AN EQUIVALENT HOMOGENEOUS CONTINUUM APPROACH TO MODELING SOLUTE TRANSPORT AND WATER FLOW IN REGULARLY STRUCTURED POROUS MEDIA

by

J. C. Parker and D. A. Barry

Virginia Polytechnic Institute and State University
Blacksburg, Virginia 24061

Project No. 810819-01-0

Project Officer

Louis G. Swaby
Office of Research and Development
U.S. Environmental Protection Agency
Washington D.C. 20460

OFFICE OF RESEARCH AND DEVELOPMENT
U.S. ENVIRONMENTAL PROTECTION AGENCY
WASHINGTON, D.C 20460

ABSTRACT

Theoretical investigations and numerical and laboratory experiments were conducted to evaluate the feasibility and limitations of describing solute transport and water flow in regularly structured porous media with an equivalent homogeneous continuum approach. For the analysis of solute transport, it is shown that distinguishing between resident and flux concentration detection modes is of fundamental importance to obtain physically meaningful solutions of the governing equations in situations when large local variations in pore water velocities occur. Effects of using erroneous detection mode are demonstrated theoretically and experimentally for porous media with bimodal velocity distributions. Using a time moment method, relationships between diffusion-controlled or first-order kinetic type mobile-immobile transport models and an "equivalent" monocontinuum dispersion model are derived and criteria for the validity of the latter approach are obtained. A generalization of the moment analysis results is presented which relates the effective dispersivity for the monocontinuum system with arbitrary bimodal structure to primary geometrical and physical properties of the system. Effects of local transverse mixing within zones of the bicontinuum are demonstrated experimentally to appeciably effect the validity of monocontinuum degeneration unless a time-dependent dispersion coefficient is adopted. The moment method is also used to evaluate constraints on the description of transport through layered media with flow transverse to the stratification as equivalent homogeneous porous media. Experimental results are employed to demonstrate the method. Finally, an analysis of the feasibility of describing flow in variably saturated porous media with heterogeneities perpendicular to the mean flow field are investigated. Comparison of numerically simulated flow in a dual medium system with predictions based on analytically calculated average conductivity-saturation-pressure relationships indicates that the averaging procedure may provide satisfactory results under a variety of imposed boundary conditions.

ACKNOWLEDGEMENTS

We acknowledge with gratitude the administrative assistance of Louis Swaby in facilitating this study. Collaboration on Chapter 2 with Rein van Genuchten of the U.S. Salinity Laboratory, Riverside, California and on Chapter 4 with Al Valocchi of the University of Illinois, was a substantial benefit to the study and a detailed review of Chapter 6 by Yves Parlange of Cornell University is gratefully acknowledged. Two-dimensional finite element flow simulations in Chapter 7 were carried out by J. J. Kaluarachchi. Appreciation is also due to James Harris and Marshall McCord who carried out the laboratory analyses involved in this study.

CONTENTS

CHAPTER 1

INTRODUCTION

Fractures, cracks, biopores, and other zones of low flow impedance in geologic media can have a profound influence on water resource management due to their effects on water and solute movement to groundwater, streams and springs. Explicit mathematical treatment of these features in flow and transport models results in a more complex model to solve which may lead at times to numerical difficulties, for example, in the case of numerical solutions for variably saturated flow with very large node to node permeability variations transverse to the mean flow direction. A more serious impediment to the explicit description of such heterogeneities is the extreme difficulty, if not impossibility, of obtaining a sufficiently detailed deterministic description of the porous medium at a scale corresponding to that of the heterogeneities. Clearly, in the usual continuum treatment of porous media, a certain degree of heterogeneity is always dealt with implicitly and reflected in the magnitude and form of the macroscopic coefficients which describe the system, e.g dispersivity, permeability, water capacity, etc. Thus, we may naturally ask what limitations constrain the implicit description of heterogeneous systems as equivalent simple continua. When it is feasible to treat heterogeneities in such a manner, data requirements for modeling the system will be diminished significantly.

It is the purpose of this research to investigate constraints on the description of heterogeneous systems as equivalent simple continua using a combination of theoretical analyses and laboratory and numerically simulated experiments. Most of our efforts have concentrated on the analysis of soluble chemical transport accompanying steady water flow in porous media with bimodal pore size distributions of various geometric configurations. In Chapter 2 a theoretical analysis of the effects of experimentally imposed and mathematically assumed boundary conditions on the interpretation of solute transport experiments in heterogeneous media is presented, followed in Chapter 3 by a laboratory investigation which demonstates these effects. In Chapter 4, a theoretical framework based on the method of moments is presented which yields a methodolgy for evaluating the applicability of an equivalent simple continuum approach in systems comprised of spheroidal microporous aggregates and in Chapter 5 the analysis is generalized to arbitrary geometry in longitudinally homogeneous media, with experimental results presented to illustrate the method. In Chapter 6 the moment method is employed to investigate the treatment of longitudinally heterogeneous media as equivalent homogeneous systems. Finally, in Chapter 7 we present the results of preliminary numerical studies into the feasibility of describing transient variably saturated flow in transversally heterogeneous media with an equivalent monocontinuum approach.

CHAPTER 2

FORMULATION OF BOUNDARY CONDITIONS

The convective-dispersive transport equation is the foundation upon which numerous mathematical analyses of solute transport in porous media have been based. Recently, questions have been raised regarding the applicability of this model to media exhibiting large variations in pore water velocities caused by the presence of continuous large pores or by field-scale variability in hydraulic properties (van Genuchten and Wierenga, 1977). Under certain limiting conditions (i.e., for low apparent dispersivities), all solutions of the classical convection-dispersion model yield symmetrical concentration distributions in time and space. Experiments on fractured or aggregated media, however, yield asymmetrical spatial and temporal concentration distributions with first moments markedly different from those anticipated for symmetric distributions [e.g., Bouma and Wösten, 1979) For such media, rapid breakthrough is observed in laboratory column tracer experiments. It is intuitively apparent that a large portion of the pore space is being more or less bypassed, resulting in a discrepancy between the effluent concentration and the volume-averaged resident pore fluid concentration in the vicinity of the exit boundary. Such a discrepancy is often regarded as incongruous with the classical convection-dispersion equation, a view seemingly corroborated by the inability of certain solutions of this equation to fit observed-breakthrough curves (e.g., Nkedi-Kizza et al., 1983).

Distinctions between flux-averaged effluent and volume-averaged resident concentrations have been made by workers in petroleum and chemical engineering (Brigham, 1974; Kreft and Zuber, 1978, 1979). We will show that it is of fundamental importance to make such a distinction in order to stipulate boundary conditions appropriate for specific experimental solute detection modes. When the assumptions implicitly invoked by various boundary conditions are given proper consideration and when mass balance constraints are carefully adhered to, we will find that certain perceived limitations of the convection-dispersion model appear to be mitigated.

THEORY

The usual continuum approach to solute transport in porous media invokes the use of concentrations which represent average quantities of solute occurring in the pore fluid within a finite representative elementary volume of the porous medium (Bear, 1972). Associating this mean value with its centroid results in the requisite function which is continuously differentiable in space. Consideration of a mass balance for nonreactive solutes in one dimension yields the continuity condition

$$\partial(C_r\theta)/\partial t = -\partial J/\partial x \qquad (2.1)$$

where C_r is the volume-averaged concentration (or resident concentration in the terminology of Kreft and Zuber, 1978) which we specifically distinguish from the flux-averaged concentration C_f, to be discussed shortly, θ is the volumetric water content, t is time, and J is the solute flux density. The constitutive relationship describing J is

$$J = qC_r - D\theta \, \partial C_r/\partial x \qquad (2.2)$$

where q is the liquid flux density and D is the dispersion coefficient representing the combined effects of diffusion and hydrodynamic dispersion on transport. Combination of (2.1) and (2.2) and restriction of our attention to the case of constant q, θ, and D for macroscopically one-dimensional transport yields the linear convection-dispersion equation

$$\frac{\partial C_r}{\partial t} = D \frac{\partial^2 C_r}{\partial x^2} - v \frac{\partial C_r}{\partial x} \qquad (2.3)$$

where $v=q/\theta$ is the mean pore water velocity.

Boundary Conditions for Volume-Averaged Equations

Considerable attention has been given to the solution of (2.3) for various initial and boundary conditions. For a semi-infinite system, an appropriate lower boundary condition is

$$\partial C_r/\partial x \; (\infty, t) = 0 \qquad (2.4)$$

If, on intuitive grounds, we assume that concentrations are continuous across the inlet boundary, and if the input solution is well mixed, a first-type boundary condition results which, for pulse-type injection, would specify

$$C_r(0,t) = C_o \qquad 0 < t \leq t_o$$
$$C_r(0,t) = 0 \qquad t > t_o \qquad (2.5)$$

Although intuitively appealing, we will show that this first-type boundary condition for C_r defined by (2.5) is improperly posed. When the input solution is not well mixed, a boundary layer may develop in the region external to the porous medium, rendering (2.5) inappropriate. However, a more general argument against the applicability of the first-type boundary condition may be posed by consideration of the physical reality underlying the representation of boundaries in mathematical continua. It is apparent that the

plane which we regard as the macroscopic boundary has no physical relevance at the microscopic level as irregularities in pore structure and morphology become manifest. If the representative elementary volume (REV) of the porous medium has a diameter ℓ, then because properties in a continuum are associated with the centroid of the averaging volume, medium properties must vary continuously from those of the external medium to those of the bulk porous medium over a finite transition zone of thickness $\ell/2$ [*Bear and Bachmat*, 1982]. Integration of (2.3) over this finite transition zone from x=0 to $x=\ell/2$ for $t<t_o$ leads to

$$qC_o - D_o\theta(0)\frac{\partial C_r(0,t)}{\partial x} = qC_r(\ell/2,t) - D\theta(\ell/2)\frac{\partial C_r(\ell/2,t)}{\partial x} + \int_0^{\ell/2}\frac{\partial C_r(x,t)\theta(x)}{\partial t}\,dx \qquad (2.6)$$

where D_o is the bulk solution molecular diffusion coefficient, D is the bulk porous medium dispersion coefficient, and $\theta(x)$ is the volumetric water content at x with $\theta(0)=1$ and $\theta(\ell/2)$ the bulk porous medium value. For a well-mixed input solution, $\partial C_r(0,t)/\partial x=0$. Evaluation of the integral in (2.6) requires a knowledge of C_r and hence D in the boundary region $0<x<\ell/2$. The case of an assumed linear variation in D within a boundary region was discussed by Pearson (1959) who noted that the indeterminacy of this function makes it desirable to impose the limiting condition that $\ell\to 0$, causing the integral to vanish. Taking ℓ as infinitesimal in (2.6) and proceeding in a similar fashion for $t>t_o$ yields, directly,

$$\left(C_r - \frac{D}{v}\frac{\partial C_l}{\partial x}\right)\Bigg|_{x=0^+} = C_o \qquad 0 < t \leq t_o$$

$$\left(C_r - \frac{D}{v}\frac{\partial C_r}{\partial x}\right)\Bigg|_{x=0^+} = 0 \qquad t > t_o \qquad (2.7)$$

which is the third-type boundary condition for pulse injection specifying the solute flux at the inlet boundary. We will refer to the quantity D/v as the apparent medium dispersivity. The designation 0^+ denotes quantities evaluated approaching x=0 from positive x (interior to the porous medium).

We may interpret the third-type boundary condition to imply the existence of a transition region within which medium dispersivity and concentration vary continuously. The transition region is treated macroscopically as being of infinitesimal thickness, resulting in apparent discontinuities in both quantities at the boundary. Actual concentrations at the pore scale will vary continuously over the finite transition region. The incongruity of a

concentration discontinuity at the boundary which increases with the apparent dispersivity must be tempered by the realization that calculated values have no physical relevance within $\ell/2$ of the boundary. To derive the first-type boundary condition for C_r (equation 2.5) from (2.6), an additional assumption to those involved for the third-type condition must be made, namely, that $\partial C_r/\partial x=0$ interior to the transition zone. Because this latter stipulation will not be met, we find that the cost of maintaining macroscopic continuity of concentration for the first-type condition is a loss of mass flux continuity. Considering the indeterminant nature of the macroscopic features of the boundary transition region, the least we can do is require that the basic condition of mass conservation be met by the boundary conditions.

The solution to (2.3), subject to the initial conditions

$$C_r(x,0) = 0 \tag{2.8}$$

and the third-type upper boundary condition (2.7) for the semi-infinite case (2.4) has been given by Lindstrom et al. (1967) as

$$C_r(x,t) = C_o A(x,t) \qquad 0 < t \leq t_o$$

$$C_r(x,t) = C_o A(x,t) - C_o A(x,t-t_o) \qquad t > t_o \tag{2.9a}$$

where

$$A(x,t) = \frac{1}{2}\,\mathrm{erfc}\left[\frac{x - vt}{2(Dt)^{1/2}}\right] + \left[\frac{v^2 t}{\pi D}\right]^{1/2} \exp\left[\frac{-(x - vt)^2}{4Dt}\right]$$

$$- \frac{1}{2}\left[1 + \frac{vx}{D} + \frac{v^2 t}{D}\right] \exp\,(vx/D)\,\mathrm{erfc}\left[\frac{x + vt}{2(Dt)^{1/2}}\right] \tag{2.9b}$$

which is the appropriate expression for evaluating volume-averaged resident concentrations.

It may be noted that a commonly employed solution for C_r is obtained by truncating the last two terms from A(x,t), thus leaving only the first erfc term. This solution may be derived explicitly if the porous medium is assumed to extend to infinity in both directions from the injection plane. The resulting spatial distribution of C_r as $t_o \to 0$ yields a normal curve with a first moment occurring at x=vt. The symmetry of this distribution is disturbed by

inlet boundaries that preclude back dispersion and skew the solute distribution away from the boundary.

Transformation to Flux-Averaged Equations

In many cases, solute flux distributions rather than pore fluid concentrations may be of primary interest. It is then convenient to define the flux-averaged concentration C_f such that

$$qC_f = J \tag{2.10}$$

or, with (2.2),

$$C_f = C_r - \frac{D}{v}\frac{\partial C_r}{\partial x} \tag{2.11}$$

which is valid for nonzero pore water velocities. Flux concentrations may be interpreted physically as representing the mean of the microscopic fluid concentrations weighted by their respective microscopic fluid velocities. The discrepancy between C_f and C_r increases with the apparent dispersivity (Kreft and Zuber, 1978). In the special case of v=0 with mixing solely by diffusion, C_f has no physical relevance and is mathematically undefined.

To evaluate $C_f(x,t)$ for a semi-infinite medium, we may employ a transformation of (2.3), (2.4), (2.5), and (2.8). Putting (2.10) into (2.1) for constant (and nonzero) v yields

$$\frac{\partial C_r}{\partial t} = - v \frac{\partial C_f}{\partial x} \tag{2.12}$$

Differentiating (2.11) with respect to time yields

$$\frac{\partial C_f}{\partial t} = \frac{\partial C_r}{\partial t} - \frac{D}{v}\frac{\partial^2 C_r}{\partial x \partial t} \tag{2.13}$$

Use of (2.12) to eliminate C_r from (2.13) gives

$$\frac{\partial C_f}{\partial t} D \frac{\partial^2 C_f}{\partial x^2} - v \frac{\partial C_f}{\partial x} \tag{2.14}$$

which is mathematically identical to (2.3) but with C_r replaced by C_f. Both equations describe the same physical processes, and D and v represent precisely the same physical quantities in both equations. This duality of interpretation of the physical meaning of the concentrations in the convection-dispersion equation imposes a need to carefully stipulate boundary conditions in keeping with the desired meaning. The identical mathematical form of (2.3) and (2.14) must not be allowed to obscure the fundamental distinction between resident and flux concentrations.

For the initial condition $C_r=0$ we have by differentiation that $\partial C_r/\partial x=0$, which leads to the transformed initial condition in terms of C_f by direct substitution in (11):

$$C_f(x,0) = 0 \tag{2.15}$$

The lower boundary condition $\partial C_r/\partial x=0$ transforms subject to the stipulation that higher order spatial derivatives of C_r are also zero at $x=\infty$, to yield

$$\partial C_f/\partial x\ (\infty,t) = 0 \tag{2.16}$$

To evaluate the transformed upper boundary condition, we eliminate C_r from (2.7) with (2.11), which gives, immediately,

$$\begin{aligned} C_f(0,t) &= C_o \qquad 0 < t \leq t_o \\ C_f(0,t) &= 0 \qquad t > t_o \end{aligned} \tag{2.17}$$

The transformation from C_r to C_f results in a mathematically identical set of equations with the exception of the upper boundary condition which changes from a third-type condition for C_r to a first-type for C_f. The solution of (2.14)-(2.17) is

$$C_f(x,t) = C_oB(x,t) \qquad 0 < t \leq t_o \tag{2.18a}$$

$$C_f(x,t) = C_oB(x,t) - C_oB(x,t-t_o) \qquad t > t_o$$

where

$$B(x,t) = \frac{1}{2}\ \mathrm{erfc}\left[\frac{x - vt}{2(Dt)^{1/2}}\right] + \exp\ (vx/D)\ \mathrm{erfc}\left[\frac{x + vt}{2(Dt)^{1/2}}\right] \tag{2.18b}$$

Obviously, the problem posed by (2.14)-(2.17) may be solved mathematically, irrespective of the subscript on C. In fact, (2.18) is most commonly presented as a solution to the volume-averaged equations for the semi-infinite case subject to a first-type upper boundary condition in C_r (equation 2.5) (Lapidus and Amundson, 1952). The form of (2.18) is then preserved, but the result is interpreted as representing $C_r(x,t)$ rather than $C_f(x,t)$. By conceding on physical grounds that a flux-type input boundary condition must be employed (i.e., the third type in C_r), we see that the foregoing interpretation of (2.18) is incorrect. Application of this equation implies that a transformation has been made from volume-averaged to flux-averaged concentrations.

RESULTS AND DISCUSSION

Spatial Concentration Distributions

Figure 2.1 compares the spatial distributions of C_r, and C_f in the x direction calculated from (2.9) and (2.18), respectively, using apparent dispersivities (D/v) that range from 0.01 to 100.0 m. Reduced concentrations C_r/C_o and C_f/C_o are plotted against the dimensionless distance X=x/vt for a pulse of duration vt_o=0.5 m and a final time given by vt=1.0m.

It is apparent that all curves for C_f pass through the origin in accordance with the boundary condition $C_f(x,t)=0$ for $t>t_o$. This is not the case for the C_r curves, which exhibit an apparent discontinuity in concentration at the inlet boundary which increases in magnitude with the dispersivity as expected.

For the lowest dispersivity medium the C_r and C_f curves are very similar (Figure 2.1). Mathematically, it is apparent from the definition of C_f that as $D/\nu \to 0$, $C_f \to C_r$. Physically, this reflects the fact that volume-averaged and flux-averaged concentrations become identical when variations in microscopic pore water velocities tend to zero. As these velocity variations increase, dispersive transport dominates over macroscopically convective transport, and the spatial distributions of C_r and C_f gradually diverge. Both distributions become markedly asymmetrical, exhibiting skewing away from the injection boundary. This skewing forces the modal and mean values of C_r and C_f to occur at greater distances from the injection boundary than would be the case for purely convective transport.

For piston flow (D=0), the distributions of C_r and C_f reduce to a square wave with a reduced concentration of unity between X=0.5 and X=1.0 (Figure 2.1). The first moment in space for piston flow accordingly occurs at X=0.75. We will designate this value of X, corresponding to the center of mass for piston flow, as X^*. The first moments of the spatial distributions of C_r and C_f may be calculated as:

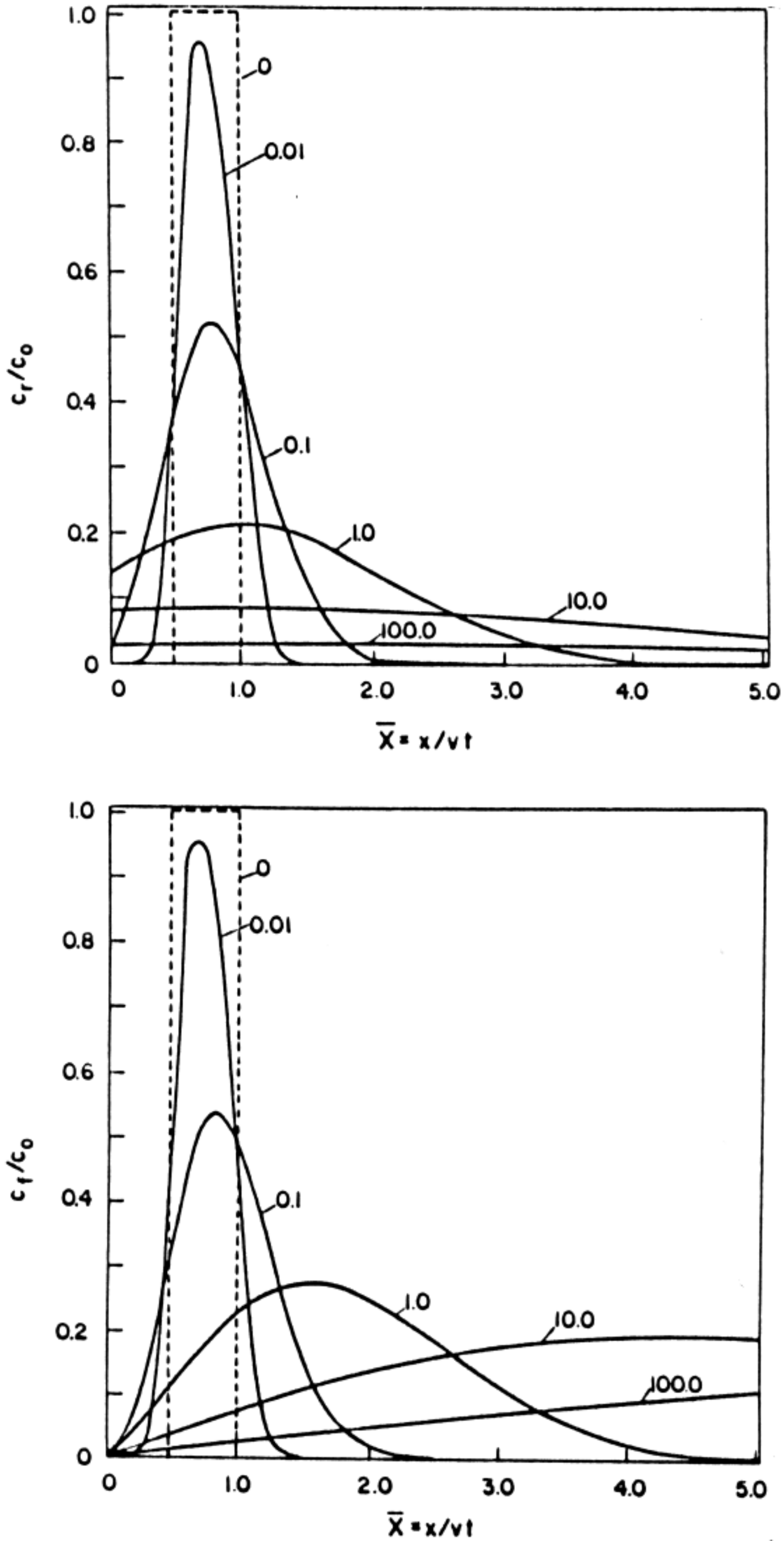

Figure 2.1. (a) Resident concentrations by (2.9) and (b) concentrations by (2.18) as functions of dimensionless distance for a pulse of duration vt_o=0.5 m at a final time vt=1.0 m for various apparent dispersivities D/v (values indicated on curves).

$$\langle X \rangle = \left[\int_0^\infty XC(X)\ dX \right] \left[\int_0^\infty C(X)\ dX \right]^{-1} \qquad (2.19)$$

where C is C_r or C_f and $\langle X \rangle$ is the dimensionless distance corresponding to the mean of the distribution function. For resident concentrations, $\langle X \rangle$ describes the center of mass of the solute distribution, while for C_f the value represents the distance at which the solute flux density attains its mean value.

Values of $\langle X \rangle$ were evaluated from (2.19) by numerical quadrature for the cases presented in Figure 2.1. Results are given in Table 2.1 as $\langle X \rangle / X^*$ values representing ratios of actual first moments of the spatial distributions to those for piston flow. Also given are reduced modal distances X_m/X^* corresponding to maxima in the C_r and C_f distributions. The first moments of C_r increase markedly beyond the piston flow mean as apparent dispersivity increases, while modal distances advance more gradually, lagging well behind mean distances. Mean and modal distances for distributions of C_f likewise increase with increasing dispersivity. Note that the modal values for C_f increase much more with increasing dispersivity than the values for C_r. Also, modal and mean values for C_f occur at larger distances than those for C_r at a given dispersivity.

TABLE 2.1. First moments of spatial distributions $\langle X \rangle$ and modal distances X_m as ratios with the piston front center of gravity X^* for various apparent dispersivities D/v with vt_o=0.5 m and vt=1.0 m

	$\langle X \rangle / X^*$		X_m/X^*	
D/v, m	C_r	C_f	C_r	C_f
0.01	1.01	1.03	0.98	0.97
0.1	1.13	1.26	1.04	1.17
1.0	1.88	2.51	1.29	2.13
10.0	4.62	6.83	1.58	5.47
100.0	13.44	20.61	1.78	16.19

It is often not appreciated that the convection-dispersion equation predicts centers of mass of concentration profiles in excess of those expected for piston flow. Analyses of solute transport are sometimes made by explicitly or implicitly decoupling convection and dispersion mechanisms (Sidle and Kardos, 1979; Rose et al., 1982). The center of mass is assumed to move at a velocity v with symmetric dispersion occurring about the mean. This decoupling is mathematically equivalent to imposing boundary conditions relevant to infinite media. For bounded media, this leads to errors which increase with apparent dispersivity as the last two terms in (2.9b) for C_r become increasingly significant. In media which exhibit large variabilities in pore water velocities, hydrodynamic dispersion becomes increasingly more important relative to convective transport, and the implied solution truncation will lead to significant errors.

To correct for observed discrepancies between measured centers of mass and piston flow values, bicontinuum models with "mobile" and "immobile" pore regions have been postulated (Skopp and Warrick, 1974; van Genuchten and Wierenga, 1976; Sidle and Kardos, 1979; Rao et al., 1980). By viewing the data in Table 2.1 in this manner, we could conclude that for the D/v = 100 m medium the "mobile" pore fraction is approximated by $X^*/\langle X\rangle$ for C_r, i.e., 1/13.44 = 0.074. This value may or may not have any physical significance, but if the medium is viewed as a simple (mono-) continuum, the information is immaterial. Microscopic features have no direct relevance to the macroscopic description except insofar as they affect the adequacy of the imposed macroscopic boundary conditions. If the scale of microscopic variations in the pore structure governs the REV, which in turn governs the thickness of the boundary transition region, as has been suggested, then the region of validity of a bulk continuum approach will be affected. So long as the flow region of interest is large compared to the scale of the microscopic heterogeneities and hence to the size of the boundary transition region, a monocontinuum approach should be valid. In such circumstances, the exclusion of a portion of the fluid-filled pore space from the porous medium continuum is physically justifiable only if (1) part of the pore fluid is encapsulated by some form of impermeable or semipermeable membrane or (2) electrochemical forces exclude solute near solid surfaces (i.e., negative adsorption).

Temporal Concentration Distributions

In many field and laboratory situations it is either more desirable or convenient to monitor temporal concentration changes at fixed points in space downstream from a tracer injection location rather than to determine spatial distributions at fixed times. Confusion between volume- and flux-averaged concentrations in such situations may lead to gross misinterpretations of observations. Values of the reduced concentrations of C_r/C_o and C_f/C_o are given in Figure 2.2 as functions of the dimensionless time T = vt/x at a fixed distance x = 0.1 m for media subject to a dimensionless pulse duration vt_o/x = 0.5 and characterized by various values of the dimensionless curves given for various D/v, we employ the dimensionless group D/vx in lieu of its inverse, which represents a Peclet number.) As was observed for the spatial distribution functions, the temporal distributions of C_r and C_f become indistinguishable as the apparent dispersivity approaches zero (piston flow).

As dispersivity increases, peak values of both C_r and C_f shift to shorter times. However, while the temporal distribution of resident concentrations becomes increasingly flat, values of C_f pass through a minimum at intermediate D/v. In the limit as $D/v \rightarrow \infty$, C_r becomes zero at all times while the distribution of C_f converges to a square wave with unit concentration between T = 0 to 0.5 (Figure 2.2). To use the terminology of *Bouma and Dekker* [1978], a "short-circuit" of zero impedance occurs, and the flux conditions imposed at x = 0 are instantaneously propagated throughout the medium. As with the piston flow scenario, this limiting case may be approached but, of course, never achieved.

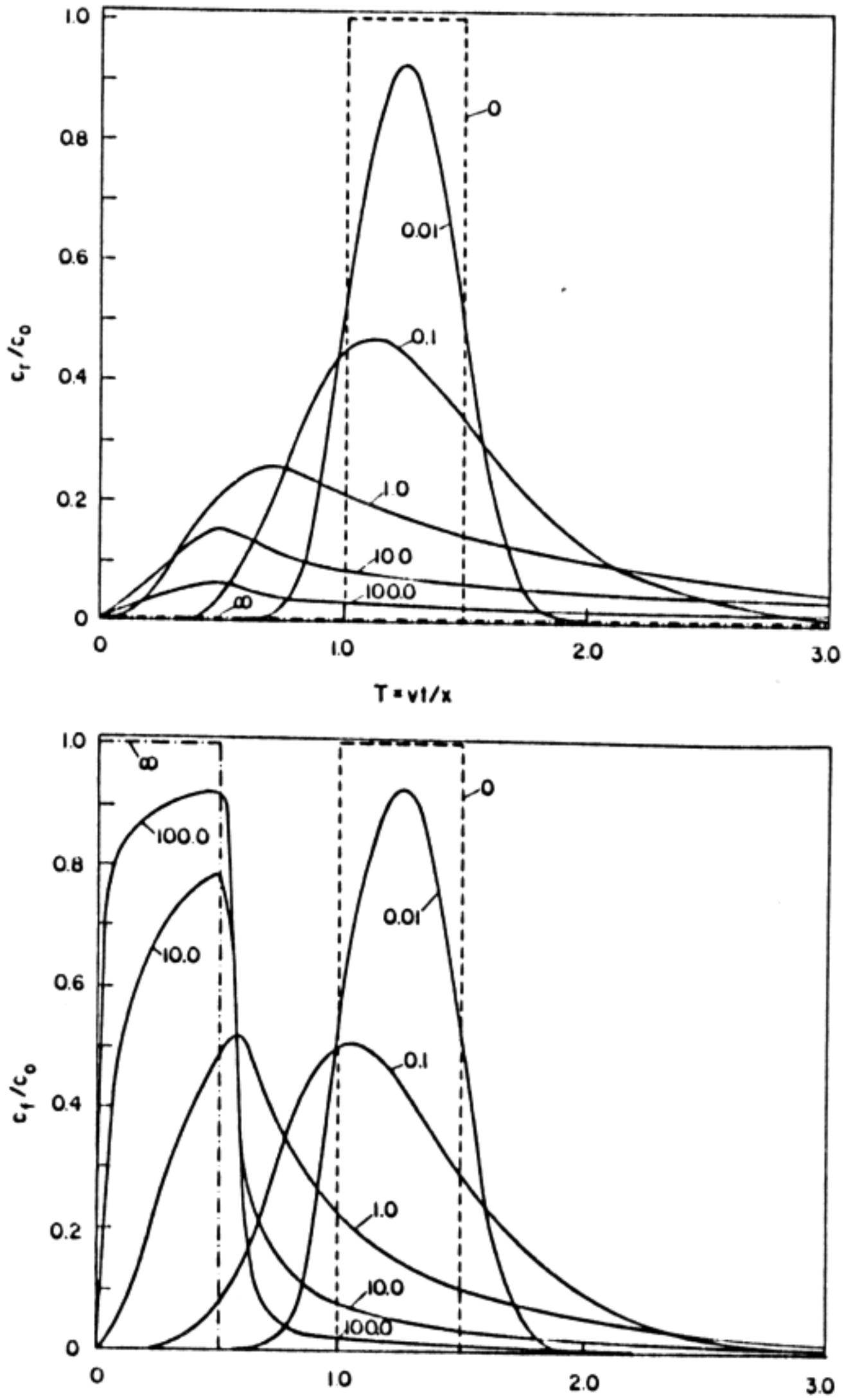

Figure 2.2. (a) Resident concentrations by (2.9) and (b) flux concentrations by (2.18) as functions of dimensionless time at x = 0.1 m for a pulse duration vt_o/x 0.5 and for various values of D/vx (values indicated on curves).

The marked differences between temporal distributions of C_r and C_f have important but generally unappreciated implications to the interpretation of laboratory tracer experiments as well as for field lysimeter and observation well data. Consider the case of transport through a finite soil column during steady water flow. Effluent solution is collected as it exits the column, and its concentration is determined as a function of time. To properly interpret the measured concentrations, it must be recognized that the values represent flux-averaged and not pore volume-averaged quantities. This is intuitively apparent if one considers the extreme case of flow through a fractured porous medium exhibiting large variations in microscopic pore water velocities. The effluent solution comes nearly exclusively from the larger pores, which "short-circuit" the input solution resulting in rapid breakthrough and extended "tailing." However, the volume-averaged concentration within the column near the outflow boundary may be much less than that of the flux-averaged effluent solution, particularly during the peak effluent concentration phase.

To pose macroscopic boundary conditions for the exit boundary, we may proceed in the same manner as for the inflow boundary by imposing a flux continuity and assuming as infinitesimal boundary transition region, to obtain

$$C_e = \left(C_r - \frac{D}{v} \frac{\partial C_r}{\partial x} \right) \Bigg|_{x=L^-} \qquad (2.20)$$

where $C_e = C_e(t)$ is the concentration in the effluent and L^- denotes that the quantities are evaluated approaching L from the interior of the porous medium. It is evident that C_e is precisely the definition of C_f at $x = L$ given by (2.11). Thus the analytical solution for C_f given by (2.18) is to be used for C_e provided that we assume that C_r for $x < L$ is unaffected by the additional condition imposed on the solution that the spatial derivatives of C_r are zero at $x = \infty$. This provision imposes a mild restriction, since the outflow boundary of a column should have no effect on the upstream velocity distribution interior to the boundary layer during steady flow. If no back mixing occurs, then the solute distribution interior to the column will be unaffected by the boundary. Since the only mechanism of back mixing is diffusion, little error should result when hydrodynamic dispersion is the dominant mechanism of dispersion in the porous medium. In most practical instances, this will be the case.

Equating C_e and C_f and employing (2.18) to describe the effluent-time data indicates that Figure 2.2b may be interpreted as a family of breakthrough curves for columns of specified length $x = L$. The dimensionless time T corresponds physically to the number of pore volumes of effluent. It should be mentioned that (2.18) often has been employed to describe effluent concentrations from column tracer experiments but on the grounds that it represents $C_r(x,t)$ and that $C_r(L,t) = C_f(L,t)$. This reasoning is incorrect, although the result is fortuitously identical so long as only flux concentrations are dealt with. However, the implication that C_r and C_f are identical will lead

to gross errors if subsequent predictions of C_r are made. Since the assumption that $C_r(L,t) = C_f(L,t)$ is intuitively unreasonable for fractured porous media, it has been assumed frequently that a monocontinuum approach in such media is infeasible. The curves of Figure 2.2b show that the rapid breakthrough and tailing typical of such systems are, in fact, predicted by the flux concentration solution (2.18) for media of high dispersivity.

If the observation scale is large compared to the scale of heterogeneity, it should be feasible to model the porous medium as a monocontinuum and employ (2.18) to determine transport coefficients from effluent breakthrough curves (e.g., van Genuchten, 1981; Parker and van Genuchten, 1984). For subsequent predictions of $C_r(x, t)$, these coefficients may be employed with (2.9). Use of (2.18) to predict $C_r(x, t)$ on the assumption that $C_r = C_f$ will lead to gross errors for high-dispersivity media. If experimental values of C_r are desired, appropriate extraction of sectioned columns must be performed.

It is noteworthy that the area under the curves of C_f versus T from T = 0 to ∞ is constant and equal to the dimensionless pulse time $vt_o/x = 0.5$ (Figure 2.2b). This indicates that the solution meets the mass balance criteria:

$$\int_o^x C_r(X,t)dX = v\int_o^t [C_o - C_f(x, \tau)]\, d\tau \qquad (2.21a)$$

$$0 < t \leq t_o$$

$$\int_o^x C_r(X,t)\, dX = v \int_o^{to} C_o\, d\tau - v \int_o^t C_f(\chi,\tau)\, d\tau \qquad (2.21b)$$

$$t > t_o$$

for any particular values of x and t were χ and τ are dummy variables. For x = L, this simply states that the solute mass in the column equals the difference between cumulative inflow and outflow. In the limit as $t \rightarrow \infty$, the left-hand side of (2.21) goes to zero, and from the definition of T = vt/x, we obtain

$$\frac{vt_o}{x} = \int_o^{\infty} \frac{C_f}{C_o}\, dT \qquad (2.22)$$

which is the observed result.

Note that the integral in (2.22) involves C_f, not C_r. In some cases, solutions for C_r have been employed to analyze effluent concentration data (e.g., Nkedi-Kizza et al., 1983]. With C_r substituted for C_f in (2.22), an inequality is obtained with the left-hand side always less than the right-hand side. This has the effect of making the apparent pore water velocity seem greater than the actual value to force a mass balance (i.e., retardation factors less than unity). The erroneous inference to be drawn is that some of the

pore volume apparently excludes solute. This difficulty is not obtained when the solution appropriate to the flux detection mode is employed.

It is useful to also note that by differentiating (2.21) with respect to time or space, two additional transformations between resident and flux concentrations are obtained; these transformations may be regarded as supplemental, but fundamentally equivalent, to that of (2.11), namely,

$$\int_o^x \frac{\partial C_r(\chi,t)}{\partial t}\, d\chi + vC_f(x,t) = vC_o \qquad 0 < t \leq t_o \qquad (2.23a)$$

$$\int_o^x \frac{\partial C_r(\chi,t)}{\partial t}\, d\chi + vC_f(x,t) = 0 \qquad t > t_o \qquad (2.23b)$$

$$C_r(x,t) = -v\int_o^t \frac{\partial C_f(x,\tau)}{\partial x}\, d\tau \qquad t > 0 \qquad (2.24)$$

The solutions which we have presented for C_r and C_f satisfy these mass balance constraints. Solutions which fail to distinguish between C_r and C_f generally will not satisfy these criteria. This is notably the case for solutions commonly applied to column tracer studies which assume that the effluent concentration is equal to the resident concentration at x = L. An exception arises for the solution of the convection-dispersion equation given by Brenner (1962). This solution imposes a third-type upper boundary condition and a zero gradient condition at x = L for C_r. Equation (2.7) and (2.20) are thus satisfied; however, the assumption that $\partial C_r(L,t)/\partial x = 0$ forces the concentration to be continuous at the outflow as (2.20) reduces to $C_e(t) = C_r(L,t)$. Use of Brenner's solution for C_r and evaluation of C_f using (2.11) satisfies the conditions stipulated by (2.23) and (2.24) (van Genuchten and Parker, 1984). Predicted concentrations at x = L thus yield physically acceptable estimates of C_e from a mass balance standpoint. However, the assumption of concentration continuity at the exit seems inconsistent with the macroscopic treatment of the upper boundary at which the concentration is discontinuous. The rationalization of the zero gradient condition at the outflow presumably arises from the intuitive argument that boundary layers cannot occur at outflow boundaries. Boundary layers external to porous media resulting from poor mixing of outflow solution indeed cannot occur. However, boundary layers may arise from the more general conception of boundary layers as transition regions within which transport parameters change from those of the bulk porous medium to those of the bulk solution. Accordingly, a macroscopic concentration discontinuity at exit boundaries may be anticipated in high-dispersivity media, and the solutions formally derived from semi-infinite systems may provide a more suitable approximation of the boundary than Brenner's explicitly finite solution, which imposes a zero gradient condition at the column exit.

This rather heuristic argument against the applicability of Brenner's finite column solution is reinforced by consideration of the limiting case as $D/v \rightarrow \infty$ which yields for Brenner's solution at $x = L$,

$$C_e/C_o = 1 - e^{-T} \qquad T \leq T_o$$
$$C_e/C_o = e^{(T_o - T)} - e^{-T} \qquad T > T_o \tag{2.25}$$

while (2.18) yields, in the limit,

$$C_e/C_o = 1 \qquad T \leq T_o$$
$$C_e/C_o = 0 \qquad T > T_o \tag{2.26}$$

where $C_e = C_e(t) = C_f(L,t)$ is the effluent concentration, $T = vt/L$ is the eluted pore volumes, and $T_o = vt_o/L$ is the reduced pulse duration. Equation (2.25) describes a breakthrough curve (C_e/C_o versus T) which for a continuous pulse passes through the origin, gradually increases to $C_e/C_o = 0.632$ at $T = 1.0$, and approaches $C_e/C_o = 1.0$ as $T \rightarrow \infty$. This function contrasts sharply with the square wave for the limiting case described by (2.26) (Figure 2.2b). Brenner's solution is incapable of predicting this "short-circuiting" behavior which, as previously mentioned, fractured porous media are observed to approach. This diminishes the utility of Brenner's solution and throws further doubt on the appropriateness of the assumptions it invokes in posing the lower boundary condition.

Analogous problems to those occurring in laboratory studies arise in the interpretation of solution concentrations in samples taken from wells or lysimeters in the field. The least ambiguous field measurements are those obtained from large monolithic pan lysimeters which yield flux concentrations for a well-defined flow region. The effect of the exit boundary on the flow pattern, particularly for unsaturated conditions, is the only uncertainty (so long as the results are not extended beyond the bounds of the monolith). Subphreatic well samples are also most appropriately viewed as (local) flux concentrations. Their significance to the interpretation of aquifer properties will depend on the formation's homogeneity and the magnitude of flow disturbances caused by the well. The interpretation of results from samples taken with small suction samplers in the unsaturated zone is much less certain. Depending on the manner in which these units disrupt the local flow pattern, the sampled concentrations may yield resident concentrations or flux concentrations or anything in between.

An additional complication to the interpretation of field solution samples arises because the sampled quantities generally represent a small proportion of the total flow region of interest. If the scale of variability of pore water

velocity is greater than the effective radius of the sampling device, then multiple samples will need to be taken to evaluate field-scale areal averages of C_r or C_f. Since scales of hydraulic property variations in geologic media are generally orders of magnitude larger than typical sampling devices, the need for numerous sampling locations is assured.

Caution should be exercised in the interpretation of areally averaged solute concentrations. While resident concentrations may be meaningfully averaged to obtain larger (e.g., field-) scale values, simple averages of flux concentrations have no corresponding direct physical interpretation. To define meaningful areally-averaged flux concentrations, local concentrations should be weighted by local hydraulic flux values so that (10) remains valid at the larger scale. Of course, the determination of field-scale values of C_r or C_f in no way guarantees their conformance to a deterministic, monocontinuum convection-dispersion model. At some scale of averaging within the plane perpendicular to flow, constraints on such an approach will arise. However, it appears likely that scale limitations may be less severe than has been thought, owing to misapplications and misinterpretations of various boundary conditions in finite and semi-infinite media.

While we have confined our discussion to one-dimensional transport accompanying steady flow, the approach may be generalized. The definition of C_f given by (2.11) may be extended to multiple dimensions, in which case the vectorial nature of the hydraulic flux must be considered. In general, the flux transformation of the convection-dispersion equation will be valid only for constant D. For transient flow problems, solutions for C_f may be obtained by local application of (2.11) after solving the nonlinear problem for C_r subject to a flux-type inlet boundary condition.

CHAPTER 3

ANALYSIS OF COLUMN TRACER EXPERIMENTS

The formulation of boundary conditions appropriate to the analysis of solute transport in finite soil columns has been the subject of considerable discussion and marked disagreement. Van Genuchten and Parker (1984) have reviewed analytic solutions of the linear one-dimensional convective-dispersive transport equation and evaluated their suitability to the analysis of column tracer experiments. Two solutions were identified which imposed flux-type conditions at inlet and outlet boundaries and satisfied mass balance constraints when applied to the analysis of effluent data. The solution of Lapidus and Amundson (1952) ostensibly for a concentration-type inlet boundary condition was shown to meet these criteria through a local transformation from volume-averaged to flux-averaged concentrations and subject to an assumption that exit boundaries do not affect concentration distributions within the porous medium. The solution of Brenner (1962) also imposes flux-type boundary conditions but simplifies the lower boundary condition by assuming that continuity of macroscopic concentrations occurs across the exit boundary. Based on heuristic arguments, use of the former solution was recommended over the latter for analysis of column effluent data, while the solution of Lindstrom et al. (1967) stipulating a flux-type upper boundary condition for the semi-infinite case was shown to be appropriate for analyzing resident concentrations within the porous medium. In Chapter 2 we suggested that by distinguishing between flux- and volume-averaged concentrations and by employing solutions appropriate to the concentration detection mode, perceived difficulties in the treatment of fractured and aggregated porous media as simple continua may in certain circumstances dissipate.

In this chapter we wish to (i) clarify the conditions governing treatment of porous media, including fractured and aggregated media, as simple continua, (ii) experimentally demonstrate the distinction between resident and flux concentrations and (iii) evaluate the adequacy of various boundary condition assumptions in describing observed spatial and temporal concentration distributions in column tracer experiments.

THEORETICAL

Relationships Between Microscopic and Macroscopic Quantities

In principle, at least, solute transport in porous media may be described at a microscopic level which considers explicitly the effects of pore geometry and fluid velocity distributions (Bear and Bachmat, 1982). For our purposes, we regard the microscopic level as small compared to pore dimensions but large enough that statistically meaningful particle ensembles may be defined (in the continuum mechanics sense). At the microscopic scale we define the

local concentration by

$$\tilde{c} = dm_s/dU_w \tag{3.1}$$

where m_s is the solute mass and U_w is the liquid volume. The velocities of the liquid and solute particles in the Lagrangian description are, respectively,

$$\tilde{v}_w = (\partial \tilde{x}_w/\partial t)\Big|_{\xi_w=\text{constant}} \tag{3.2}$$

$$\tilde{v}_s = (\partial \tilde{x}_s/\partial t)\Big|_{\xi_s=\text{constant}} \tag{3.3}$$

where $\tilde{x}_w$ and $\tilde{x}_s$ are the microscopic-scale position vectors of the respective particles; ξ_w and ξ_s are their corresponding initial coordinates; and t is time.

The mass flux density of solute at the microscopic scale is given by

$$\tilde{j} = \tilde{c}\ \tilde{v}_s \tag{3.4}$$

which is useful to decompose into

$$\tilde{j} = \tilde{c}\ \tilde{v}_w + \tilde{c}(\tilde{v}_s - \tilde{v}_w) \tag{3.5}$$

where the first term on the right-hand side may be identified as a convective flux and the second as a diffusive flux.

The microscopic mass balance equation for a nonreactive solute is

$$(\partial \tilde{c}/\partial t) + \nabla\cdot\tilde{j} = 0. \tag{3.6}$$

Since the terms in (3.6) represent rates of change in solute mass per unit volume of the liquid phase, integration over an arbitrary volume is permissible. To pass from the microscopic to macroscopic domains, it is desired to integrate over a region U_o characterizing the representative elementary volume (REV) as

$$\int_{(U_o)} \left[\frac{\partial \tilde{c}}{\partial t} + \nabla\cdot\tilde{j}\right] dU = 0. \tag{3.7}$$

The expressed integration may be meaningfully carried out to define the macroscopic realm if a region U_o exists such that mean values of extensive quantities associated with centroids of U_o vary continuously in time and space. Bear and Bachmat (1982) show that integration of (3.7) then leads to the macroscopic equations:

$$(\partial C_r/\partial t) + \nabla\cdot j = 0 \tag{3.8}$$

$$j = vC_r - D\nabla C_r \tag{3.9}$$

where D is a dispersion tensor reflecting the effects of molecular diffusion and microscopic pore water velocity variations; and the macroscopic fluid concentration, fluid velocity, and solute mass flux density relative to the pore fluid domain (C_r, v, and j, respectively) are defined by expressions of the form

$$E(\mathbf{x},t) = (1/U_{ow})\int_{(U_{ow})} e(\mathbf{x},t)\,dU_w \tag{3.10}$$

where e represents the microscopic quantity ($\tilde{c}$, $\tilde{v}_w$, $\tilde{j}$); E is the corresponding macroscopic quantity (C_r, v, j); U_{ow} is the volume of the fluid within the REV of volume U_o; U_w is the water domain; and the macroscopic position vector x represents the centroid of U_o. The macroscopic volumetric fluid flux density and solute mass flux density relative to the porous medium domain are given, respectively, by $J = j\theta$ and $q = v\theta$ where $\theta = U_{ow}/U_o$ is the volumetric water content. From the implied assumption that extensive quantities vary linearly within the REV, it follows that the integration in (3.10) could be equivalently carried out within the bulk porous medium over a representative area (REA) rather than a volume (Bear and Bachmat, 1983).

The quantities C_r, v and j clearly represent mean values within the water phase of the REV or REA with microscopic values effectively weighted according to their microscopic ensemble volumes or areas. Employing the terminology of Kreft and Zuber (1978), we designate C_r as the resident concentration in order to distinguish it from the flux concentration defined macroscopically by

$$C_f = j/v = J/q \tag{3.11}$$

or via (3.9)

$$C_f = C_r - (D/v)\nabla C_r. \tag{3.12}$$

Equations (3.11) and (3.12) indicate that at the macroscopic level C_f may be regarded as an equivalent concentration which would occur if transport were purely convective (i.e., as if D = 0). It should be noted that defined in this fashion C_f unlike C_r is a vector quantity which achieves a maximum parallel to the velocity field and a minimum at right angles in directions of decreasing C_r. In multidimensional applications it may be more useful to define flux concentrations by the norm of this quantity. In the case of one-dimensional transport when fluid and solute fluxes are necessary parallel, this distinction will not be of concern. As dispersive mechanisms become more dominant (D/v increasing) C_f and C_r will increasingly diverge. From (3.4), (3.10) and (3.11), we obtain the microscopic definition of C_f as

$$C_f(x,t) = \frac{\int_{(U_{ow})} \tilde{c}(\tilde{x},t)\tilde{v}_s(\tilde{x},t)dU_w}{\int_{(U_{ow})} \tilde{v}_w(\tilde{x},t)dU_w} \qquad (3.13)$$

which clearly shows that C_f represents a flux-weighted mean concentration. Comparison of (3.13) with (3.10) for C_r indicates that the difference between C_r and C_f will tend to zero as the microscopic diffusive velocity ($\tilde{v}_s - \tilde{v}_w$) diminishes and as the covariance between $\tilde{c}$ and $\tilde{v}_w$ likewise tends to zero. Increases in the covariance between $\tilde{c}$ and $\tilde{v}_w$ may arise due to increases in the correlation between $\tilde{c}$ and $\tilde{v}_w$ or to increases in the variance of $\tilde{v}_w$. If $\tilde{c}$ and $\tilde{v}_w$ are completely uncorrelated the covariance is zero regardless of the variance of $\tilde{v}_w$ and $C_r \propto C_f$ for $\tilde{v}_s - \tilde{v}_w \propto 0$. Physically, such a condition would be approached by a porous medium in which the particle arrangement and pore geometry are random. In the limiting case of perfect correlation between $\tilde{c}$ and $\tilde{v}_w$ as for a bundle of noninteracting parallel tubes, the covariance for $\tilde{c}$ and $\tilde{v}_w$ and the difference between C_r and C_f will increase as the variance of the velocity distribution increases. This will occur irrespective of the form of the distribution function -- i.e., normal, lognormal, bimodal, etc. In aggregated or fractured porous media with continuous large pores, a high covariance between $\tilde{c}$ and $\tilde{v}_w$ may be anticipated due to autocorrelation between $\tilde{c}$ and $\tilde{v}_w$ associated with channeling phenomena as well as to the tendency for velocity distributions to be quite broad. The net effect will be a marked difference between resident and flux concentrations in such media.

Macroscopic Boundary Conditions and Solutions

To pose macroscopic boundary conditions in finite porous media, caution must be exercised in passing from the microscopic to macroscopic domains. If ℓ is the diameter of a spherical REV, difficulties will arise in assigning meaningful macroscopic values of extensive quantities to locations within a distance $\ell/2$ of the boundary. Within this boundary region the REV extends partially beyond the boundary while the centroid remains within the porous medium. Within the boundary region there is no way to pose macroscopic

transport equations in any exact fashion since the effect of the boundary of the microscopic velocity field and hence on the macroscopic dispersion tensor is unknown as is the magnitude of ℓ itself.

To deal with the boundaries macroscopically, we note that for a continuum analysis to be appropriate, the flow region must be large relative to the REV. If we formally assume the REV and thus the boundary region are infinitesimally small then from a mass balance over the boundary region we obtain the flux-type boundary condition (Pearson, 1959; Chapter 2, this report):

$$\left[C_r - (D/v)\nabla C_r\right]\Big|_{x=b} = C_{ext} \qquad (3.14)$$

where **b** is the macroscopic position vector normal to the boundary and $C_{ext} = C_{ext}(\mathbf{b},t)$ is the concentration of entering or exiting fluid external to the porous medium at this location. Owing to the assumption of an infinitesimal REV, the dispersion tensor is regarded as equal to that of the bulk porous medium interior to the boundary region. The quantities on the left-hand side of (3.14) must be evaluated approaching **b** from the interior of the porous medium because by stipulating a flux continuity and an infinitesimal boundary region, continuity in concentration across the boundary is sacrificed. This apparent incongruity must be tempered by the realization that the REV is in reality finite so that predicted concentrations with a distance $\ell/2$ of the boundary have no physical significance.

Comparison with (3.12) indicates that the left-hand side of (3.14) is identically equal to $C_f(\mathbf{b},t)$. Thus, while flux concentrations within the bulk porous medium represent conceptual rather than directly measurable quantities, at (macroscopic) boundaries a direct physical interpretation arises. This is most clearly visualized at an outflow boundary where collected effluent may be regarded as being flux-averaged relative to the resident concentration in the porous medium -- that is, the effluent concentration will be weighted towards the concentrations occurring in pores where the fluid velocity is greatest.

Mathematically, the identity between $C_f(\mathbf{b},t)$ and $C_{ext}(\mathbf{b},t)$ indicates that the third-type boundary condition in C_r (eq. 3.14) transforms to a first-type condition in C_f. Furthermore, C_f has the property of obeying a linear convection-dispersion equation of the same form as that for C_r in one dimension (Kreft and Zuber, 1978; Chapter 2, this report):

$$\frac{\partial C_f}{\partial t} = D\,\frac{\partial^2 C_f}{\partial x^2} - v\,\frac{\partial C_f}{\partial x} \qquad (3.15)$$

for transport in the x direction for the case of constant D and where D and v are precisely the same physical quantities as in the analogous expression for C_r. The transformation follows in a straightforward manner from (3.8), (3.9) (3.11), and (3.12) of the linear one-dimensional case. This property of C_f facilitates its analytic evaluation but also lends a duality of interpretation of the macroscopic convection-dispersion equation which has led to some confusion over the physical meaning of various solutions to it.

For a finite column at constant water content subjected to steady one-dimensional flow in the x direction with pulse-type injection, the upper boundary condition described by (3.14) becomes

$$\left(C_r - \frac{D}{v}\frac{\partial C_r}{\partial x}\right)\Bigg|_{x=0} = \begin{cases} C_o & 0 < t \leq t_o \\ 0 & t > t_o \end{cases} \qquad (3.16)$$

where the coordinate origin is set at the inflow boundary; t_o is the pulse duration; and C_o is the influent concentration during the pulse. The left-hand side of (3.16) is identically $C_f(0,t)$.

For a column of length L, $C_{ext}(L,t) = C_f(L,t)$ is the effluent concentration and (3.14) yields

$$\left(C_r - \frac{D}{v}\frac{\partial C_r}{\partial x}\right)_{x=L} = C_f(L,t). \qquad (3.17)$$

This stipulation in itself, however, does not adequately define the physical system since $C_f(L,t)$ is unknown. An additional equation is needed. One approach to completing the system of equations is to assume that back-mixing at the column exit is negligible, allowing the porous medium to be treated mathematically as a semi-infinite medium for which $\partial C_r(\infty,t)/\partial X = 0$.

Solutions to (3.8) and (3.9) for C_r and to (3.15) for C_f subject to the above boundary conditions and to the initial condition $C_r(x,0) = 0$ (hence $C_f(x,0) = 0$) have been given respectively, by Lindstrom et al. (1967) and Lapidus and Amundson (1952), as

$$C_r(x,t) = \begin{cases} C_o A(x,t) & 0 < t \leq t_o \\ C_o A(x,t) - C_o A(x,t-t_o) & t > t_o \end{cases} \qquad (3.18a)$$

where

$$A(x,t) = \frac{1}{2}\,\mathrm{erfc}\left[\frac{x - vt}{2(Dt)^{1/2}}\right]$$

$$+ \left[\frac{v^2 t}{\pi D}\right]^{1/2} \exp\frac{-(x - vt)^2}{2(Dt)^{1/2}} \qquad (3.18b)$$

$$- \left[\frac{1}{2} + \frac{vx}{2D} + \frac{v^2 t}{2D}\right] \exp(vx/D)\ \mathrm{erfc}\left[\frac{x + vt}{2(Dt)^{1/2}}\right]$$

and

$$C_f(x,t) = \begin{cases} C_o B(x,t) & 0 < t \leq t_o \\ C_o B(x,t) - C_o B(x,t-t_o) & t > t_o \end{cases} \qquad (3.19a)$$

where

$$B(x,t) = \frac{1}{2}\,\mathrm{erfc}\left[\frac{x - vt}{2(Dt)^{1/2}}\right]$$

(3.19b)

$$+ \frac{1}{2} \exp(vx/D)\ \mathrm{erfc}\left[\frac{x + vt}{2(Dt)^{1/2}}\right] .$$

Another approach to completing the lower boundary condition which has been advocated is to assume that concentration is continuous across the lower boundary. Accordingly, $C_f(L,t) = C_r(L,t)$ or equivalently

$$\left.\frac{\partial C_r}{\partial x}\right|_{x=L} = 0. \qquad (3.20)$$

The solution for C_r subject to this exit boundary condition with other conditions as previously stipulated is (Brenner, 1962)

$$C_r(x,t) = C_o \left[1 - \sum_{m=1}^{\infty} E_m\right] \tag{3.21a}$$

where

$$E_m = 2P\beta_m \left[\beta_m \cos f_m + \frac{P}{2} \sin f_m\right]$$

$$\cdot \exp\left[\frac{vx}{2D} - \frac{v^2 t}{4DR} - \frac{\beta_m D t}{L^2 R}\right] \tag{3.21b}$$

$$\cdot \left\{\left[\beta_m^2 + (P/2)^2 + P\right]\left[\beta_m^2 + (P/2)^2\right]\right\}^{-1}$$

$$P = vL/D \tag{3.21c}$$

$$f_m = \beta_m X/L \tag{3.21d}$$

and where the eigenvalues β_m are the positive roots of

$$\beta_m \cot \beta_m - \beta^2{}_m/P + P/4 = 0. \tag{3.21e}$$

Owing to the lower boundary condition assumption that $C_r(L,t) = C_f(L,t)$, (3.21) also yields the effluent concentration.

METHODS AND MATERIALS

Since one objective of this study was to test the validity of solutions for resident and flux concentrations, it was desired to employ a porous medium which should exhibit marked divergence between distributions of C_f and C_r. To obtain such a medium, a mixture of medium quartz sand with 0.11, 0.17, and 0.13 mass fractions of added tile grout, bentonite clay, and water, respectively, was compacted in a column with a 1.7-mm diameter wire passing axially through its center. The 52-mm diam by 190 mm long column was constructed of PVC pipe divided into 19-mm lengths glued together with silicone cement to facilitate later sectioning.

After the packed material was cured, the column was placed vertically and ponded continuously with 0.01M $CaCl_2$ for several days. The hydraulic conductivity of the fine matrix (with the wire still occupying the axial pore) was 2.4×10^{-5} m s^{-1}. Following this wetting procedure the wire was removed from the column and at the moment the ponded solution level reached the

column surface, 0.01 M $MgBr_2$ was added. The axial pore remained stable during the experiment owing to cementation afforded by the cured grouting. A total of 0.65 pore volumes of Br solution was added gradually to maintain a 10- to 20-mm pressure head. This was followed by a chaser of 0.01M $MgCl_2$ added in the same manner until a total of 1.8 pore volumes of Br and Cl solutions had been added. Effluent solution was collected in 4- to 8-mL aliquots as it dripped from the column exit into collection tubes via a funnel. The volumetric water content θ of the column was determined gravimetrically to be 0.371 $m^3\ m^{-3}$ and the hydraulic flux density during the tracer experiment was 4.65 x 10^{-4} m s^{-1} giving a mean pore water velocity of 1.25 x 10^{-3} m s^{-1} (assuming an effective water content equal to θ). The Br^- concentrations in the effluent were determined using a Br^- selective electrode.

A second experiment was performed on a replicate column in the same manner but after the Br slug had been absorbed, the column was turned horizontally to minimize axial redistribution of solute and quickly sectioned into 19 mm segments. The material from the sections was leached by a vacuum filtration procedure with $CaCl_2$ solution. Bromide concentrations in the extracts were analyzed with a Br^- selective electrode and converted back to pore fluid concentrations from the known dilution ratios.

RESULTS AND DISCUSSION

The experimental Br breakthrough curve is presented in Figure 3.1 as reduced effluent concentrations $C_e(t) = C_{ext}(L,t)/C_o$ vs. eluted pore volumes or reduced time $T = vt/L$. The best-fit of (3.19) to the effluent data was determined by a least-squares fitting procedure (Parker and van Genuchten, 1984) assuming $C_{ext}(L,t) = C_f(L,t)$ and using the measured mean pore water velocity v and pulse duration t_o. The dispersion coefficient (D) obtained for the best-fit curve (Fig. 3.1) is 0.10 $m^2\ s^{-1}$ which indicates an apparent dispersivity (D/v) of 81 m and a column Peclet number (vL/D) of 0.0023.

Also shown in Fig. 1.1 is the best-fit to Brenner's solution (eq. 3.21) which is attained by the limiting case of $D \rightarrow \infty$ described by

$$C_f(L,t)/C_o = \begin{cases} 1 - \exp(-T) & (T \leq T_o) \\ \exp(T_o - T) - \exp(-T) & (T > T_o) \end{cases} \qquad (3.22)$$

where $T = vt/L$ and $T_o = vt_o/L$. From the inadequacy of (3.21) in describing the effluent data, it may be concluded that the assumption of continuity in macroscopic concentrations across the lower boundary is inappropriate. Conversely, the assumptions implied by (3.19) that a macroscopic concentration discontinuity occurs at the exit and that the upstream concentration distribution is unaffected by the outflow boundary yield a quite accurate description of the breakthrough curve. To preclude the possibility that this fit is merely fortuitous, we should ensure that the resident concentration distribution is consistent with the effluent (flux) concentration data.

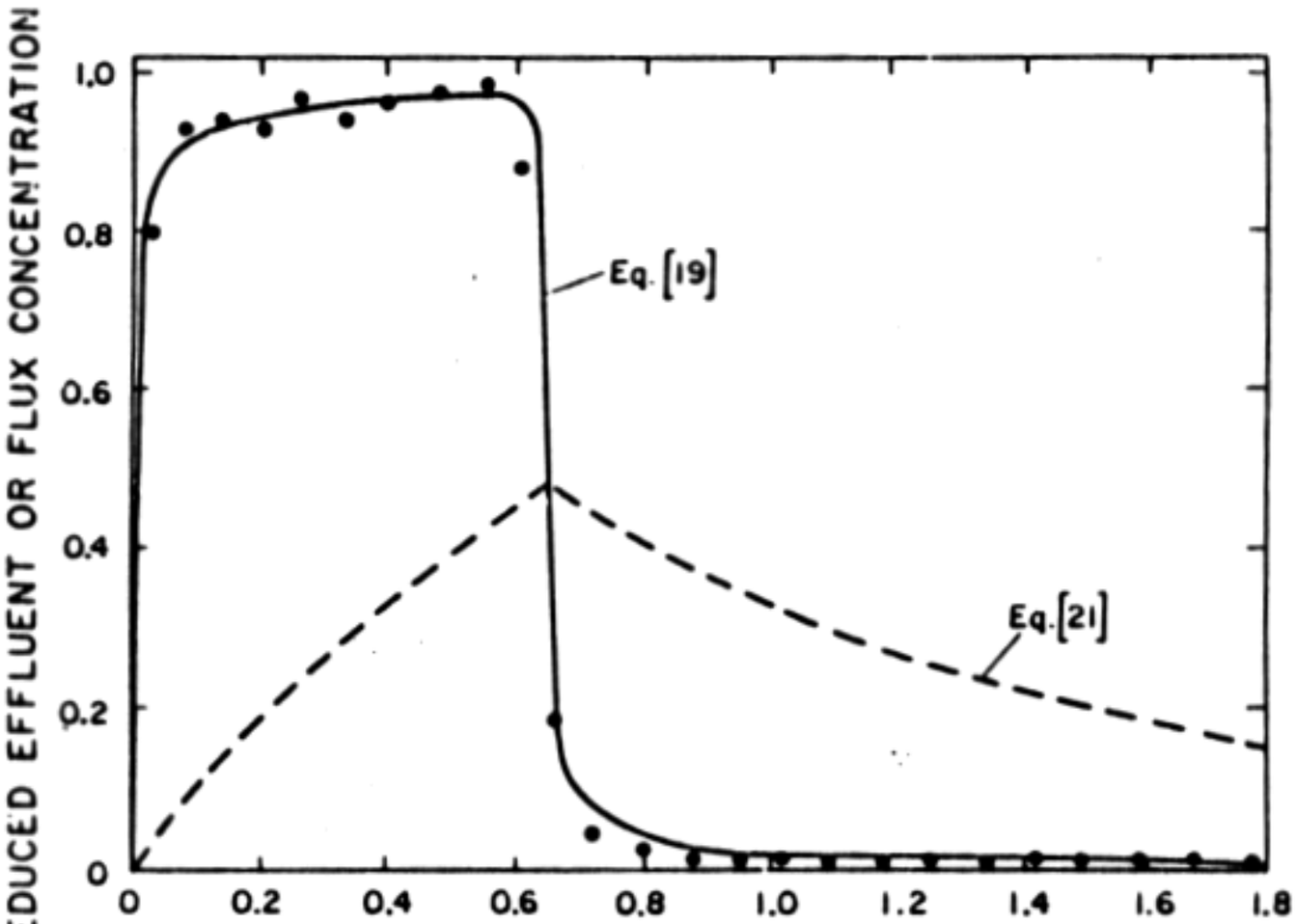

Figure 3.1. Breakthrough curve for a pulse addition of 0.65 pore volumes of Br tracer plotted as reduced effluent concentration versus reduced time or eluted pore volumes. Data points are observed values: smooth curve is best-fit to (3.19) for C_f with $D = 0.10\ m^2\ s^{-1}$ using measured values of v and t_o; dashed line is solution of Brenner (1962) for $D \rightarrow \infty$.

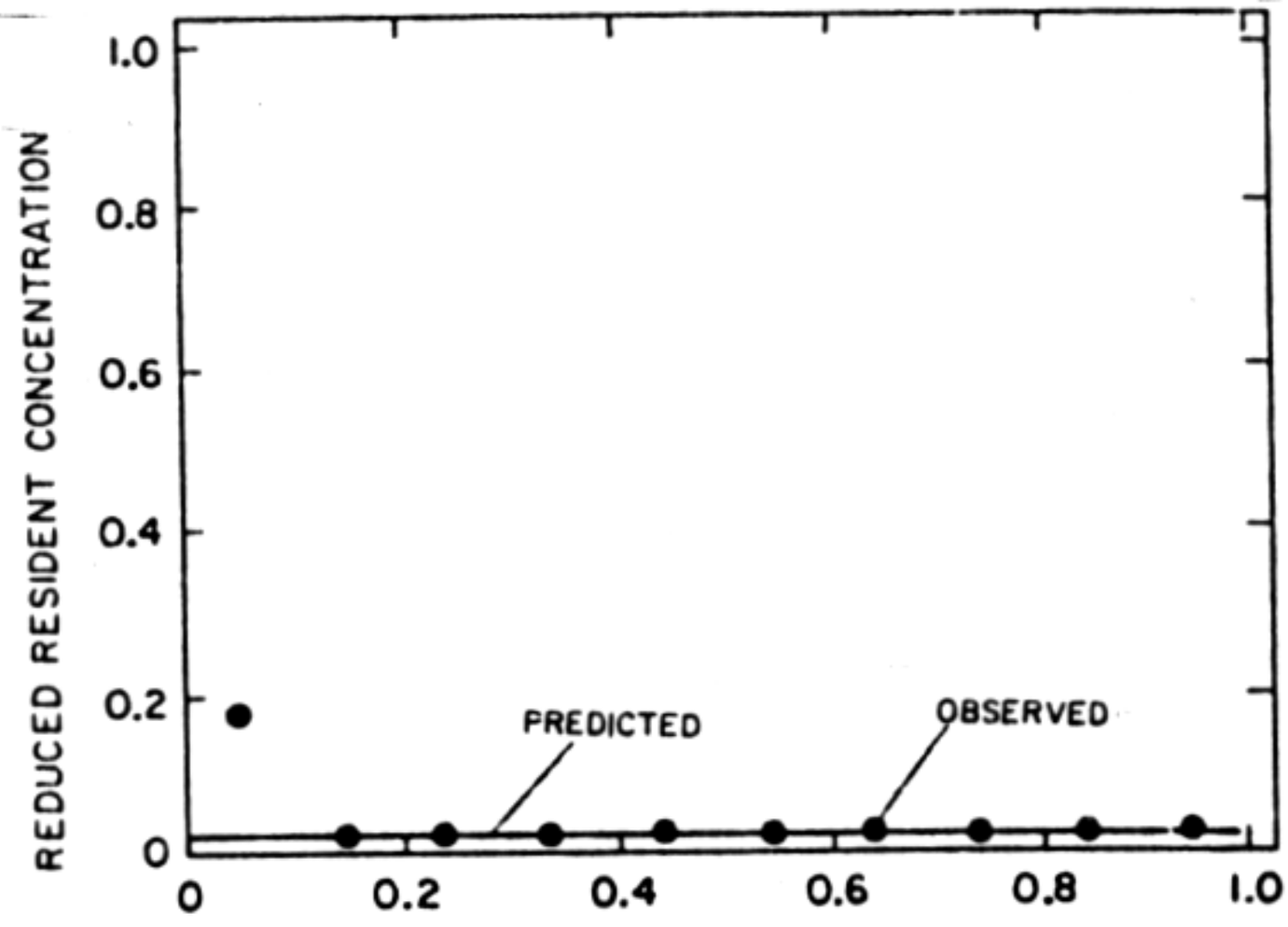

Figure 3.2. Reduced resident concentrations of Br^- vs. relative position in column after injection of 0.65 pore volumes of tracer. Data points represent measured mean concentrations in 19-mm sections; smooth curve is predicted distribution by (3.18) using dispersion coefficient fitted to effluent data.

The resident concentration distribution in the sectioned column after injection of 0.65 pore volumes of Br tracer is shown in Figure 3.2. Measured values represent mean concentrations in each 19-mm section plotted against their midplane coordinates and expressed as reduced values $C_r = C_r/C_o$. Comparison of Figures 3.1 and 3.2 indicates that a large difference between resident and flux concentrations occurred in the vicinity of the column exit just prior to sectioning. While the mean value of C_r in the lower column section was only 0.025, the corresponding value of C_e was 0.98. Such a discontinuity in concentration at the column exit is predicted by the solutions for resident and flux concentrations given by (3.18) and (3.19) which impose a zero gradient condition at infinity. The observation of a large concentration difference at the column exit clearly contradicts the assumption of a zero concentration gradient at the outflow invoked by (3.21) and explains the inability of this solution to describe the breakthrough curve and the resident concentration distribution.

Using the value of D fitted to the effluent data for (3.19), the resident concentration profile $C_r(x,t_f)$ was calculated from (3.18) for time t_f corresponding to the moment the Br slug was completely absorbed and the column was sectioned. Calculated concentrations correspond very closely to the measured values (Fig. 3.2) except in the upper-most section where the measured value is higher than predicted. This discrepancy should be anticipated since the analytical solution implies an infinitesimal REV thus forcing a discontinuity in medium dispersivity and concentration at the macroscopic boundary.

In reality, the REV is finite and a boundary region of thickness $\ell/2$ will exist within which areally-averaged concentrations vary continuously but nonlinearly, thus invalidating the continuum approach. From the symmetry of the pore geometry, the characteristic length ℓ of the REV for the column under study may be estimated as om the order of the column radius of 26 mm. As anticipated, the discrepancy between observed and predicted concentrations appears to be confined to a region within about $\ell/2 \simeq 13$ mm of the column end. A significant discrepancy between measured and predicted concentrations did not occur at the exit boundary probably because the experimental arrangement allowed effluent to drip freely from the outflow minimizing back-mixing.

Errors in resident concentrations in the boundary region may be expected to affect the flux concentration distribution throughout the column. This fact is readily apparent from the more general integral definition of C_f which imposes no assumption regarding the REV size (Chapter 2);

$$C_f(x,t) = C_{ext}(0,t) - \frac{1}{v}\int_o^x \frac{\partial C_r(\chi,t)}{\partial t}\, d\chi. \qquad (3.23)$$

Equation (3.23) simply stipulates that the flux on any plane satisfies a mass balance over the column segment. Any error in C_r in the boundary region ($0 \leq x \leq \ell/2$) will affect C_f estimates at all downstream locations. The magnitude of the error will diminish as the discrepancy between C_r and C_f narrows (small D/v) and as the distance x from the boundary increases (becoming

negligible when $x \gg \ell/2$).

Due to the artifice of assuming an infinitesimal REV, concentrations in the porous medium near the inlet boundary will be underpredicted by the analytical solution during an injection phase ($\partial C_r/\partial x < 0$, $x = 0^+$) while during a flushing period ($\partial C_r/\partial x > 0$, $x = 0^+$) overprediction will occur. As a result more solute than predicted will be retained in the porous medium within the boundary region. Since concentration changes in the boundary region should occur during a relatively brief interval following a change in influent concentration, effluent concentrations should change less rapidly than predicted following a step change in inlet concentration. This error in C_f will be damped with increasing distance from the source. For the column length used in this study, such errors appear to have diminished to the point of being on the order of the experimental error in observed concentrations.

SUMMARY AND CONCLUSIONS

When analyzing the results of column tracer studies, it is important to realize that the proper formulation of macroscopic boundary conditions leads to a discrepancy between effluent concentrations and resident concentrations within the porous medium near the column exit. Physically such a discontinuity may be rationalized by regarding the effluent concentration to be a flux-weighted mean concentration relative to the resident concentration C_r at the exit. It is analytically convenient to define the flux concentration C_f as such a flux-weighted mean at the microscopic level which leads to a macroscopic definition of C_f as the ratio of the macroscopic solute mass flux density to the fluid volumetric flux density. The utility of this definition arises because C_f obeys a macroscopic convection-dispersion equation identical in form to that for C_r which may be solved explicitly upon appropriate transformation of boundary conditions. Transport through a finite column is shown to be accurately analyzed by considering the flow region to represent a section of an effectively semi-infinite column on the assumption that back-mixing at the column outlet is minimal. Solutions which assume equality of resident and flux concentrations at the outlet fail to describe the experimental effluent data and resident concentration distributions.

Theory indicates that large differences in resident and flux concentrations should occur in fractured or aggregated porous media having continuous relatively large pores. The experimental results confirm this expectation and indicate that the analytical solution of Lapidus and Amundson (1952) is appropriately used to analyze resident concentration distributions in the bulk porous medium exclusive of boundary regions within $\ell/2$ of the column ends.

If the flow region is large compared to the REV, it should be feasible to treat fractured and aggregated porous media as simple continua. Many of the difficulties which researchers have perceived in the treatment of such media as simple continua may be traced to the misapplication and misinterpretation of macroscopic boundary conditions and to a failure to distinguish between resident and flux concentration modes.

CHAPTER 4

MOMENT ANALYSIS FOR AGGREGATED MEDIA

Nonequilibrium between mobile and immobile pore regions in fractured or aggregated porous media can have marked effects on chemical transport. Approaches to modeling transport in such media generally fall into one of three types: (1) bicontinuum approach with interchange between mobile and immobile zones of specified geometry governed by Fick's law; (2) bicontinuum approach with interchange described by an empirical first-order kinetic expression; and (3) equivalent monocontinuum approach which assumes residence times are sufficiently large to achieve negligible concentration differences between mobile and immobile pore regions. In this Chapter we will refer to the later condition as 'local equilibrium'.

Diffusionally controlled bicontinuum transport models have been developed by a number of researchers for various assumed pore geometries and reaction mechanisms. Analytic solutions for homogeneous media during steady flow have been given for single and multiple parallel fracture systems (Tang et al., 1981, Grisak and Pickens, 1981; Sudicky and Frind, 1982) for cylindrical macropores (van Genuchten et al., 1984) and for systems of spherical aggregates (Rasmuson and Neretnieks, 1980). Van Genuchten (1985) has presented a unified approach to the analysis of systems of varying pore geometry and has shown that to fair approximation, systems with varying geometry can be described with a generic diffusional model by including in the diffusion equation a shape factor which depends on the specific pore geometry.

Analytic solutions for first-order kinetic inter-region transfer have been available in the literature longer than those for diffusional kinetics (e.g., Deans, 1963; Coats and Smith, 1964; van Genuchten and Wierenga, 1976) and have been rather widely used to analyze transport in structured soils. First-order kinetic models avoid the difficulty of specifying the exact system geometry but at a price of losing *a priori* physical significance of the rate coefficient. In practice the coefficient has generally been obtained by curve-fitting to data from tracer experiments (van Genuchten and Wierenga, 1976; Parker and van Genuchten, 1984). Rao et al. (1980) compared diffusional and first-order kinetic models for spherical aggregate systems under no flow conditions and found first-order rate coefficients to be time dependent--reaching asymptotic values at times which depend on the aggregate size and diffusion coefficient. Expressions for apparent first-order rate coefficients in terms of parameters in diffusional kinetic models have been obtained for various pore geometries by Raats (1981,1984) and van Genuchten (1985).

Under certain circumstances a monocontinuum approach which assumes local equilibrium between mobile and immobile regions may satisfactorily describe transport in structured soils. Such circumstances should arise when observations are made sufficiently far downstream from the injection point that mean residence times are great enough to mitigate diffusional gradients between mobile and immobile zones. In the monocontinuum approach, the

effect of diffusive mass transfer into and out of stagnant pore zones is modeled by utilizing a modified dispersion coefficient in the classical convection-dispersion model. Passioura (1971) presented an analysis of the effective monocontinuum dispersion coefficient for nonreactive solute transport in a system of spherical aggregates. A similar analysis was discussed by Bolt (1982) who considered effects of different pore geometries. Baker (1977) and De Smedt and Wierenga (1984) considered the degeneration of a first-order kinetic bicontinuum model for nonreactive solutes to an equivalent monocontinuum model to obtain an apparent dispersion coefficient defined in terms of the first-order kinetic model parameters. Raats (1981,1984) has shown that both the local equilibrium and first-order kinetic models represent degenerate cases of diffusional kinetics which will be valid under limiting conditions. Criteria for the degeneration of diffusional kinetics to the local equilibrium case have been investigated by various authors who have suggested a number of different indices of equilibrium (Passioura, 1971; James and Rubin, 1979; Rao and Jessup, 1983). Generally, these criteria have been either empirically determined or derived by utilizing analogies with nonflowing systems. Recently, Valocchi (1985) utilized a method of moments to evaluate criteria for the use of equilibrium models.

The purpose of this Chapter is to present a unified treatment of the relationship between parameters in diffusional kinetic, first-order kinetic, and equilibrium transport models and to evaluate criteria for the equivalency between these models. A moment analysis will be utilized and results tested by evaluation of model predictions for previously published as well as some newly derived analytic solutions for nonequilibrium and equilibrium transport.

SPHERICAL DIFFUSION MODEL

The equation describing one-dimensional transport during steady flow in a system comprised of mobile and immobile pore regions is taken following van Genuchten et al. (1984)

$$\theta_m R_m \frac{\partial c_m}{\partial t} + \theta_{im} R_{im} \frac{\partial c_{im}}{\partial t} = \theta_m D_m \frac{\partial^2 c_m}{\partial x^2} - q \frac{\partial c_m}{\partial x} \qquad (4.1)$$

where x and t are distance and time, c_m and c_{im} respectively represent mean resident solution concentrations in mobile and immobile regions, θ_m and θ_{im} represent mobile and immobile region water content such that the total water content $\theta = \theta_m + \theta_{im}$, D_m is a mobile zone dispersion coefficient, q the hydraulic flux density, and R_m and R_{im} are retardation factors for the mobile and immobile zones defined by

$$R_m = 1 + \rho_m k_m / \theta_m \qquad (4.1a)$$

$$R_{im} = 1 + \rho_{im} k_{im} / \theta_{im} \qquad (4.1b)$$

where ρ_m and ρ_{im} are partial densities of mobile and immobile zones such that the total bulk density $\rho = \rho_m + \rho_{im}$, and k_m and k_{im} are slopes of linear adsorption isotherms for the two regions given as mass adsorbed per mass solid phase versus solution concentration. It is assumed in (4.1) that adsorption is equilibrium-controlled within each zone. Assuming the immobile zone to be comprised of uniform spherical aggregates, c_{im} is the mean resident concentration in the spheres given by

$$c_{im}(x,t) = \frac{3}{a^3}\int_0^a r^2 c_a(x,r,t)dr \qquad (4.2)$$

where c_a is the local concentration in the aggregate, r is the radial coordinate in the aggregate, and a is the aggregate radius. Diffusion into or out of the aggregates is described by

$$R_{im}\frac{\partial c_a}{\partial t} = \frac{D_a}{r^2}\frac{\partial}{\partial r}\left[r^2\frac{\partial c_a}{\partial r}\right] \qquad (4.3)$$

where D_a is the effective diffusion coefficient in the aggregates. It is convenient to recast the spherical diffusion (SD) model of (4.1) - (4.3) in dimensionless form as

$$\beta R\frac{\partial C_m}{\partial T} + (1-\beta)R\frac{\partial C_{im}}{\partial T} = \frac{1}{P_m}\frac{\partial^2 C_m}{\partial X^2} - \frac{\partial C_m}{\partial X} \qquad (4.4)$$

$$\frac{\partial C_a}{\partial T} = \gamma\frac{1}{\zeta^2}\frac{\partial}{\partial \zeta}\left(\zeta^2\frac{\partial C_a}{\partial \zeta}\right) \qquad (4.5)$$

$$C_{im} = 3\int_0^1 C_a\,\zeta^2 d\zeta \qquad (4.6)$$

where

$$T = \frac{qt}{(\theta_m+\theta_{im})L} = \frac{qt}{\theta L} = \frac{vt}{L} \qquad (4.7)$$

$$X = x/L \qquad (4.8)$$

$$\zeta = r/a \qquad (4.9)$$

$$P_m = qL/\theta_m D_m = vL/\phi D_m \qquad (4.10)$$

$$R = \frac{\theta_m R_m + \theta_{im}R_{im}}{\theta} = \phi R_m + (1-\phi)R_{im} \qquad (4.11)$$

$$\beta = \Phi R_m/R \tag{4.12}$$

$$\gamma = \frac{D_a\theta L}{a^2 q R_{im}} = \frac{D_a L}{a^2 v R_{im}} \tag{4.13}$$

where P_m is the mobile zone Peclet number, R is the net porous medium retardation factor, $\theta = \theta_m + \theta_{im}$ is the bulk medium water content, $v = q/\theta$ is the mean pore water velocity over the entire porous medium, $\Phi = \theta_m/\theta$ is the mobile pore fraction, and L is an arbitrary distance. For column tracer studies L is typically the column length in which case T represents the number of pore volumes leached. Concentrations written in plain upper case letters here and subsequently represent relative concentrations of the form C = c/c_o where c_o is the influent concentration for continuous injection or for a pulse of finite duration and c denotes c_a, c_m, or c_{im}. Dimensionless concentrations of this form will be useful when we consider continuous injection but for inlet pulses of finite or infinitesimal duration, it will be desirable to normalize concentrations to the total mass injected into the system. Thus we define also cumulative mass-normalized dimensionless concentrations of the general form

$$\overline{C} = \frac{c}{m/\theta L} = \frac{c}{M} \tag{4.14}$$

where m is the total mass per unit area introduced into the system and M is the concentration equivalent to mixing the injected mass in one pore volume. For a square pulse input function with influent concentration c_o over time t=0 to t_o corresponding to a reduced time $T_o=vt_o/L$ then $M=c_oT_o$ hence

$$\overline{C} = \frac{c}{c_o T_o} = \frac{C}{T_o} \tag{4.15}$$

We consider first the solution of (4.4) - (4.6) for a semi-infinite system subject to the initial and boundary conditions

$$C_m(X,0) = C_a(X,\zeta,0) = 0 \tag{4.16}$$

$$(C_m - \frac{1}{P_m}\frac{\partial C_m}{\partial X})\ (0,T) = \begin{cases} 1 & 0<T<T_o \\ 0 & T>T_o \end{cases} \tag{4.17}$$

$$\frac{\partial C_m}{\partial X}\ (\infty,T) = 0 \tag{4.18}$$

and to the continuity constraints

$$C_m(X,T) = C_a(X,1,T) \tag{4.19}$$

$$\frac{\partial C_a}{\partial \zeta}(X,0,T) = 0 \tag{4.20}$$

the solution for $\bar{C}_m$ is

$$\bar{C}_m(X,T) = \begin{cases} \frac{1}{T_o} C_m(X,T) & 0 \leq T \leq T_o \\ \\ \frac{1}{T_o}\left[C_m(X,T) - C_m(X,T-T_o)\right] & T > T_o \end{cases} \tag{4.21a}$$

where $C_m(X,\tau)$ is the solution for c_m/c_o for continuous injection given by van Genuchten et al. (1984) and van Genuchten (1985) as

$$C_m(X,\tau) = \frac{1}{2} + \frac{2P_m}{\pi}\int_0^\infty \frac{\exp(P_m X/2 - z_p X)}{[(P_m/2 + z_p)^2 + z_m^2]}$$

$$\cdot[(P_m/2+z_p)\sin(2\gamma\lambda^2\tau - z_m X)$$

$$-z_m\cos(2\gamma\lambda^2\tau - z_m X)]\frac{d\lambda}{\lambda} \tag{4.21b}$$

where

$$z_p = \left[\frac{1}{2}(r_p+\Omega_1)\right]^{1/2} \tag{4.21c}$$

$$z_m = \left[\frac{1}{2}(r_p-\Omega_1)\right]^{1/2} \tag{4.21d}$$

$$r_p = (\Omega_1^2 + \Omega_2^2)^{1/2} \tag{4.21e}$$

$$\Omega_1 = P_m^2/4 + \gamma P_m(1-\beta)R\psi_1 \tag{4.21f}$$

$$\Omega_2 = 2\gamma P_m \beta R\lambda^2 + \gamma P_m(1-\beta)R\psi_2 \tag{4.21g}$$

$$\psi_1 = \frac{3\lambda(\sinh 2\lambda + \sin 2\lambda)}{\cosh 2\lambda - \cos 2\lambda} - 3 \tag{4.21h}$$

$$\psi_2 = \frac{3\lambda(\sinh 2\lambda - \sin 2\lambda)}{\cosh 2\lambda - \cos 2\lambda} \tag{4.21i}$$

A solution for the flux concentration which represents the ratio of solute flux density to hydraulic flux density may be obtained by use of the relation

$$C_f = C_m - \frac{1}{P_m} \frac{\partial C_m}{\partial X} \qquad (4.22)$$

where $C_f = c_f/c_o$ is the reduced flux concentration. For finite systems of length L, we may interpret the flux concentration as the effluent concentration at X=1 as shown in Chapter 2.

The solution for C_f can be obtained by applying (4.22) to (4.21) or by transforming the original system of equations [4]-[6] and [16]-[20] and solving directly. The solution for mass normalized flux concentration is

$$\bar{C}_f(X,T) = \begin{cases} \frac{1}{T_o} C_f(X,T) & 0 < T \leq T_o \\ \\ \frac{1}{T_o} [C_f(X,T) - C_f(X,T-T_o)] & T > T_o \end{cases} \qquad (4.23a)$$

where $C_f(X,\tau)$ is the solution for c_f/c_o for continuous injection obtained by Rasmuson and Neretnieks (1980) and given also van Genuchten (1985) as

$$C_f(X,\tau) = \frac{1}{2} + \frac{2}{\pi} \int_0^\infty \exp(P_m X/2 - z_p X) \sin(2\gamma\lambda^2\tau - z_m X) \frac{d\lambda}{\lambda} \qquad (4.23b)$$

where z_p and z_m are given as in (4.21).

We are interested also in evaluating the solution for c_{im}. First, we define a total concentration c_t to be the mass of chemical in both adsorbed and solution phases of mobile and immobile regions expressed per net solution volume at a given point in time and space. Hence

$$C_t = (1-\beta)RC_{im} + \beta RC_m \qquad (4.24)$$

where $C_t = c_t/c_o$. Owing to the definition of flux concentration, we may write the continuity condition for the bulk porous medium as

$$\frac{\partial C_t}{\partial T} = - \frac{\partial C_f}{\partial X} \qquad (4.25)$$

Employing (4.23) for C_f and integrating (4.25) with respect to time gives:

$$\bar{C}_t(X,T) = \begin{cases} \frac{1}{T_o} C_t(X,T) & 0 < T \leq T_o \\ \frac{1}{T_o} [C_t(X,T) - C_t(X,T-T_o)] & T > T_o \end{cases} \qquad (4.26a)$$

$$C_t(X,\tau) = \frac{1}{\pi\gamma} \int_0^\infty \exp(\frac{P_m X}{2} - z_p X) \left\{ z_m [\sin(2\gamma\lambda^2\tau - z_m X) + \sin(z_m X)] \right.$$

$$\left. + (\frac{P_m}{2} - z_p)[\cos(2\gamma\lambda^2\tau - z_m X) - \cos(z_m X)] \right\} \frac{d\lambda}{\lambda^3} \qquad (4.26b)$$

The solution for C_{im} can be obtained from (4.24) using (4.21) and (4.26) for C_m and C_t, respectively. We may also evaluate mean resident concentrations c_r in the bulk porous medium defined by

$$C_r = \Phi C_m + (1-\Phi) C_{im} \qquad (4.27)$$

where again $C_r = c_r/c_o$. From (4.24) and (4.27) we obtain

$$C_r = \frac{(\Phi-\beta)}{(1-\beta)} C_m + \frac{(1-\Phi)}{(1-\beta)R} C_t \qquad (4.28)$$

which yields C_r via (4.21) and (4.26). Note that the solution for c_r requires stipulation of Φ as well as P_m, γ, β, and R while solutions for c_m, c_{im}, c_t and c_f do not require explicit specification of Φ.

Because pulse duration will be found to affect the degeneration of the spherical diffusion model to simpler forms, we wish to consider also the limiting case of instantaneous injection of a quantity of chemical $M=c_o T_o$ as $T_o \to 0$. The inlet boundary condition thus becomes

$$(\bar{C}_m - \frac{1}{P_m} \frac{\partial \bar{C}_m}{\partial X})(0,T) = \delta(T) \qquad (4.29)$$

where $\delta(T)$ is the dirac delta function. Solutions may be obtained from those given for finite pulse durations by noting that

$$\lim_{T_o \to 0} \frac{c(T) - c(T-T_o)}{c_o T_o} = \frac{\partial (c/c_o)}{\partial T} \qquad (4.30)$$

For flux concentrations the solution for mass normalized concentration for dirac injection is accordingly $\bar{C}_f^{\delta} = \partial C_f / \partial T$ which yields

$$\bar{C}_f^{\delta}(X,T) = \frac{4\gamma}{\pi}\int_0^{\infty}\exp(P_m X/2 - z_p X)\cos(2\gamma\lambda^2 T - z_m X)\lambda d\lambda \qquad (4.31)$$

Evaluation of equations (4.21), (4.23), (4.26) and (4.31) was carried out with an algorithm discussed by Rasmusen and Neretnieks (1980) and van Genuchten et al. (1984). Gaussian integration is performed over half-periods of the decaying sine-cosine functions with convergence of the alternating series accelerated by repeated averaging of partial sums.

LOCAL EQUILIBRIUM MODEL

The usual approach to modeling transport during steady flow under the assumption of local equilibrium (LE) within the entire porous medium employs the monocontinuum convection-dispersion equation

$$\theta R\frac{\partial c_r}{\partial t} = \theta D_e\frac{\partial^2 c_r}{\partial x^2} - q\frac{\partial c_r}{\partial x} \qquad (4.32)$$

where D_e is an effective dispersion coefficient for the monocontinuum model and other terms are identical to those previously defined. The equivalence of R employed here and in the SD model may be noted by observing that the slope k of the effective system isotherm will be given by

$$k = \frac{\rho_m k_m + \rho_{im} k_{im}}{\rho} \qquad (4.33)$$

Comparison of $R=1+\rho k/\theta$ for the monocontinuum model with [11] indicates the terms are identical. Subsequently we will show that D_e reflects combined effects of diffusive mixing arising from transfer between mobile and immobile zones in addition to mixing due to hydrodynamic dispersion in mobile pore zones so that $D_e > D_m$.

In dimensionless variables the LE model becomes

$$R\frac{\partial C_r}{\partial T} = \frac{1}{P_e}\frac{\partial^2 C_r}{\partial X^2} - \frac{\partial C_r}{\partial X} \qquad (4.34)$$

where all variables are precisely the same as for the SD model except $P_e=vL/D_e$. The initial and boundary conditions analogous to those of (4.16) - (4.18) are

$$C_r(X,0) = 0 \qquad (4.35)$$

$$\left(C_r - \frac{1}{P_e}\frac{\partial C_r}{\partial X}\right)(0,T) = \begin{cases} 1 & 0 < T \leq T_o \\ 0 & T > T_o \end{cases} \tag{4.36}$$

$$\frac{\partial C_r}{\partial X}(\infty,T) = 0 \tag{4.37}$$

The resulting solutions for C_r and C_r are (Lindstrom et al., 1967)

$$\bar{C}_r(X,T) = \begin{cases} \frac{1}{T_o} C_r(X,T) & 0 < T \leq T_o \\ \frac{1}{T_o}\left[C_r(X,T) - C_r(X,T-T_o)\right] & T > T_o \end{cases} \tag{4.38a}$$

$$C_r(X,\tau) = \frac{1}{2}\,\mathrm{erfc}(f_m) + \left(\frac{\tau P_e}{\pi R}\right)^{1/2} \exp(-f_m^2)$$

$$- \frac{1}{2}\left(1+P_eX+\frac{\tau P_e}{R}\right)\exp(P_eX)\,\mathrm{erfc}(f_p) \tag{4.38b}$$

where

$$f_m = \frac{RX-\tau}{2(R\tau/P_e)^{1/2}} \tag{4.38c}$$

$$f_p = \frac{RX+\tau}{2(R\tau/P_e)^{1/2}} \tag{4.38d}$$

To evaluate flux concentrations, the analog of (4.22) for the monocontinuum analysis is

$$C_f = C_r - \frac{1}{P_e}\frac{\partial C_r}{\partial X} \tag{4.39}$$

Solutions for C_f and $\bar{C}_f$ subject to the preceding initial and boundary conditions are

$$\bar{C}_f(X,T) = \begin{cases} \frac{1}{T_o} C_f(X,T) & 0 < T \leq T_o \\ \frac{1}{T_o}\left[C_f(X,T) - C_f(X,T-T_o)\right] & T > T_o \end{cases} \tag{4.40a}$$

$$C_f(X,\tau) = \frac{1}{2}\,\mathrm{erfc}(f_m) + \frac{1}{2}\exp(P_eX)\,\mathrm{erfc}(f_p) \tag{4.40b}$$

For the case of a dirac inlet condition, the solution for mass normalized flux concentration is obtained immediately from (4.40) upon applying (4.30) to yield

$$\bar{C}_f^{\delta}(X,T) = \frac{1}{2T\pi^{1/2}} \left[f_p \exp(-f_m^2) + f_m \exp(P_e X - f_p^2) \right] \qquad (4.41)$$

where f_p and f_m are as given in (4.38) with τ=T.

RELATIONSHIP BETWEEN DIFFUSION AND LOCAL EQUILIBRIUM MODELS

In order to evaluate the relationship between SD and LE model parameters and to develop criteria for the validity of the latter, we will utilize a time moment analysis described in detail by Valocchi (1985) who reported moments of C_f^{δ} versus T for the models under consideration. For finite duration inlet pulses, we must add to the n^{th} moment of solution for the dirac inlet case an additional term corresponding to the n^{th} moment of the input function. For SD and LE models the first absolute moments are identical and equal to XR + $T_o/2$. As $T_o \to 0$ this moment represents the mean (reduced) residence time of solute at a distance x from the inlet. After correcting for slight notational differences between reduced parameter definitions here and in Valocchi (1985) and adding appropriate terms for the finite pulse, we obtain second central moments of $C_f(T)$ for the two models given by

$$\mu_2^{LE} = \frac{2XR^2}{P_e} + \frac{T_o^2}{12} \qquad (4.42)$$

$$\mu_2^{SD} = \frac{2XR^2}{P_m} + \frac{2XR(1-\beta)}{15\gamma} + \frac{T_o^2}{12} \qquad (4.43)$$

When the LE model is a valid approximation of the SD model, both should have the same second moment. Forcing this condition by equating (4.42) and (4.43) yields

$$\frac{1}{P_e} = \frac{1}{P_m} + \frac{1}{P_{im}} \qquad (4.44a)$$

$$\frac{1}{P_{im}} = \frac{(1-\beta)}{15R\gamma} \qquad (4.44b)$$

where $1/P_{im}$ represents the component of the dimensionless apparent

dispersion ($1/P_e$) arising from diffusive transfer between mobile and immobile regions. If $P_e=P_m$ (e.g., see Valocchi, 1985) then $1/P_{im}\rightarrow 0$ is a criterion for the validity of the monocontinuum approach. Note that the form of the input function is immaterial to (4.44) since it drops from the analysis. Thus (4.44) may be applied quite generally even to the case of continuous injection for which moments cannot be formally defined. In terms of the primary SD model variables, we obtain an expression for the effective monocontinuum dispersion coefficient:

$$D_e = \Phi D_m + \frac{(1-\Phi)a^2v^2R_{im}^2}{15D_a[\Phi R_m+(1-\Phi)R_{im}]^2} \qquad (4.45)$$

indicating that the radial diffusion contribution to D_e increases as D_a and Φ decrease and as v, a and R_{im}/R increase. It is noteworthy that this model leads to a quadratic relation between D_e and v rather than the usually assumed linear relation. For the special case of nonreactive solute, $R_m = R_{im} = 1$ and (4.45) reduces to

$$D_e = \Phi D_m + \frac{(1-\Phi)a^2v^2}{15D_a} \qquad (4.46)$$

which, aside from notational differences, is identical to the equation for D_e derived by Passioura (1971) and by Raats (1984) via quite different analyses.

We consider first the application of (4.45) to predict C_r and C_f for the SD model and equivalent LE model assuming R=1, $\Phi=\beta=0.1$, X=1, $P_m=30$ and for $\gamma=0.01$ and $\gamma=1$ subject to continuous injection. To facilitate subsequent evaluation of effects of X and R on LE model validity, we plot relative concentrations versus a time variable (T/XR) which is normalized against the first absolute time moment. On this scale the normalized "residence time" will always be unity. For the case $\gamma=0.01$ (Figure 4.1a) a large difference is observed between C_r and C_f predictions for the SD model reflecting significant disequilibrium between mobile and immobile regions. Calculations of C_m indicate that they are nearly equal to C_f reflecting the relatively high P_m (see equation 4.22) while C_{im} values deviate from C_m by as much as 0.6 reduced concentration units. Comparison of SD and LE model predictions using in the latter an effective P given by (4.44) indicates significant discrepancies although the general trends in C_f and C_r predicted by the LE model are still preserved. For the case of $\gamma = 1$ (Figure 4.1b) the discrepancy between C_f and C_r and between SD and LE model predictions becomes much narrower. Differences between C_m and C_{im} for this case are calculated to be no more than 0.06 units indicating approach to "equilibrium" between mobile and immobile zones. Since for $1/P_m\rightarrow 0$ we find $C_m\rightarrow C_f$, and local equilibrium implies $C_m = C_{im} = C_r$, then equality of SD and LE model predictions for large P_m will correspond to the condition that $C_r \approx C_f$ which implies also $1/P_e\rightarrow 0$.

The foregoing arguments indicate that 'exact' correspondence between SD and LE model predictions will occur as $1/P_{im} \rightarrow 0$ and hence as $P_e \rightarrow P_m$ which is the situation investigated by Valocchi (1985). However, in practice exact correspondence may be a moot objective since measurement error and soil variability always overlay appreciable uncertainty on the model. Our purpose here is to determine practical constraints on the LE model when the assumption of local equilibrium is not rigorously met and hence when P_e and P_m become divergent. Before attempting to derive explicit error criteria for SD to LE model degeneration, we consider the effects of the various system variables on LE model validity by parametric analysis.

Effects of the porous medium variables γ, β, R and P_m and observation location X on C_f versus T/XR for continuous injection for parameter values stipulated in Table 4.1 as Cases 1-5, respectively, are illustrated in Figures 4.2-4.6. Ranges in parameter values are chosen to represent a span observable in field and laboratory studies (e.g. Rao and Jessup, 1983). As anticipated from the preceding discussion, increasing γ, β, R and P_m lead to closer correspondence between SD and LE predictions. In Case 5 (Table 4.1, Figure 4.6) effects of observation location on SD to LE model degeneration are investigated showing that LE model validity improves as one moves downstream. This effect reflects the fact that with increasing travel distance, mean residence time increases and eventually becomes large relative to the characteristic time for diffusion into immobile pore regions. To investigate the effects of pulse duration on LE model validity, we reconsider the effect of γ for the parameter values of Case 1 but now for dirac rather than continuous injection (Figure 4.7). Comparison of Figures 4.2 and 4.7 indicates that for any given set of parameter values the deviation between SD and LE model predictions is more severe for the dirac boundary condition. Evaluating effects of variable pulse duration from T_o=0.1 to 1.0 for other parameter values as for Case 3a (Figure 4.8) indicates that the degree of correspondence between SD and LE models increases continuously with increasing T_o for constant mass loading M.

It is apparent that no single reduced variable in the SD model can be employed as an index of equilibrium. We might expect $1/P_{im} \rightarrow 0$ would provide an index of equilibrium at X=1 (or $1/P_{im}X \rightarrow 0$ for $X \neq 1$), however, P_{im} will not reflect effects of P_m or pulse duration. To obtain a more general index of LE model validity we again use time moment analysis and propose as a feasible criteria of equilibrium the deviation between third moments of LE and SD models. We utilize moments of C_f with respect to the normalized time variable T/XR. The relative third moments of $C_f(T/XR)$ are

$$\mu_3^{LE} = \frac{12}{X^2 P_e^2} \tag{4.47}$$

$$\mu_3^{SD} = \frac{12}{(P_m X)^2} + \frac{4(1-\beta)}{5 P_m X^2 \gamma R} + \frac{4(1-\beta)}{105 (X\gamma R)^2} . \tag{4.48}$$

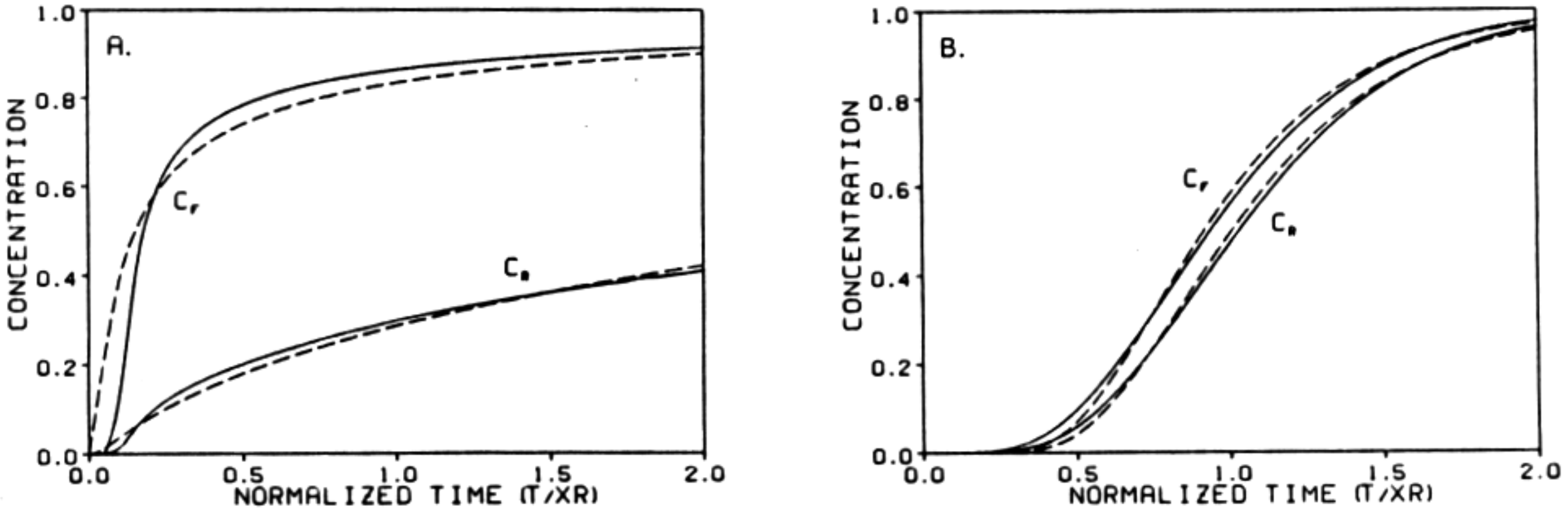

Figure 4.1. Resident and flux concentrations for spherical diffusion model (solid lines) and local equilibrium model (dashed lines) for continuous injection with R = 1, $\phi = \beta = 0.1$, X = 1, $P_m = 30$ and (a) $\gamma = 0.01$ or (b) $\gamma = 1$.

Table 4.1. Parameter values for continuous injection simulations

Case Number	X	γ	β	R	P_m	P_{im}	P_e
1a	1.0	0.03	0.1	1.0	30.0	0.50	0.49
b	1.0	0.30	0.1	1.0	30.0	5.00	4.29
c	1.0	3.00	0.1	1.0	30.0	50.00	18.75
2a	1.0	0.3	0.01	1.0	30.0	4.55	3.95
b	1.0	0.3	0.50	1.0	30.0	8.99	6.92
c	1.0	0.3	0.99	1.0	30.0	451.30	28.13
3a	1.0	0.1	0.1	1.0	30.0	1.66	1.57
b	1.0	0.1	0.1	10.0	30.0	16.66	10.71
c	1.0	0.1	0.1	100.0	30.0	166.66	25.42
4a	1.0	1.0	0.1	1.0	1.0	16.66	0.94
b	1.0	1.0	0.1	1.0	10.0	16.66	6.25
c	1.0	1.0	0.1	1.0	100.0	16.66	14.28
5a	0.01	10.0	0.1	1.0	30.0	166.66	25.42
b	0.10	10.0	0.1	1.0	30.0	166.66	25.42
c	1.00	10.0	0.1	1.0	30.0	166.66	25.42

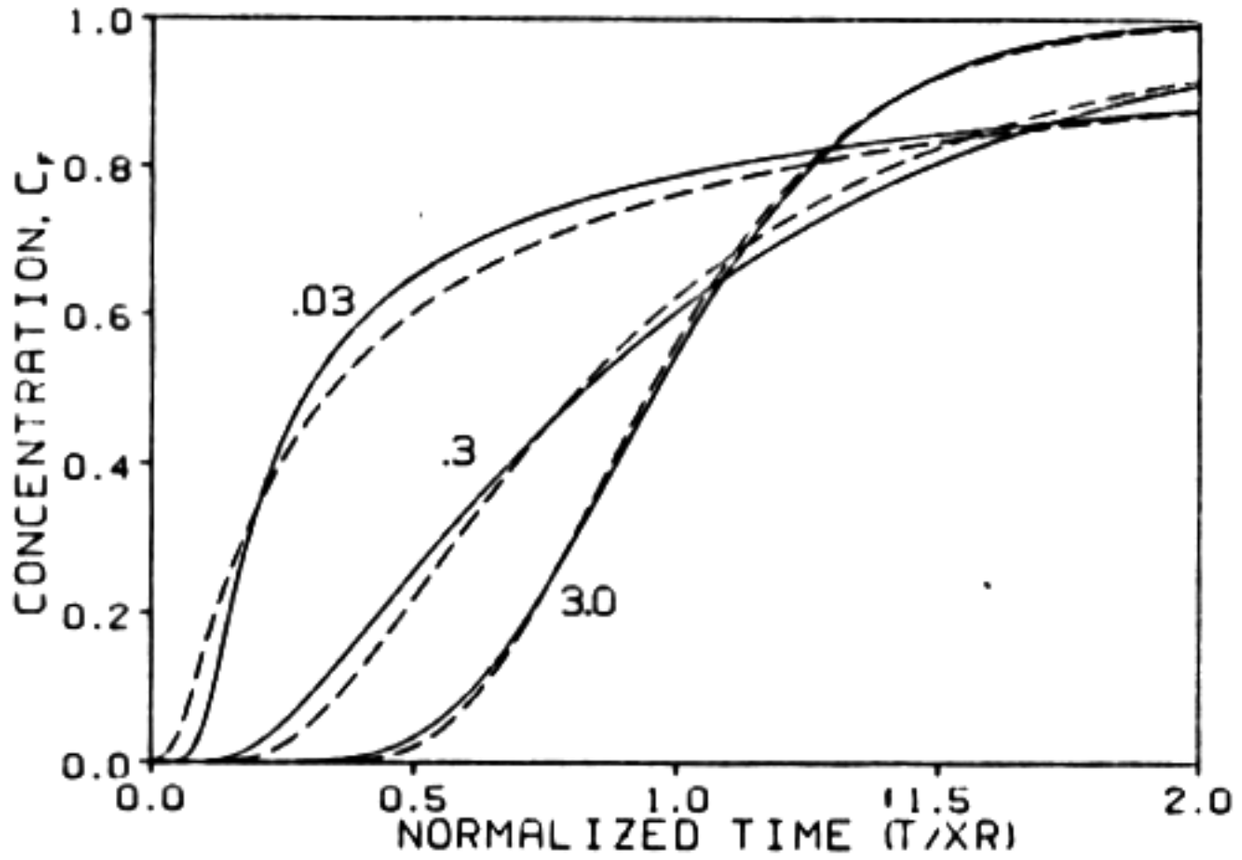

Figure 4.2. Effect of c on flux concentrations for spherical diffusion model (solid lines) and local equilibrium model (dashed lines) for case 1 of Table 1 with continuous injection and b = 0.1, R = 1, P_m = 30, X = 1. Values of c indicated on curves.

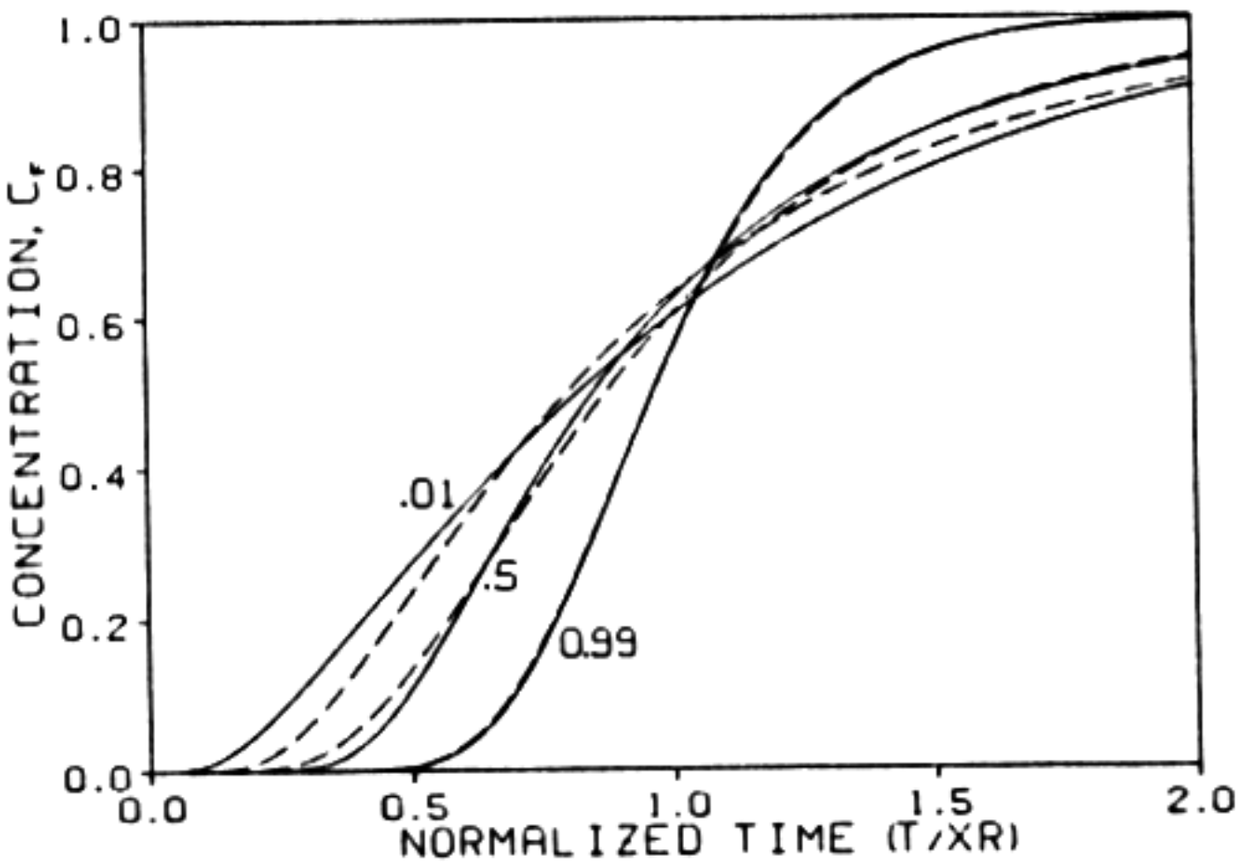

Figure 4.3. Effect of b on flux concentrations for spherical diffusion model (solid lines) and local equilibrium model (dashed lines) for case 2 of Table 1 with continuous injection and c = 0.3, R = 1, P_m = 30, X = 1. Values of b indicated on curves.

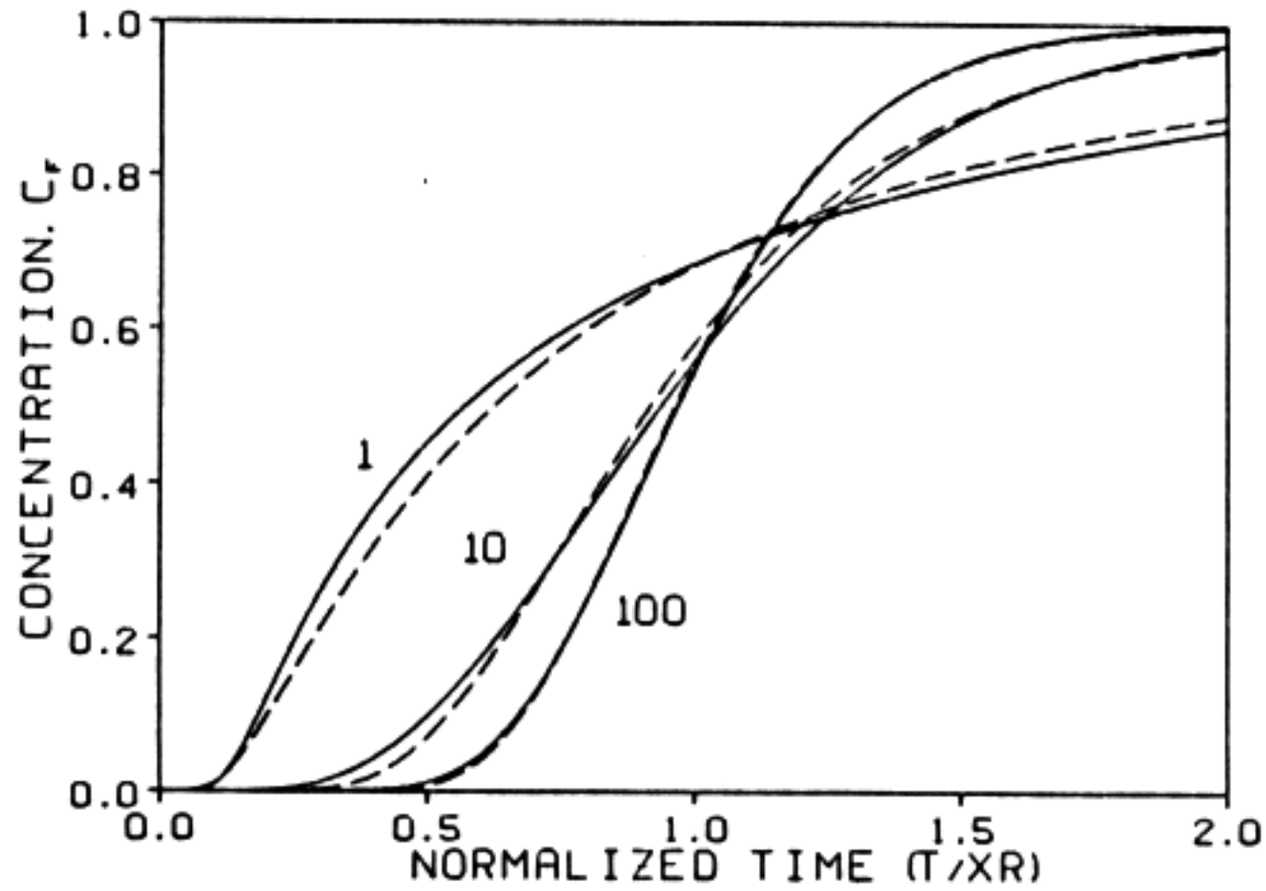

Figure 4.4. Effect of R on on flux concentrations for spherical equilibrium model (solid lines) and local equilibrium model (dashed lines) for case 3 of Table 1 with continuous injection and c = 0.1, B = 0.1, P_m = 30, X = 1. Values of R indicated on curves.

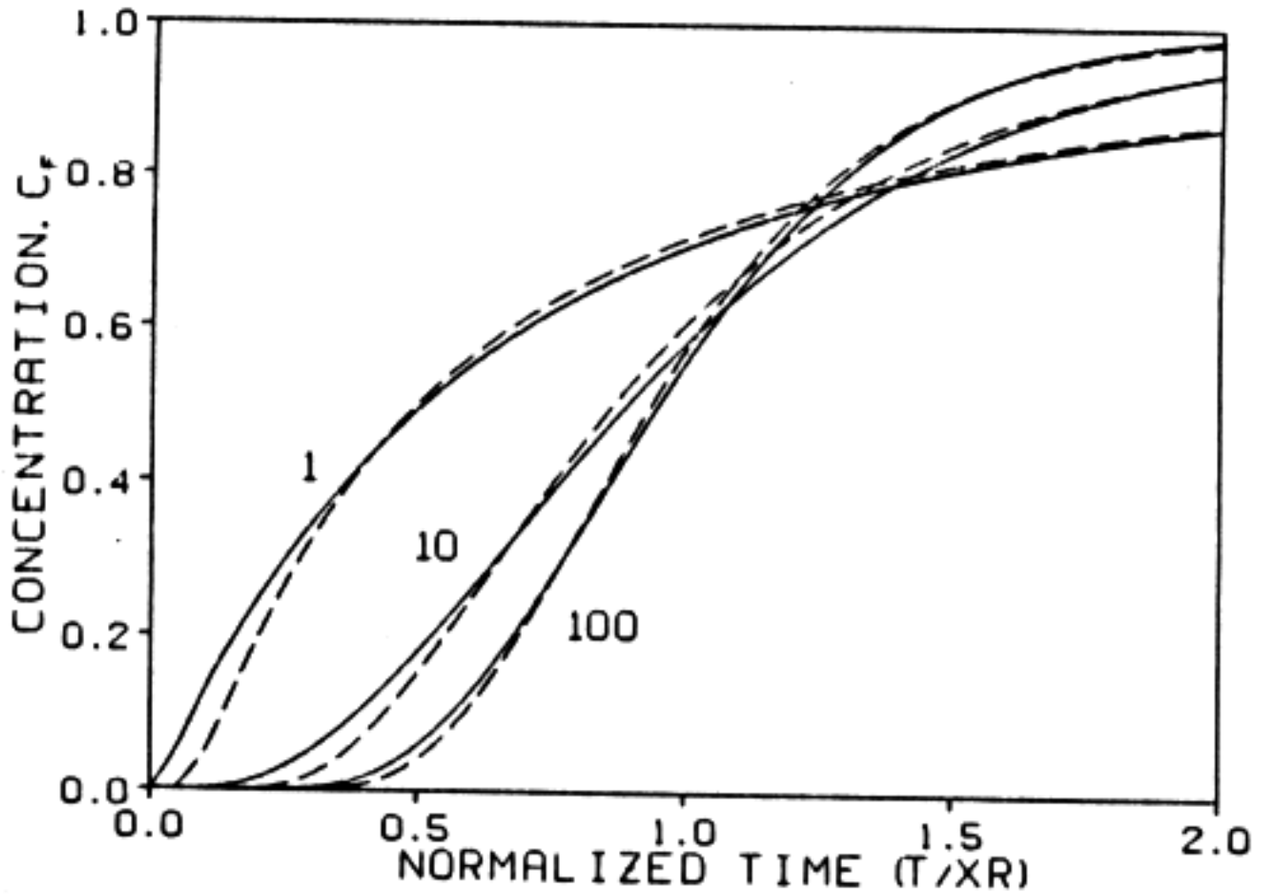

Figure 4.5. Effect of P_m on flux concentrations for spherical diffusion model (solid lines) and local equilibrium model (dashed lines) for case 4 of Table 1 with c = 1, b = 0.1, R = 1, X = 1. Values of P_m indicated on curves.

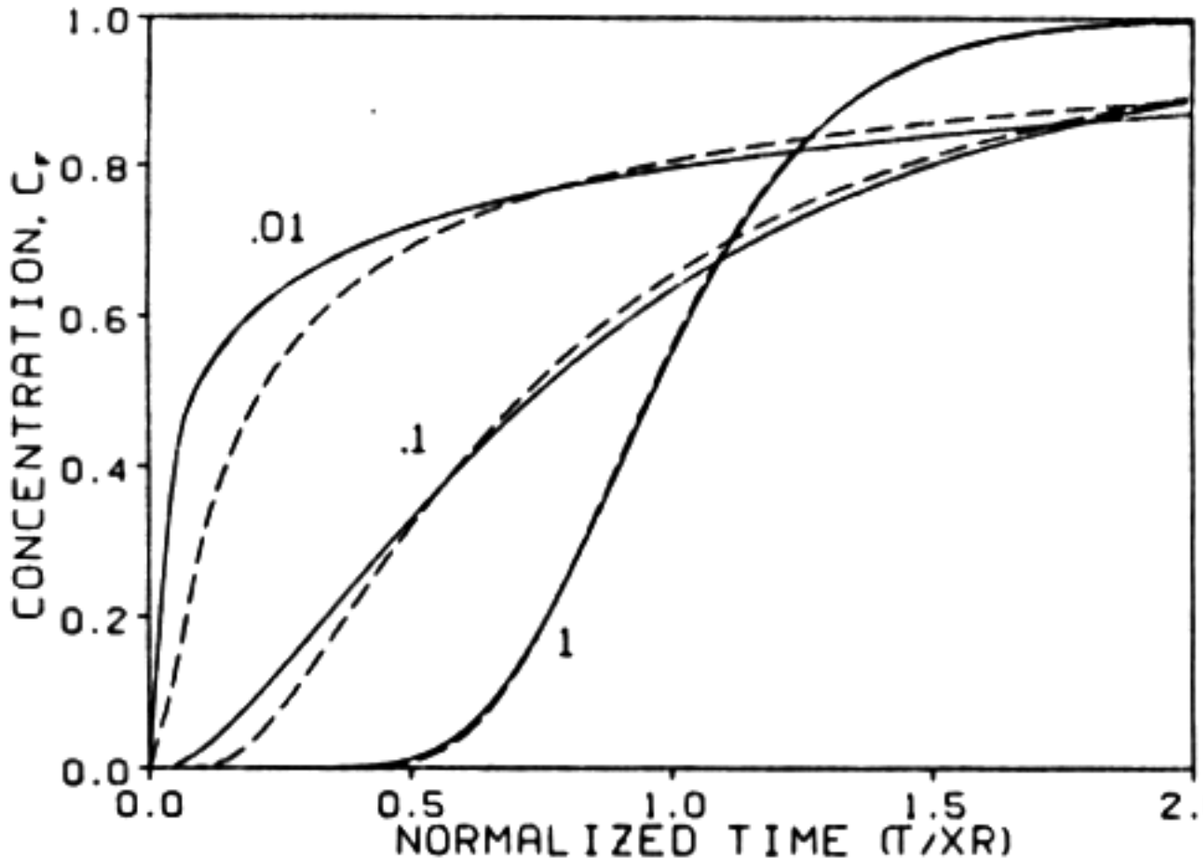

Figure 4.6. Effect of X on flux concentrations for spherical diffusion model (solid lines) and local equilibrium model (dashed lines) for case 5 of Table 1 with c = 10, b = 0.1, R = 1, P_m = 30. Values of X indicated on curves.

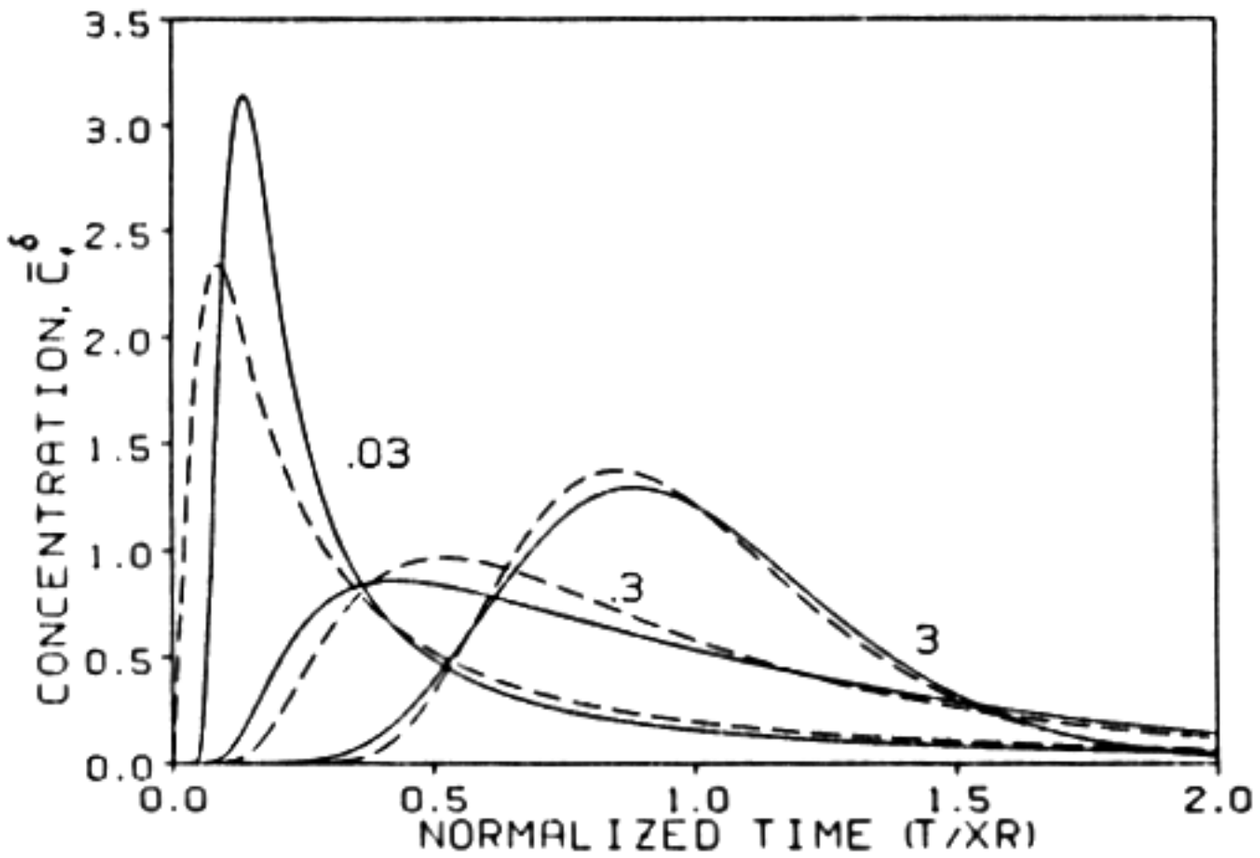

Figure 4.7. Effect of c on flux concentrations for spherical diffusion model (solid lines) and local equilibrium model (dashed lines) for dirac injection and B = 0.1, R = 1, P_m = 30, X = 1. Values of c indicated on curves.

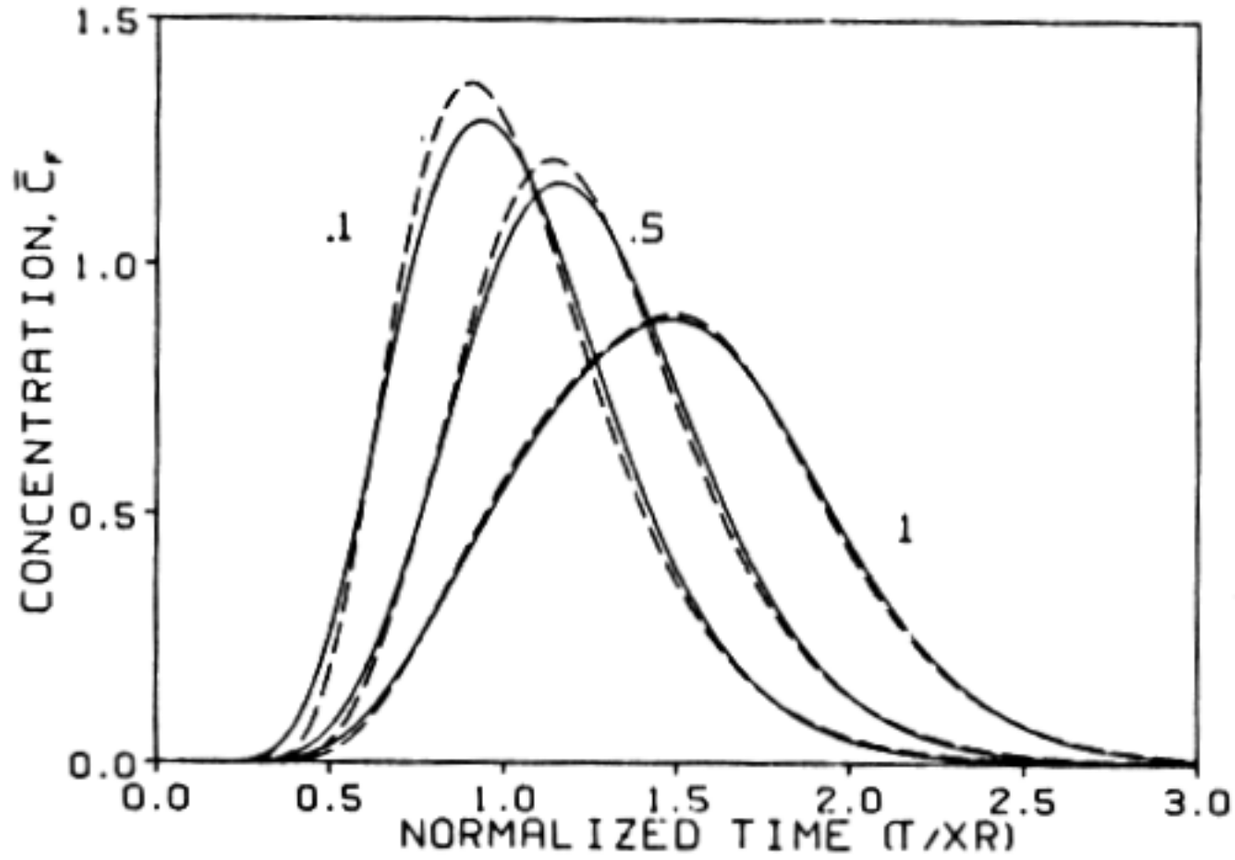

Figure 4.8. Effect of T_o on flux concentrations for spherical diffusion model (solid lines) and local equilibrium model (dashed lines) for pulse injection of fixed mass with c = 0.1, b = 0.1, R = 1, P_m = 30, X = 1. Values of T_o indicated on curves.

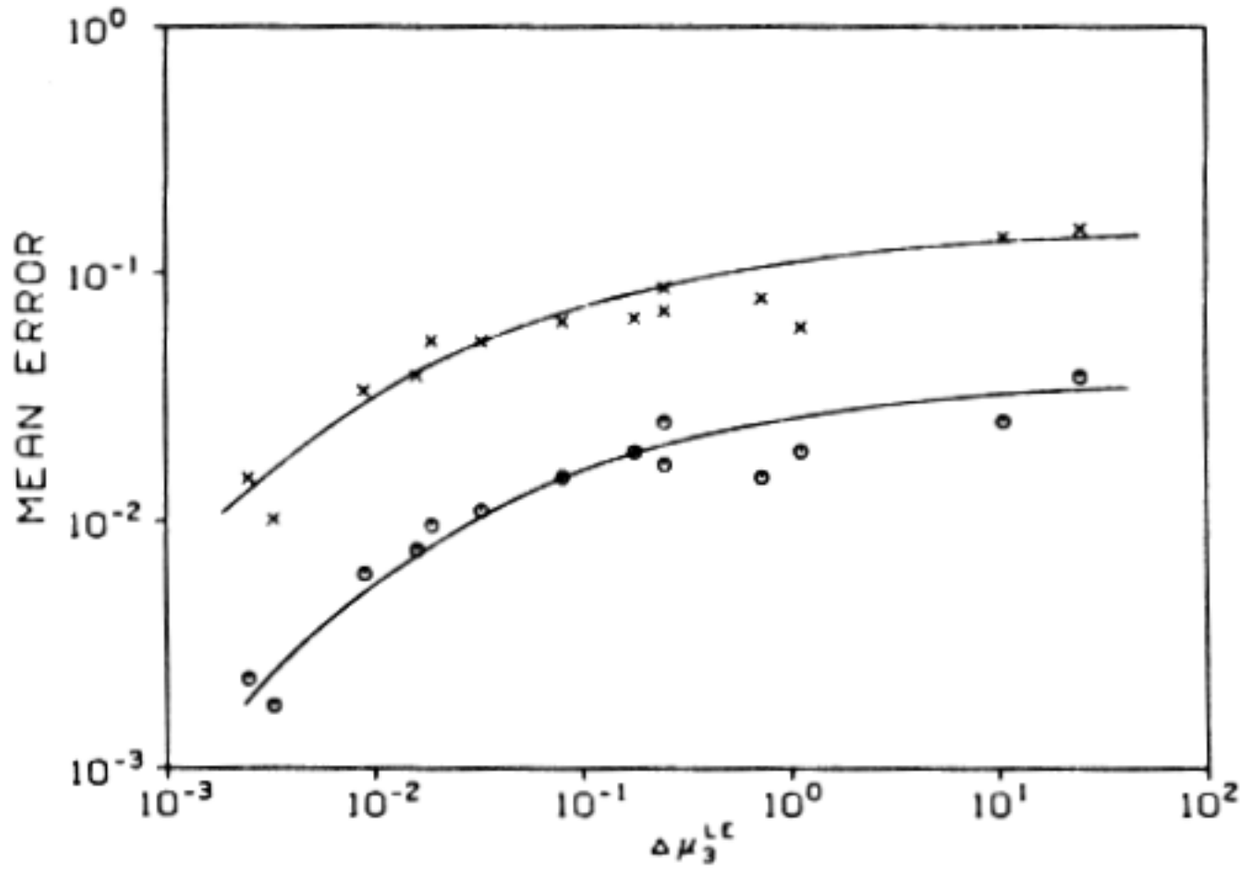

Figure 4.9. Observed mean error versus third-moment deviation between spherical diffusion model and local equilibrium model for cases 1-5 of Table 1 with continuous injection (circles) and for corresponding cases with dirac injection (crosses).

The deviation between third moments is then

$$\Delta\mu_3^{LE} \equiv \left|\mu_3^{LE} - \mu_3^{SD}\right| \tag{4.49a}$$

$$= \frac{4(1-\beta)}{5X^2\gamma R}\left|\frac{1}{P_m} + \frac{(2-7\beta)}{105\gamma R}\right| \tag{4.49b}$$

where (4.44) has been used to eliminate P_e from (4.47) yielding an expression for the deviation between LE and SD models in terms of SD model parameters. No term for the input function arises in (4.47) or (4.48) and hence in (4.49) since a square pulse has zero third moment. Therefore, we will deal with effects of dirac and continuous injection separately to determine the endpoint behavior.

To evaluate the utility of (4.49) to describe LE model faithfulness to SD model predictions, we require some objective measure of LE model accuracy. For this purpose we define the mean error between LE and SD model predictions as

$$E = \frac{1}{n}\sum_{i=1}^{n}\left| Y_i^{SD} - Y_i^{LE} \right| \tag{4.50}$$

where Y_i^{SD} and Y_i^{LE} are reduced concentrations for SD and LE models calculated at n=40 equally spaced T/XR values from T/XR=0 to 2. Mean errors E calculated for all cases in Table 4.1 for continuous injection increase in a fairly consistent fashion with third moment deviations $\Delta\mu_3^{LE}$ (Figure 4.9). This relationship allows one to evaluate the feasibility of using the LE model in lieu of the more complex SD model subject to a specified accuracy. For example, to obtain $E \leq 0.01$, which in most practical cases should be quite adequate accuracy, requires $\Delta\mu_3^{LE} \leq 0.05$; an accuracy of $E \leq 0.02$ will be obtained if $\Delta\mu_3^{LE} \leq 0.25$.

For pulse injection less accurate results are anticipated for a given $\Delta\mu_3$. To evaluate this, SD and LE model predictions were obtained for the dirac inlet condition for each case in Table 4.1. Errors calculated by (4.50) for these simulations are nearly an order of magnitude higher than those for continuous injection at any given $\Delta\mu_3^{LE}$ value (Figure 4.9). To attain an accuracy of $E \leq 0.01$ now requires $\Delta\mu_3^{LE} \leq 0.002$, while for $\Delta\mu_3^{LE} = 0.01$ the mean error will be about 0.03. Criteria for finite pulse inlet conditions are intermediate between the dirac and continuous results with the relationship between E and T_o for the simulations of Figure 4.8 approximately linear (r=-0.98).

FIRST-ORDER KINETIC MODEL

An alternative method of formulating an expression for mobile-immobile region interchange to couple with (4.1) is to assume in lieu of (4.2) and (4.3) the linear transfer function

$$\theta_{im}R_{im}\frac{\partial c_{im}}{\partial t} = \alpha(c_m - c_{im}) \tag{4.51}$$

where α is the first-order rate coefficient. In dimensionless form we have

$$(1-\beta)R\frac{\partial C_{im}}{\partial T} = \omega(C_m - C_{im}) \tag{4.52}$$

where $\omega=\alpha L/q$ and other terms are as defined for the SD and LE models. We will only consider here the solution of (4.4) and (4.52) for flux concentration subject to continuous injection. The result is (Parker and van Genuchten, 1984).

$$C_f = \int_0^T g(X,\tau)\ J(a,b)\ d\tau \tag{4.53a}$$

where

$$g(X,\tau) = \frac{X}{\tau}\left[\frac{P_m\beta R}{4\pi\tau}\right]^{1/2} \exp\left[-\frac{P_m(\beta RX-\tau)^2}{4\beta R\tau}\right] \tag{4.53b}$$

$$J(a,b) = 1 - e^{-b}\int_0^a e^{-\lambda}\ I_o(2\sqrt{b\lambda})d\lambda \tag{4.53c}$$

$$a = \omega\tau/\beta R \tag{4.53d}$$

$$b = \omega(T-\tau)/(1-\beta)R \tag{4.53e}$$

where I_o is a zero-order modified Bessel function.

As was done for the LE model, we wish to investigate the relationship between the first-order kinetic (FO) model and the SD model. As before we evaluate the equivalence of the two models by equating expressions for the second moments since first moments of FO, LE and SD models are all identical. For the FO model the second moment of C_f versus T is

$$\mu_2^{FO} = \frac{2XR^2}{P_m} + \frac{2XR^2(1-\beta)}{\omega} + \frac{T_o^2}{12} \tag{4.54}$$

Equating (4.54) with (4.43) for μ_2^{SD} gives on solving for ω

$$\omega = 15\gamma R(1-\beta) \tag{4.55}$$

which indicates the physical significance of ω in terms of the SD model reduced parameters under certain limiting conditions when SD to FO model degeneration is valid. In terms of the original model coefficients we note

$$\alpha = 15D_a\theta(1-\Phi)/a^2 \qquad (4.56)$$

A similar relation to that given by (4.55) and (4.56) has been derived empirically by van Genuchten (1985) by matching solutions for no-flow systems at relative concentrations of 0.5 yielding in lieu of the constant factor 15, a value of approximately 22.7 (inverse of squared 'shape factor'). The factor 15 is also obtained by Raats (1984) using a series expansion method.

To investigate the ability of the FO model with rate constant given by (4.55) to reproduce the diffusional kinetics of the SD model we consider again Case 1 of Table 4.1. At γ=3 the FO model is virtually indistinguishable from the SD model (Figure 4.10) and superior to the LE model (compare Figure 4.2). However, at γ=0.03 the FO model greatly deviates from the SD model predictions -- surprisingly, even more so than the LE model.

These effects may be quantified by again deriving error criteria by comparing third moments, now of the SD and FO models. The third moment of C_f versus T/XR for the FO model is found to be

$$\mu_3^{FO} = \frac{12}{(P_mX)^2} + \frac{12(1-\beta)^2}{\omega P_mX^2} + \frac{6(1-\beta)^3}{(\omega X)^2} \qquad (4.57)$$

The error criteria for SD-FO model degeneration is thus obtained from (4.48) and (4.57) as

$$\Delta\mu_3^{FO} \equiv \left|\mu_3^{FO} - \mu_3^{SD}\right| \qquad (4.58a)$$

$$= \frac{2(1-\beta)}{175(X\gamma R)^2} \qquad (4.58b)$$

Comparing (4.49) and (4.58) it is seen that $\Delta\mu_3^{FO}$ and $\Delta\mu_3^{LE}$ are related via

$$\Delta\mu_3^{LE} \equiv \left|\frac{12}{P_mP_{im}X^2} - \frac{14\beta-4}{3}\,\Delta\mu_3^{FO}\right| \qquad (4.59)$$

Apparently, as nonequilibrium behavior becomes more pronounced, the FO model may perform better or worse than the LE model depending on the relative magnitude of the first and second terms on the RHS of (4.59).

In the limit as $\Delta\mu_3^{FO}\to 0$ (4.59) indicates that $\Delta\mu_3^{LE}$ is still finite and equal to $12/P_mP_{im}X^2$. Hence, as observed in Figure 4.10, the FO model yields a more accurate approximation of the SD model than does the LE model as local equilibrium is approached. Values of $\Delta\mu_3^{FO}$ versus calculated mean errors E between SD and FO models for continuous injection using (4.50) are found to fall along the corresponding curve of E versus $\Delta\mu_3^{LE}$ of Figure 4.9 when $E\leq 0.02$. Thus $E\leq 0.02$ may be obtained by requiring $\Delta\mu_3^{FO}\leq 0.25$.

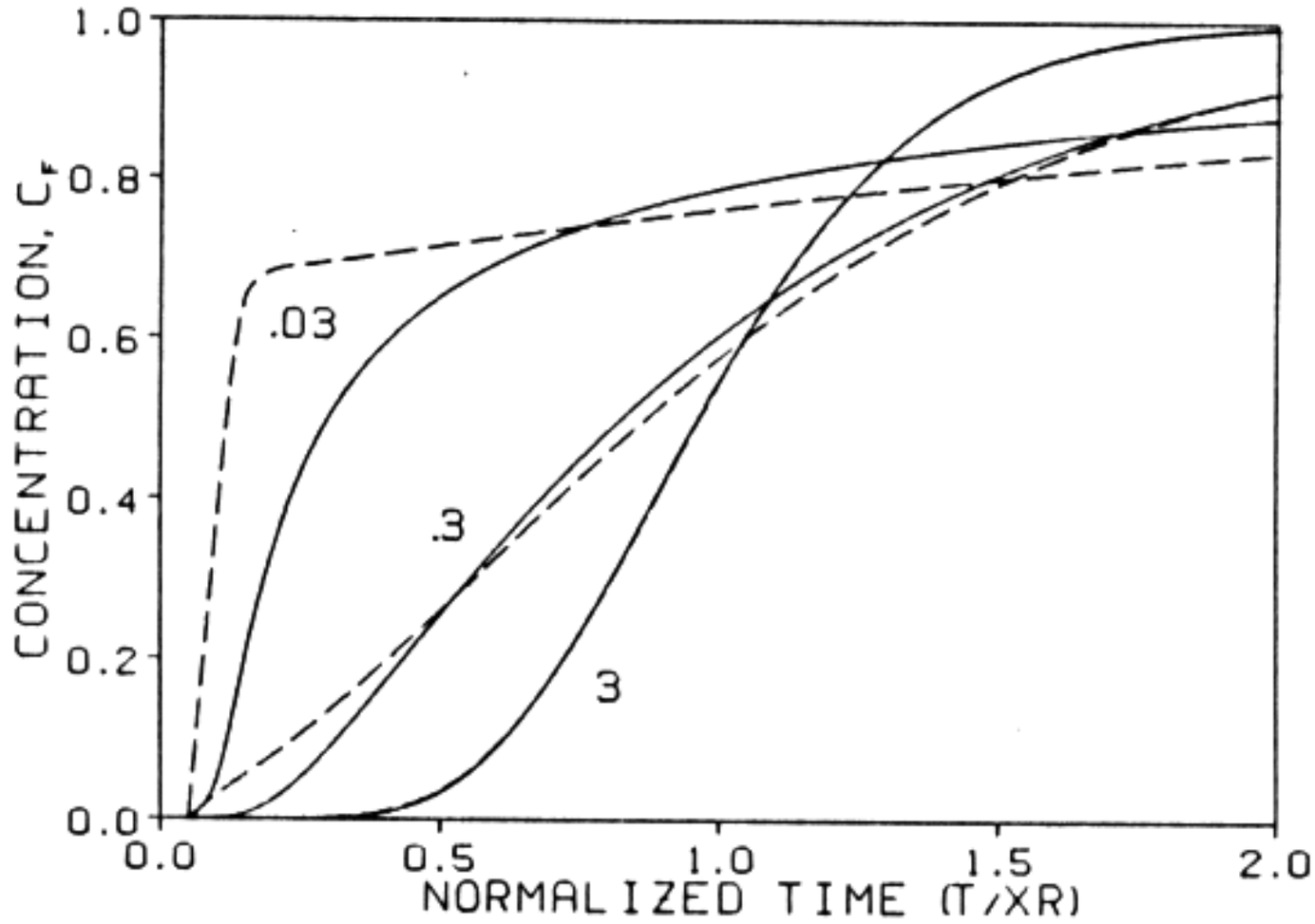

Figure 4.10. Effect of γ on flux concentrations for spherical diffusion model (solid lines) and first-order kinetic model (dashed lines) for continuous injection and β = 0.1, R = 1, P_m = 30, X = 1. Values of γ indicated on curves.

CONCLUSIONS

In spite of strict failure to meet the requirement of local equilibrium the LE model may describe with sufficient accuracy transport in soils with spheroidal aggregates. By comparing analytic expressions for time moments we are able to formulate an equivalent monocontinuum dispersion coefficient for the LE model in terms of SD model parameters which have direct physical relevance. The moment analysis yields also criteria for SD to LE model degeneration which provide quantitative guidelines for LE model suitability. LE model accuracy increases with decreasing aggregate size and immobile zone retardation factor and with increasing mobile zone retardation factor, mobile pore fraction, mobile zone diffusion coefficient and distance from inlet boundary. Degeneration criteria are presented for the two endcases of instantaneous and continuous injection with criteria for the former being more stringent than for the latter. As deviation between SD and LE models increases the distinction between resident and flux concentrations becomes increasingly important.

Applying similar methods of time moment analysis to a first-order kinetic model shows that the first-order rate constant may be related to the SD model parameters as was done for the dispersion coefficient in the LE model. Constraints on the validity of the FO model are similarly obtained. For only small deviation from local equilibrium, the FO model simulates SD predictions more accurately than does the LE model, although in both cases the discrepancies are minimal. However, as nonequilibrium conditions become more severe, the FO model may in some cases actually yield a less accurate representation of the SD predictions. For spherical geometry at least, there appears to be little gained by using the FO approach over the even simpler LE approach. However, for other geometries this may not be the case. The time moment method presented here is quite general in applicability and should provide a means to quantitatively evaluate the applicability of simple transport models in structured soils.

CHAPTER 5

EXTENSION TO ARBITRARY GEOMETRY

Our purpose in this chapter is to extend the analysis of Chapter 4 for bicontinuum-monocontinuum transport model degeneration to porous media with arbitrary macrostructure geometry and to investigate the adequacy of the degenerate models by analyzing experiments performed on systems involving adsorbed and nonadsorbed solutes in porous media containing immobile zones of spherical and planar geometries. Effects of experimental conditions on the applicability of resident and flux concentration solutions of the governing equations will be investigated.

THEORY

We begin by assuming that the physical system can be represented as a bicontinuum comprised of mobile and immobile regions of arbitrary geometry with diffusive mass exchange between regions. The dimensions of the mobile region are regarded as small enough to be well mixed so that transverse dispersion may be disregarded. The governing equations are thus given in the one dimensional case by

$$\theta_m R_m \frac{\partial c_m}{\partial t} + \theta_{im} R_{im} \frac{\partial c_{im}}{\partial t} = \theta_m D_m \frac{\partial^2 c_m}{\partial x^2} - q \frac{\partial c_m}{\partial x} \qquad (5.1)$$

$$c_{im}(x,t) = \frac{1}{V_{im}} \iiint_{(V_{im})} c_a(x,\zeta,t)\, dV_{im} \qquad (5.2)$$

$$R_{im} \frac{\partial c_a}{\partial t} = D_a \nabla^2 c_a \qquad (5.3)$$

where c_m and c_{im} respectively represent mean resident solution concentrations in mobile and immobile regions at global position x and time t, c_a is the concentration within the immobile region of volume V_{im} at global position x and local position vector ζ, θ_m and θ_{im} represent mobile and immobile region water contents such that the total water content $\theta = \theta_m+\theta_{im}$, D_m is a mobile zone dispersion coefficient, D_a is the diffusion coefficient within the immobile zone, q the hydraulic flux density, and R_m and R_{im} are retardation factors for the mobile and immobile zones.

In addition to c_m and c_{im}, it is useful to define the average resident concentration in the porous medium by

$$c_r = \Phi c_m + (1-\Phi) c_{im} \qquad (5.4)$$

where $\phi=\theta_m/\theta$ is the mobile pore fraction. We define also the flux concentration by

$$c_f = c_m - \frac{v}{D_m}\frac{\partial c_m}{\partial x} \tag{5.5}$$

where $v = q/\theta$ is the pore water velocity. The solution to (5.1) - (5.5) subject to a uniform initial condition, flux inlet condition, and semi-infinite lower boundary condition has been presented in Chapter 4 for the case in which the immobile region is comprised of spherical aggregates. Solutions for plane sheets, rectangular blocks, cylindrical cavities, and other geometries have been given by various authors (e.g. van Genuchten, 1985) and obtain forms similar to those for the spherical case.

In the preceding chapter, it was shown that the spherical diffusion model may be approximated under certain conditions by an "equivalent" monocontinuum model with effective dispersion coefficient given by

$$D_e = \phi D_m + \frac{(1-\phi)r^2v^2R_{im}^2}{15D_a[\phi R_m+(1-\phi)R_{im}]^2} \tag{5.6}$$

where r is the radius of the spherical aggregate. Similar formulae for D_e pertinent to other specific immobile zone geometries may be derived by application of the moment analysis described in the preceding chapter to the appropriate model solutions. In lieu of this model-specific approach, we consider here a simpler and more general method of extending (5.6) to a system of arbitrary geometry.

Let us assume that an immobile region exists which has a characteristic volume V_{im} and a surface area in contact with the mobile region equal to A_{im}. For such a region, the ratio $\lambda = V_{im}/A_{im}$ may be regarded as a characteristic length related to the average diffusion path length in the immobile region. For example, for rectangular blocks of dimensions a × b × c

$$\lambda = (2/a + 2/b + 2/c)^{-1} \tag{5.7}$$

and for spheres of radius r we have

$$\lambda = r/3 \tag{5.8}$$

The spherical equivalent, with respect to characteristic diffusion path length, of a block of given dimensions may be obtained by equating (5.7) and (5.8) which indicates

$$r_e = 3/(2/a + 2/b + 2/c) \tag{5.9}$$

where r_e denotes the equivalent spherical radius of the block. For the

special case of infinite slabs of thickness a with b = c → ∞, (5.9) degenerates to

$$r_e = 1.5\ a. \tag{5.10}$$

Thus, we assume that for a system comprised of planar sheets oriented parallel to the mean flow direction, the monocontinuum model will be obeyed under conditions outlined in the previous chapter subject to (5.6) with r replaced by r_e of (5.10) or, for general geometry, by r_e corresponding to λ for the specific case.

We consider in the following two sections, experimental evaluations of the equivalent monocontinuum model for porous media having immobile zones comprised of spherical aggregates and plane sheets. Monocontinuum and bicontinuum models will be compared with the experimental results and effects of experimental conditions on the appropriateness of resident and flux concentration solutions will be evaluated.

SPHERICAL DIFFUSION MODEL EXPERIMENTS

Breakthrough curves were determined from 3 cm long columns of a porous medium comprised of 1:1 dry mass proportions of 315 μm glass beads (mobile zone material) and 1.0 - 1.25 mm-sieved water stable aggregates from a Dunning soil (immobile zone material). Glass beads and aggregates were placed dry in a chromatography column in such a manner to acheive a uniform mixture. The column was wet with 0.2 meq mL^{-1} $CaCl_2$ through a fritted plastic plate on the bottom of the column and subsequently leached with several pore volumes of the same solution injected at a flux q of 864 cm d^{-1} from a feed line at the top of the porous medium. A displacing solution of 0.2 meq mL^{-1} $MgCl_2$ was subsequently introduced at the same flow rate. Effluent was collected in aliquots and analyzed for Mg by atomic absorption spectrometry.

At the completion of the experiment the column was dried to determine average water content, θ = 0.519 cm^3cm^{-3}, and bulk density, ρ = 1.36 g cm^{-3}. From gravimetric determinations of the saturated water content of aggregates, the immobile zone water content was computed to be θ_{im} = 0.356 cm^3 cm^{-3} and hence Φ = 1 - θ_{im}/θ = 0.314. Average aggregate volume was determined by water displacement for a known number of aggregates and employed to compute the mean aggregate radius of 1.16 mm assuming spherical shape.

Solute retardation factors were determined for the media from the cation adsorption capacities. Cation adsorption for glass beads is negligible, hence k_m = 0. Cation exchange capacity of the aggregates was measured to be 0.204 meq g^{-1}. Assuming a linear Ca-Mg binary exchange isotherm at a constant total cation concentration of 0.2 meq mL^{-1} yields k_{im} = 0.204 meq g^{-1}/0.2 meq mL^{-1} = 1.02 mL g^{-1} and for the bulk porous medium, k = 0.50 mL g^{-1}. The corresponding retardation factors are computed to be R_{im} = 2.84, R_m = 1.0 and R = 2.26.

The only parameters in the spherical diffusion model which now remain to be determined are D_a and D_m. From tabulated sources (Weast, 1985), we estimate the diffusion coefficient, D_o, of $MgCl_2$ in bulk water at 0.2 meq mL^{-1} concentration to be 0.88 $cm^2\ d^{-1}$. Results of DeSmedt and Wierenga (1984) indicate a tortuosity factor, τ, of about 0.75 for a porous medium of similar porosity to that employed in the present studies. Theoretical calculations (Lyman, et al., 1982) yield somewhat lower values. We will take $D_a = \tau D_o \approx 0.5$ $cm^2\ d^{-1}$ as a reasonable estimate of the immobile zone diffusion coefficient. To estimate D_m we follow the method of Dullien (1979, p.344) based on the particle size of the glass beads and the known pore water velocity to give $D_m \approx 200$ $cm^2\ d^{-1}$. For the monocontinuum model, the apparent dispersion coefficient computed from (5.6) is 1175 $cm^2\ d^{-1}$.

The observed Mg breakthrough curve for the glass bead-aggregate medium is shown in Figure 5.1 along with predicted curves for the spherical diffusion bicontinuum model and degenerate monocontinuum model using independently estimated parameters as described above. For each model both resident and flux solutions (as given in Chapter 4) are shown. The bicontinuum flux concentration solution is observed to describe the experimental data very closely. The monocontinuum flux solution follows the bicontinuum model fairly closely but somewhat overestimates effluent concentrations at early times and underestimates at intermediate times. Resident concentration solutions are clearly inappropriate for the conditions of this experiment in which effluent is collected from the entire cross section of a laboratory column.

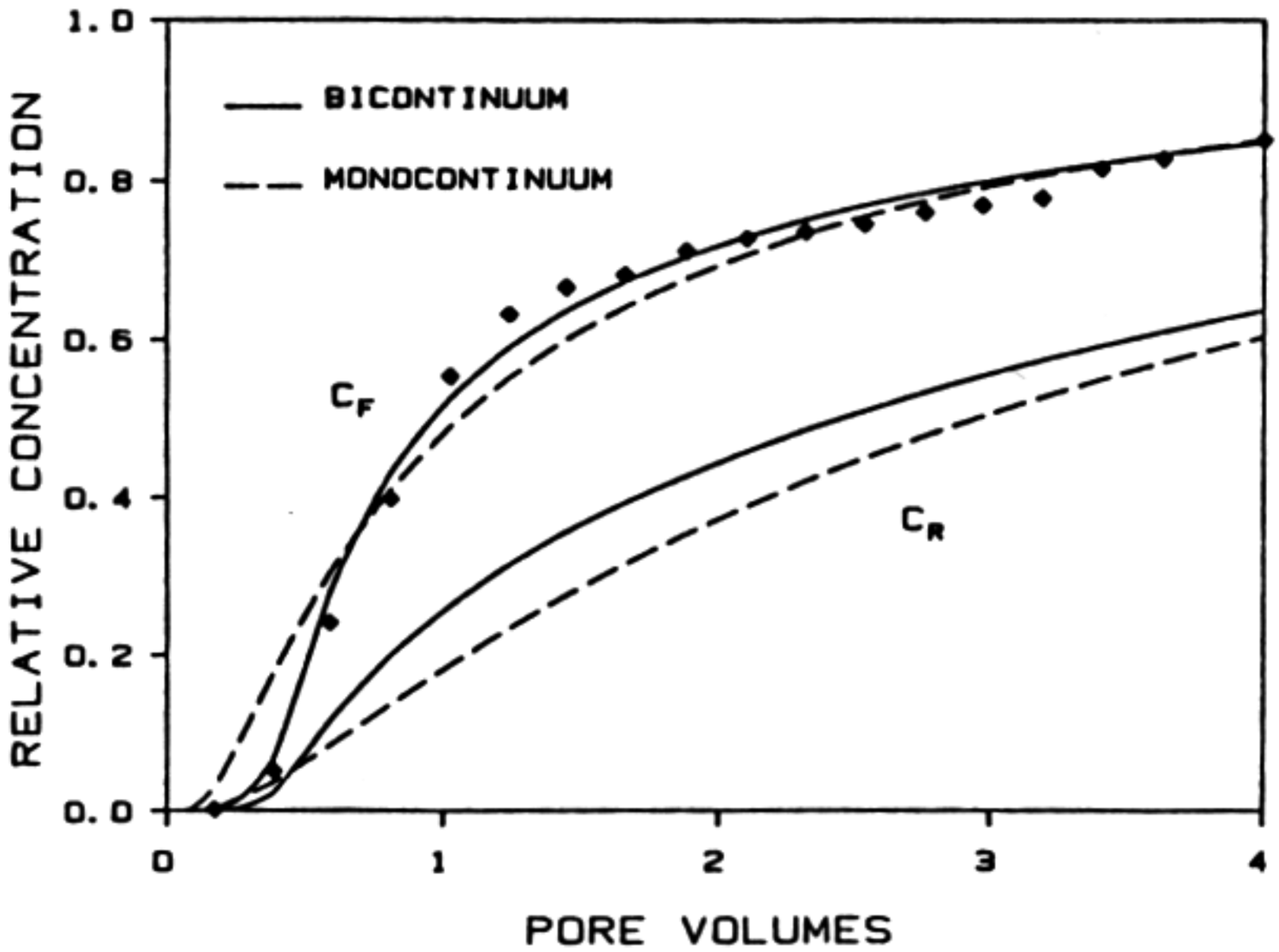

Figure 5.1. Observed Mg breakthrough data for glass bead-aggregate column and independent predictions of resident and flux soltions for bicontinuum and corresponding monocontinuum models.

PLANE SHEET DIFFUSION MODEL EXPERIMENTS

In order to evaluate the bicontinuum model degeneration under substantially different experimental conditions from those in the preceding column studies, experiments were undertaken on a stratified porous medium with flow parallel to the layers. Alternating layers of clay and glass beads each approximately 1 cm in thickness were packed into a plexiglass tank of dimensions shown in Figure 5.2. At two opposite ends of the tank, the porous medium was separated from the tank walls by a rigidly supported screen to enable introduction and free exit of tracer solution. Observation wells were installed at various locations downstream of the injection plane using different types of well designs in each of two different experiments.

Experiment I

In the first experiment, observation wells were constructed of 17 mm diameter PVC pipe with 1 mm slots sawed radially such that about 5% of the well surface area was slotted. Each well was covered with cotton cloth and installed in the porous medium with no adjacent backfill by placing the wells in the tank prior to building up the soil layers about them. After the layers were constructed from dry soil, the medium was wet over a period of two days by slowly adding 0.01 meq mL^{-1} $CaCl_2$ to the tank via one of the end plates. A steady flow regime was established at a flux of 9 cm d^{-1} and maintained for a period sufficient to displace several pore volumes through the tank before beginning tracer injection of 0.01 meq mL^{-1} $MgBr_2$ at the same flow rate. Solution samples were taken from the observation wells at various times by pipetting 1 mL samples after first stirring the well bore to ensure a well-mixed sample.

Bromide concentrations in the well 6 cm downstream of the inlet measured by a specific ion electrode are shown versus time in Figure 5.3 along with predicted bicontinuum and monocontinuum model resident and flux concentrations. Bicontinuum model solutions which explicitly consider the planar geometry of the system have forms identical to those of (4.21) - (4.28) but with parameters ψ_1 and ψ_2 given by

$$\psi_1 = \frac{\lambda(\sinh 2\lambda - \sin 2\lambda)}{(\cosh 2\lambda + \cos 2\lambda)} \qquad (5.11)$$

$$\psi_2 = \frac{\lambda(\sinh 2\lambda + \sin 2\lambda)}{(\cosh 2\lambda + \cos 2\lambda)} \qquad (5.12)$$

when the immobile layer half thickness, a/2, is used in lieu of the aggregate radius, r. From direct measurements on the system, a/2 = 1 cm, ρ = 1.2 g cm^{-3}, θ = 0.5, and Φ = 0.5. For Br we assume $R_m = R_{im} = R = 1$, and estimate D_a = 0.5 cm^2 d^{-1} and D_m = 0.1 cm^2 d^{-1} in the same manner as for the spherical aggregate experiments. Monocontinuum model predictions were made via (5.6) and (5.10).

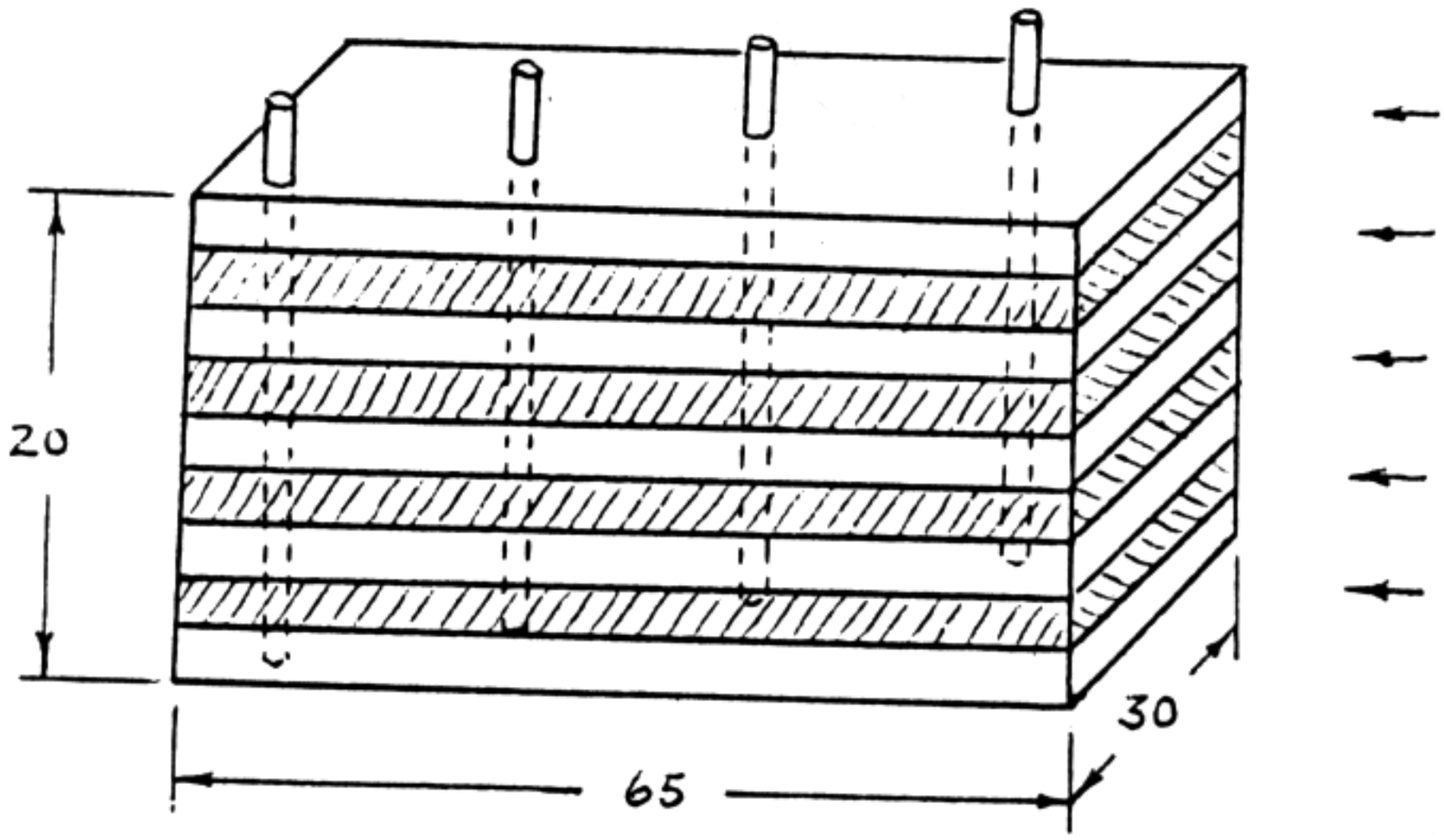

Figure 5.2. Physical arrargement of porous media in "plane sheet" diffusion model experiments.

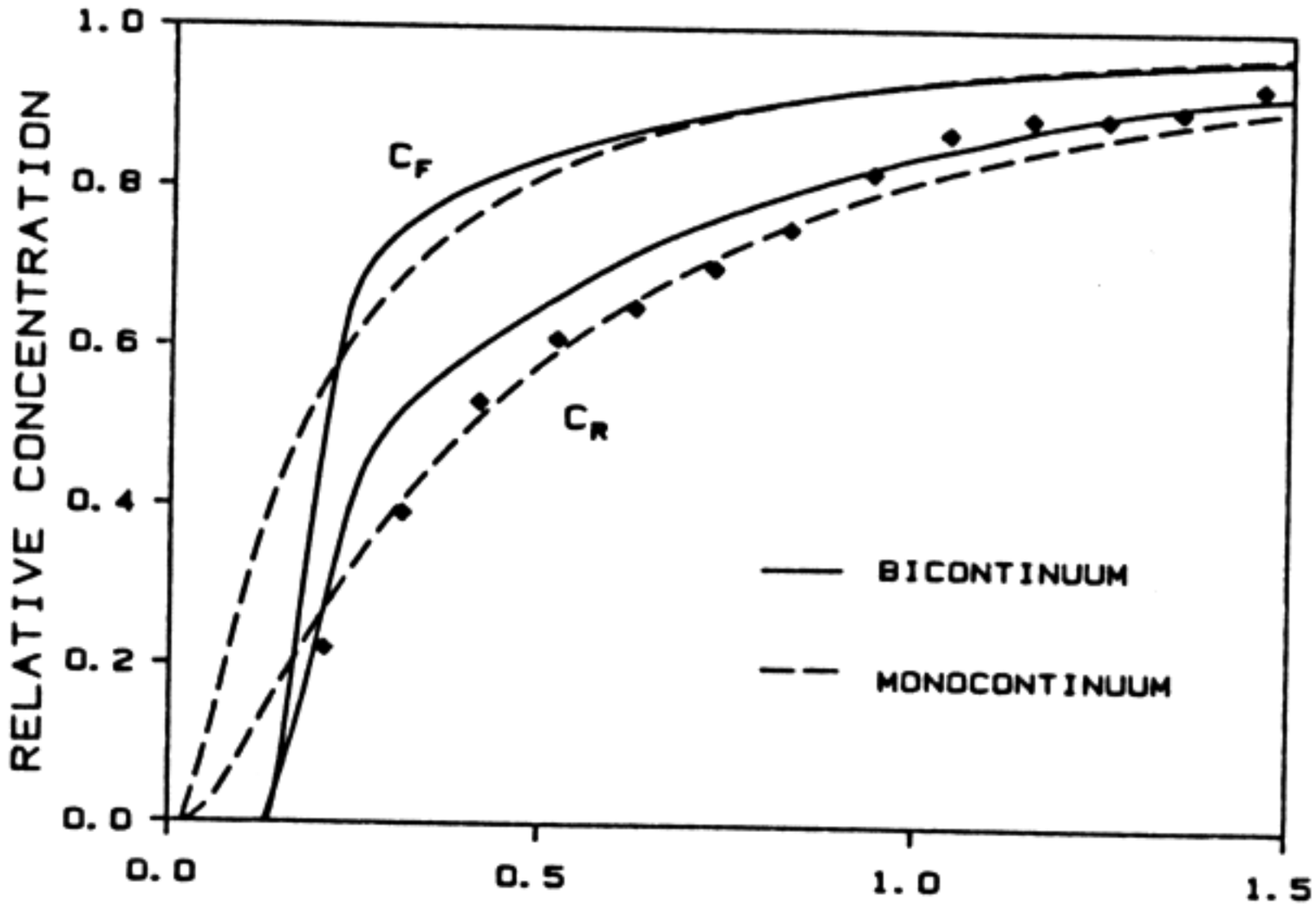

Figure 5.3. Observed and predicted Br breakthrough curves for well at 6 cm in Experiment I.

Neither the resident nor flux concentration solutions to the bicontinuum model correspond well with the observed data although the resident solution is much closer to the measured results. At short times the data correspond more closely with monocontinuum resident concentration solution than with the bicontinuum model, however, this is undoubtedly a fortuitous occurence. Poor correspondence with flux concentration solutions indicates impedance in the flow field in the vicinity of the well. As a result, the well concentration may be controlled to a significant extent by radial diffusion from the surrounding porous medium. This radial diffusional limitation may explain the tendency of observed concentrations to lag behind predicted resident values. Similar results for other wells were observed. Due to the well design, however, it is apparent that unambiguous interpretation of the results is not feasible; hence, we procede to discuss results of a second experiment performed with a modified well design.

Experiment II

In the second experiment, a modified well design was employed to preclude flow restriction through the sampling wells. The slotted area of the well was increased to 50%. To prevent soil entry into the wells, the well exteriors were covered with a highly permeable nylon fabric and a 1 cm wide coarse sand backfill was emplaced in a 1 cm circumference around each well. Experimental conditions and procedures were similar to those of Experiment I, but in this case $q = 19$ cm d^{-1}, $\theta = 0.55$ cm^3 cm^{-3}, $\phi = 0.37$, $\rho = 1.19$ g cm^{-3}, $\rho_m/\rho = 0.59$, and $a = 0.72$ cm. From measurements of the cation exchange capacity at a solution concentration of 0.06 meq mL^{-1} at which the tracer experiment was conducted, we obtain for Mg: $k_m = 0$, $k_{im} = 1.0$ mL g^{-1}. We continue to assume $D_a = 0.5$ cm^2 d^{-1} and for the flow rate of this experiment calculate via the method of Dullien $D_m = 3$ cm^2 d^{-1}.

Observed Mg breakthrough curves and predicted flux concentrations for the bicontinuum and degenerate monocontinuum models for wells at $x = 15$, 30, 45, and 60 cm locations downstream of the injection surface are shown in Figure 5.4. Agreement between predicted and observed concentrations is observed to vary markedly with sampling location. To investigate this problem further, the observed data were used to conduct parameter estimation analyses by fitting selected model parameters using a nonlinear regression procedure similar to that of Parker and van Genuchten (1984). Agreement of bicontinuum model predictions with the data was markedly improved when D_m or D_a were permitted to vary for each well. When D_m was best-fit separately for each well with other parameters held at their measured or independently estimated values, optimum values obtained were 3, 565, 1220 and 2260 cm^2 d^{-1} at $x = 15$, 30, 45, and 60 cm, respectively. Somewhat better fits were obtained when D_a values were fit with other parameters held constant yielding estimates of 1.0, 0.5, 0.33 and 0.21 cm^2 d^{-1} at the respective wells. Via (5.6) we observe that this trend in apparent D_m or D_a values for the bicontinuum model indicates that D_e in the monocontinuum model will exhibit an approximately linear increase with distance to the sampling point. Clearly, the apparent variation of D_a and D_m is not physically tenable and signals an inadequacy of the assumed bicontinuum representation of this system which in turn precludes relevance of the corresponding degenerate monocontinuum model.

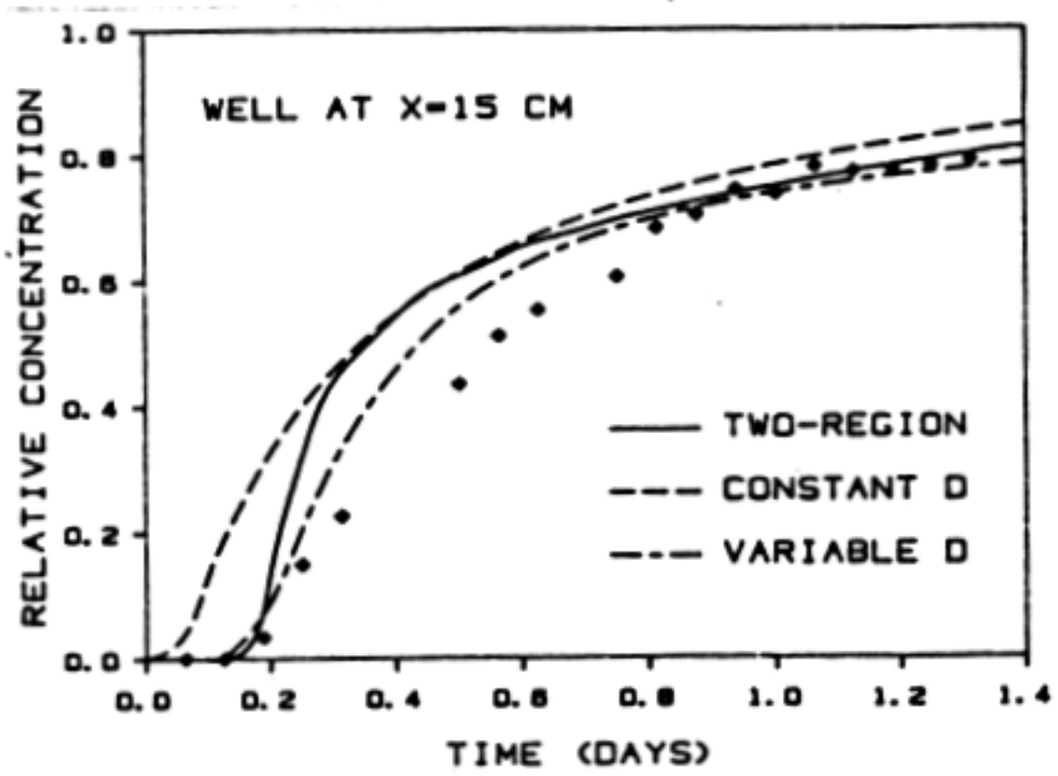

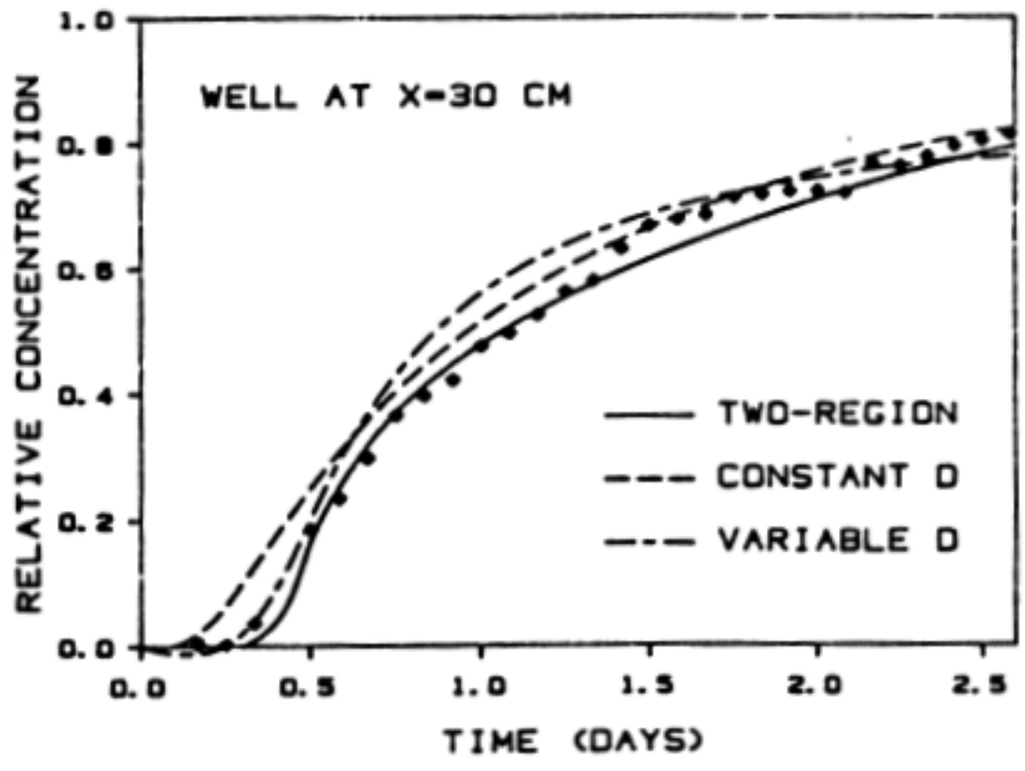

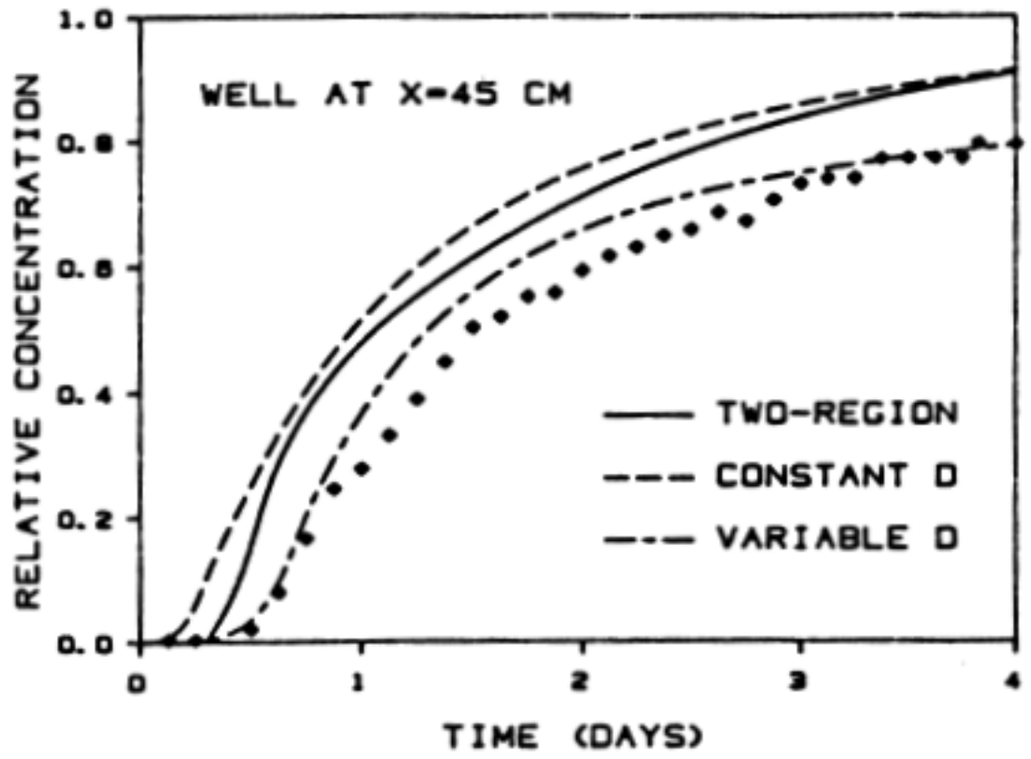

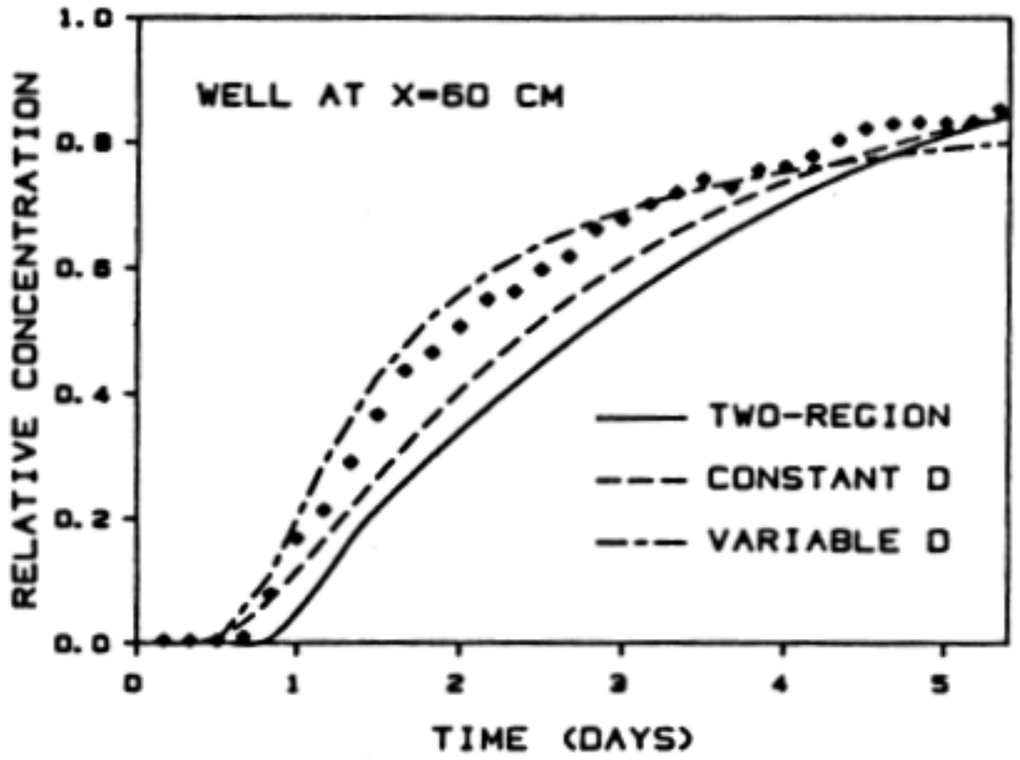

Figure 5.4. Observed Mg breakthrough data for wells at 15, 30, 45 and 60 cm in Experiment II and predicted curves using mobile-immobile model and degenerate monocontinuum model with constant D_e with all model parameters independently determined and predicted curves for monocontinuum model with fitted exponential time-dependent dispersion function.

The likely cause of this failure of the mobile-immobile model and of its monocontinuum analog is the inadequacy of the implicit assumption that solute in the mobile zone is perfectly mixed in the direction transverse to the mean flow field. A theoretical study of transport in stratified porous media by Güven et al. (1894) indicates that transverse mixing will result in an apparent time-dependence of the bulk system longitudinal dispersion which asymptotically approaches a constant value. Güven et al. indicate that the form of the time-dependent effective longitudinal dispersion coefficient should be closely approximated by

$$D(t) = D_{lim} [1 - \exp(\chi t)] \qquad (5.13)$$

where D_{lim} is the asymptotic dispersion coefficient and χ is a parameter related to the system geometry and transverse dispersion. An approximate solution of the monocontinuum convection-dispersion equation for time-dependent dispersion has been presented by Dieulin et al. (1981) for the case of continuous injection of concentration C_o as

$$c(x,t) = \frac{C_o}{2} \operatorname{erfc} \left[\frac{x - vt}{2[D(t)t]^{1/2}} \right]. \qquad (5.14)$$

Values of χ and D_{lim} obtained by fitting (5.13) and (5.14) to the observed breakthrough curves simultaneously for the four wells are 5650 $cm^2 d^{-1}$ and 0.085 d^{-1}, respectively. Predicted curves corresponding to these parameters shown in Figure 5.4 indicate that a reasonably consistent description of the data can be obtained with the time-dependent dispersion formulation.

We conclude that under conditions in which transverse mixing within mobile zones is important, application of a monocontinuum analysis will necessitate use of a time-dependent dispersion coefficient the magnitude of which should be amenable to determination by giving explicit consideration to transverse dispersion.

CHAPTER 6

MOMENT ANALYSIS FOR LAYERED MEDIA

Mass transport in layered porous media occurs in many natural geologic situations for which accurate predictions of chemical fluxes are necessary, e.g., to quantify hazardous waste transport. Although phenomenologically based (Kreft, 1981b), the convection-dispersion model is commonly used in a predictive role to describe the transport and spreading of dissolved chemicals in layered and nonlayered hydrologic systems, as well as in problems arising in fields of chemical and petroleum engineering (Moranville *et al.*, 1977).

In contrast with the extensive body of literature dealing with many aspects of the convection-dispersion model for single-layer systems, not much attention has been given to multilayer porous media, particularly in terms of purely analytical methods. In this paper we consider the analysis of chemical transport in systems with flow perpendicular to layers which are each homogeneous and well-defined. Fluid flow in the systems is considered to be uniform and steady with a known flux. We assume, for simplicity, that the systems are composed of two layers corresponding, for example, to a lagoon with a clay liner between the waste and the underlying profile. The methods used can be applied to more than two layers, albeit with increasing algebraic and computational complexity.

In previous chapters we have shown the necessity of distinguishing between flux and resident concentration detection modes when using the convection-dispersion model (see also Brigham, 1974; Kreft and Zuber, 1978); van Genuchten and Parker, 1984). For example, sectioning a soil core and measuring concentration over the soil volume corresponds to resident concentration. In practice, it often occurs that breakthrough curves at a fixed position are of primary concern and these are more properly analyzed in terms of flux concentrations (Chapter 3). Thus we will consider flux concentrations while noting that marked differences between model predictions of flux and resident concentrations will appear only when the dispersivity is relatively large, as demonstrated in Chapter 2.

Previous analytical approaches to this problem, most notably Shamir and Harleman (1967), follow the transfer function approach used in linear system analysis, e.g. as applied to electrical networks (LePage, 1961). Shamir and Harleman (1967) make the assumption that, with respect to solute transport, each layer acts independently. This allows each layer to be treated, mathematically, as if it were semi-infinite. The semi-infinite solution for the first layer is used to give the upper boundary condition for the second layer, and so on. As deduced by Shamir and Harleman (1967), this assumption implies that the order of the layers has no effect on predicted breakthrough curves and thus lengths of the layers in the profile with the same dispersivity can be summed and treated as a single layer. Shamir and Harleman (1966), as well as Selim *et al.* (1977), have presented experimental results indicating that layer ordering had little effect on measured effluent concentrations. However, on physical grounds, there is no reason to assume,

a priori, that solute transport is unaffected by the order of the layers. This point will be considered in more detail subsequently.

Other investigations utilizing the same assumption as Shamir and Harleman (1967) include: for nonreactive transport, Bruch (1970), Moranville *et al.* (1977), Ultman and Blatman (1977) and Pendse *et al.* (1978); and for transport involving radionuclide decay, Gureghian and Jansen (1985). The analyses reported by all these authors were predominantly analytical. The results show clearly that the assumption of noninteracting layers is a useful one, given that the error involved is acceptably small. As well as quantifying this error, we formalize the approach so that it can easily be applied to other transport scenarios, e.g. diffusion of solute from mobile to immobile regions.

In practice it will often be convenient to treat the layered system as an equivalent single layer for purposes of making predictions of the system response to a certain input disturbance. In essence, the procedure is to cast the transport parameters for the simple single-layer convection-dispersion model in terms of the more complex model. As noted by Fried (1975), the "idea of replacing a complex problem by an elementary well-known equivalent problem is very natural and is the base of the philosophy of the scale change."

This approach has been followed by a number of authors to simplify the analysis of nonequilibrium transport associated with diffusional or chemical kinetics (Passioura, 1971; Baker, 1977; De Smedt and Wierenga, 1984; Valocchi, 1985; van Genuchten, 1985; Chapter 4, this report). Marle *et al.* (1967) considered an equivalent layer approach to stratified media for the case of flow parallel to the direction of layering. Here we follow the time moment analysis of Marle *et al.* (1967) and Valocchi (1985). Based on Aris (1958), this method consists of equating the moments calculated for the various transport models with the moments of the simple linear equilibrium model. Aris (1958) showed that moments can be calculated from solutions in the Laplace domain while noting that distributions can be conveniently and relatively accurately defined in terms of their first few moments. These properties have great practical use, especially when exact analytical solutions are not available, as is the case for solute transport in layered soils.

Our purpose is to analyze breakthrough curves from a medium consisting of two distinct layers. The time moment method will be used to define the parameters of the two-layer system in terms of an equivalent single layer model and give conditions under which the latter model will accurately simulate layered system breakthrough curves. Additionally, the approach of Shamir and Harleman (1967) is examined, checked for accuracy and applied to a more complex transport model.

MATHEMATICAL MODEL

The mathematical model for solute transport perpendicular to the stratification is given by the system of equations

$$R_i\frac{\partial c_i}{\partial t} = D_i\frac{\partial^2 c_i}{\partial x^2} - v_i\frac{\partial c_i}{\partial x}, \qquad i = 1,\ldots,n \tag{6.1}$$

The n equations given by (6.1) apply to n homogeneous soil layers, with each layer referred to by the subscript i. In the following analyses we take n = 2. R_i, c_i, D_i and v_i are the retardation factor (Lindstrom *et al.*, 1967), solute flux concentration, hydrodynamic dispersion coefficient and mean pore-water velocity, respectively, for each layer. Distances in each layer are referenced to a common origin. Assuming a constant volumetric flow rate, q, for the entire system and taking the water contents, θ_i, to be constant within each layer, the mean pore-water velocity for each layer is

$$v_i = q/\theta_i. \tag{6.2}$$

For convenience we rewrite (6.1) as

$$\frac{\partial c_i}{\partial t} = D_i\frac{\partial^2 c_i}{\partial x^2} - v_i\frac{\partial c_i}{\partial x}, \qquad i = 1,\ldots,n \tag{6.3}$$

where the retarded mean pore-water velocity is defined as $v_i = v_i/R_i$ and the retarded coefficient of dispersion is $D_i = D_i/R_i$. In a multilayered soil, the mean retarded pore-water velocity between the origin and location x is

$$\bar{v} = \frac{qx}{R_1\theta_1 L_1 + \ldots + R_n\theta_n(x - L_{n-1})} \tag{6.4}$$

where L_i denotes the thickness of the i^{th} layer.

The flux boundary conditions to be applied in the solution of (6.3) are (Kreft, 1981b)

$$c_o(t) = c_1(0^+,t), \tag{6.5}$$

$$c_i(L_i^-,t) = c_{i+1}(L_i^+,t), \tag{6.6}$$

$$v_i\frac{\partial c_i(L_i^-,t)}{\partial x} = v_{i+1}\frac{\partial c_{i+1}(L_i^+,t)}{\partial x} \qquad \text{and} \tag{6.7}$$

$$\lim_{x\to\infty} c_i(x,t) = \text{finite}, \tag{6.8}$$

where $c_o(t)$ is the concentration of the influent solution. Since we are considering a two-layer system, in the following we take the length of the first layer to be L, while the second layer is semi-infinite. We impose a uniform initial condition such that

$$c_i = 0, \qquad x > 0,\ t = 0 \tag{6.9}$$

while noting that there is no loss of generality in imposing (6.9) since superposition may be used to construct solutions for arbitrary initial conditions from the solution subject to (6.9) (e.g., see van Genuchten and Alves, 1982).

The solution for the second layer in the Laplace domain, $\bar{c}_2(x,s)$, is (Kreft, 1981a)

$$\bar{c}_2(x,s) = \frac{2\bar{c}_0(s)q_1(1+q_2)\exp[v_1L(1-q_1)/(2D_1)+v_2(x-L)(1-q_2)/(2D_2)]}{(1+q_1)(q_2+q_1)-(1-q_1)(q_2-q_1)\exp[-q_1v_1L/D_1]} \qquad (6.10)$$

where $q_i = (1 + 4sD_i/v_i^2)^{1/2}$, s is the Laplace transform variable and $\bar{c}_0(s)$ is the Laplace transform of $c_0(t)$. Note that there is no difficulty in writing the solution for $\bar{c}_1(x,s)$ which has a form similar to (6.10). However, our interest is in breakthrough curves as affected by the layering and hence we consider only the second-layer flux concentration solution.

"Exact" solutions to (6.10) for $c_2(x,t)$ can be found by numerical inversion using readily available algorithms (e.g. Javendel *et al.*, 1984). In common with any numerical solution, this method, which is undoubtedly useful in some applications, gives little understanding of the behavior of the system under consideration. For a profile consisting of many layers, a Laplace domain solution is not necessarily available. Furthermore, any numerical method may be subject to instability for certain combinations of the parameters, especially in the case of more complex systems. Later we consider a layered profile containing mobile-immobile regions for which numerical inversion gave inaccurate results. Thus, not only does the following analysis give insight into transport in layered profiles, the approximations may be more widely applicable and numerically stable than Laplace transform inversion.

ANALYSIS AND DISCUSSION

Time-Moment Analysis

Aris (1958) has shown that a finite quantity of material moving in a dispersive medium possesses a set of time moments, m_j, defined by

$$m_j = \int_0^\infty t^j c(x,t)\, dt, \qquad j = 0,\ 1,\ 2,\ldots \qquad (6.11)$$

where $c(x,t)$ describes the concentration distribution in space and time. The moments given by (6.11) can be normalized with respect to m_0, the total mass injected per unit area. For example m_1/m_0 ($\equiv \bar{\mu}$), is the normalized mean residence time which we refer to subsequently simply as the mean. Higher order moments are commonly expressed relative to the mean by the central moments

$$\mu_j = \frac{1}{m_o}\int_o^\infty \left[t - \bar{\mu}\right]^j c(x,t)\ dt. \tag{6.12}$$

Thus $\mu_o = 1$ and $\mu_1 = 0$. The variance of the distribution is given by

$$\mu_2 = \frac{m_2}{m_o} - \bar{\mu}^2, \tag{6.13}$$

and the skewness is

$$\mu_3 = \frac{m_3}{m_o} - 3\bar{\mu}\mu_2 - \bar{\mu}^3, \tag{6.14}$$

which is also expressed as the coefficient of skewness (Skopp, 1984)

$$S = \mu_3(\mu_2)^{-3/2}. \tag{6.15}$$

Observe that c(x,t) need not be known explicitly to evaluate the moments since m_j can be calculated from (Aris, 1958)

$$m_j = (-1)^j \lim_{s\to o} \left[\frac{d^j\bar{c}(x,s)}{ds^j}\right] \tag{6.16}$$

which, in general, is a straightforward calculation.

An Equivalent Single-Layer

Table 6.1 gives expressions for the mean, variance and skewness of the single- and two-layer system breakthrough curves obtained via (6.10) for a Dirac surface condition, i.e. (Kreft, 1981a)

$$c_o(t) = \frac{m_o\delta(t)}{q}. \tag{6.17}$$

For the single-layer results, a subscript e has been used to denote "equivalent" two-layer parameters. Equating single- and two-layer means yields

$$v_e = \frac{x}{\frac{L}{v_1} + \frac{x - L}{v_2}}. \qquad (6.18a)$$

Note, as we expect, $v_e = \bar{v}$ in (6.4) when the latter equation is written for the two-layer case. Similarly, equating the variances in Table 6.1 gives an equation for the equivalent dispersion coefficient, D_e

$$D_e = \frac{x^2}{\left[\frac{L}{v_1} + \frac{x-L}{v_2}\right]^3}\left\{\frac{D_1 L}{v_1^3} + \frac{D_2(x-L)}{v_2^3} + \frac{D_1}{v_1^2}\left[\frac{D_2}{v_2^2} - \frac{D_1}{v_1^2}\right][1 - \exp(-P_1)]\right\} \qquad (6.18b)$$

where $P_1 = v_1 L/D_1$. We note that D_e and v_e are functions of position. Although the entries in Table 6.1 were calculated for a Dirac (instantaneous) condition, the calculated equivalent single layer parameters are independent of the surface condition duration. However, differences between the equivalent single-layer and the exact two-layer breakthrough curves will decrease as the duration of the surface condition increases as has been observed in other cases where a similar approach was used (Valocchi, 1985; Parker and Valocchi, 1986).

By definition, breakthrough curves calculated assuming an equivalent single layer will have the same mean and variance as the two-layer system. An error criterion for breakthrough curves calculated using this procedure can be derived by requiring the relative difference between the exact and equivalent normalized skewness coefficients, calculated using Table 6.1 and (6.15), to be small. Note that the μ_i of Table 6.1 are normalized to dimensionless time (Nauman and Buffham, 1983), $T = t\bar{v}/x$, by dividing by $(x/\bar{v})^i$. Alternatively, the following empirical condition is extremely simple and thus may be more useful in practice. The Péclet number of the equivalent single layer ($P_e = v_e x/D_e$) will be equal to the sum of the layer Péclet numbers [$P_1 = v_1 L/D_1$ and $P_2 = v_2(x-L)/D_2$] for two layers with the same dispersivities, i.e. $D_1/v_1 = D_2/v_2$. In this case the ratio of the equivalent layer Péclet number to the sum of the Péclet numbers of the individual layers is unity. In practice the greater the difference of this ratio from unity, the less accurate the equivalent single layer approximation becomes. We find that the equivalent single layer approximation is reasonably accurate if

$$\frac{P_e}{P_1 + P_2} > \frac{1}{2}. \qquad (6.19)$$

Figures 6.1 and 6.2, which give breakthrough curves for continuous solute injection, demonstrate the use of condition (6.19). In Figure 6.1, condition (6.19) is satisfied, while in Figure 6.2 it is not.

Table 6.1. One- and two-layer time moments calculated for a Dirac surface condition.

$\bar{\mu}$	One Layer	Two Layer (Exact)	Two Layer (Convolution)
$\bar{\mu}$	$\frac{x}{v_e}$	$\frac{L}{v_1} + \frac{x - L}{v_2}$	$\frac{L}{v_1} + \frac{x - L}{v_2}$
μ_2	$\frac{2xD_e}{v_e^3}$	$\frac{2D_1}{v_1^2}\left\{\frac{L}{v_1} + \left[\frac{D_2}{v_2^2} - \frac{D_1}{v_1^2}\right]\left[1 - \exp\left(\frac{-v_1 L}{D_1}\right)\right]\right\} + \frac{2D_2(x-L)}{v_2^3}$	$\frac{2LD_1}{v_1^3} + \frac{2D_2(x - L)}{v_2^3}$
μ_3	$\frac{12xD_e^2}{v_e^5}$	$\frac{12D_1}{v_1^2}\left[\frac{D_2^2}{v_2^4} + \frac{D_1 D_2}{v_1^2 v_2^2} - \frac{2D_1^2}{v_1^4}\right]\left[1 - \exp\left(\frac{-v_1 L}{D_1}\right)\right]$ $+ \frac{12LD_1^2}{v_1^5}\left[1 + \exp\left(\frac{-v_1 L}{D_1}\right)\right] + \frac{12D_2^2(x - L)}{v_2^5}$ $- \frac{12LD_1 D_2}{v_1^3 v_2^2}\exp\left(\frac{-v_1 L}{D_1}\right)$	$\frac{12LD_1^2}{v_1^5} + \frac{12D_2^2(x - L)}{v_2^5}$

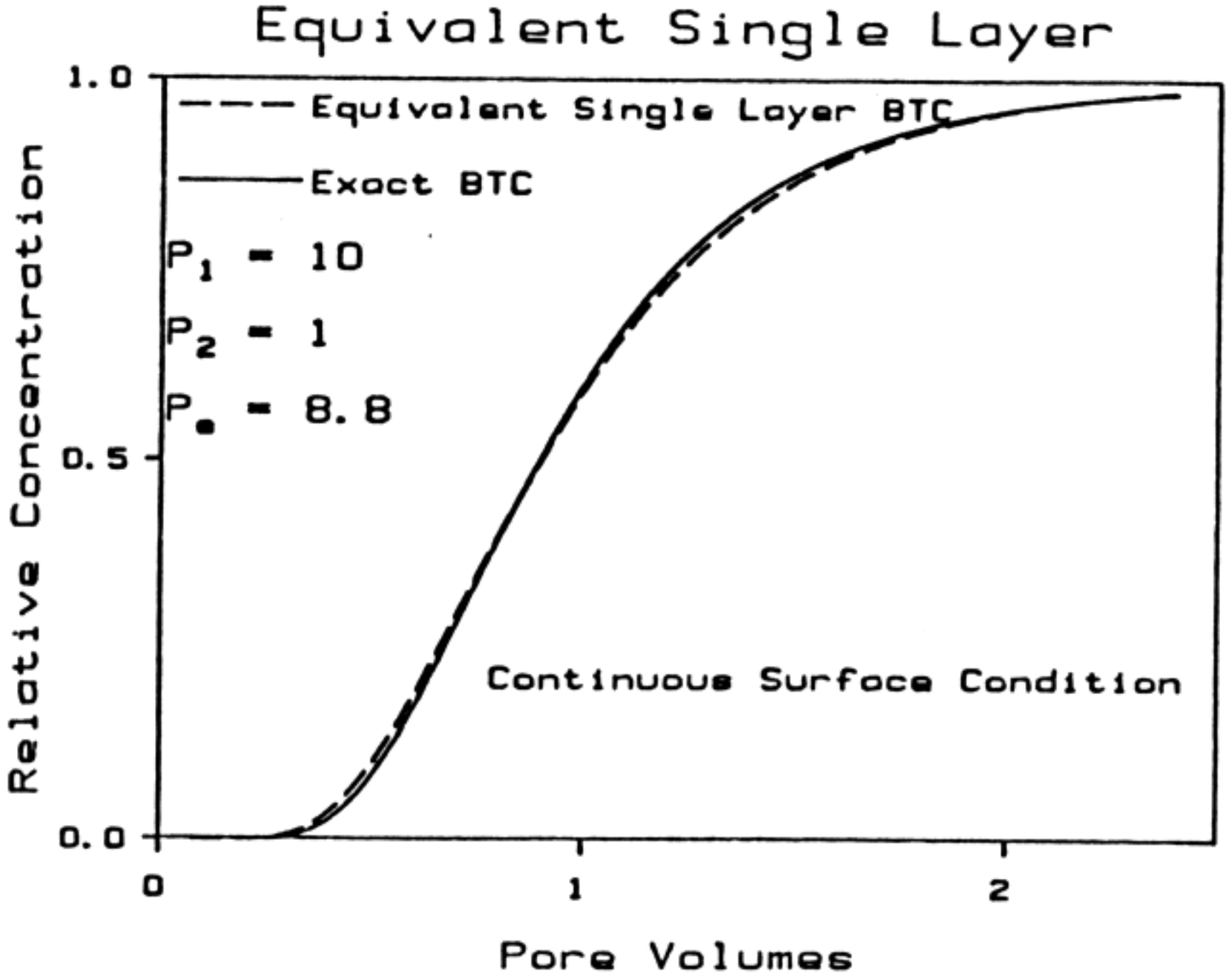

Figure 6.1. Equivalent single-layer predictions when condition (6.19) is satisfied. Note that x/L = 1.5.

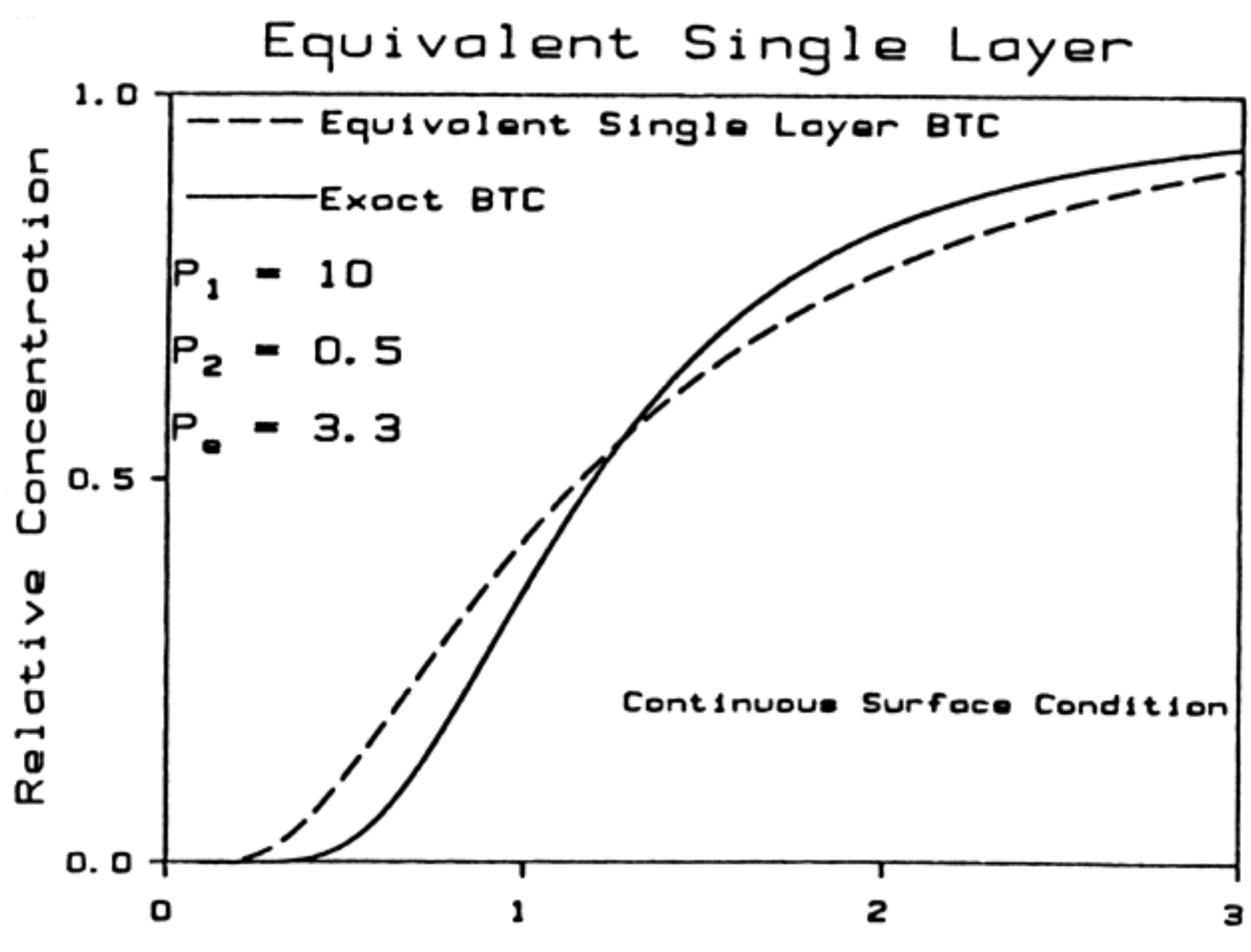

Figure 6.2. Equivalent single-layer predictions when condition (6.19) is not satisfied. Note that x/L = 1.5.

Effect of Layer Ordering

The effect of switching the layer order in a profile may be quantified using the variance calculated for the two-layer system as given in Table 6.1. Because the model assumes a finite first layer and a semi-infinite second layer, we expect that switching layers will generally result in different calculated variances. Note that the mean is unaffected by the layer order. It is of interest to determine when the layer ordering has a noticable effect on breakthrough curves or, conversely, when it has little effect. Layer ordering may be presumed to have negligible effect on breakthrough curves if, for each ordering, the absolute difference between the variances is much less than the sum of the variances, i.e. if

$$\frac{\frac{D_2}{v_2^2}\left[\frac{D_2}{v_2^2} - \frac{D_1}{v_1^2}\right]\left[1 - \exp(-P_2)\right]}{\frac{D_1 L}{v_1^3} + \frac{D_2(x - L)}{v_2^3}} \ll 1, \qquad \frac{D_2 v_1^2}{D_1 v_2^2} > 1 \tag{6.20a}$$

or,

$$\frac{\frac{D_1}{v_1^2}\left[\frac{D_1}{v_1^2} - \frac{D_2}{v_2^2}\right]\left[1 - \exp(-P_1)\right]}{\frac{D_1 L}{v_1^3} + \frac{D_2(x - L)}{v_2^3}} \ll 1, \qquad \frac{D_2 v_1^2}{D_1 v_2^2} < 1 \tag{6.20b}$$

hold. Qualitatively, we observe that condition (6.20) is satisfied if $D_2 v_1^2/(D_1 v_2^2) \simeq 1$, or if one layer is relatively long compared with the other.

Comparison of Semi-Infinite and Finite Solutions

In laboratory tracer experiments, breakthrough curves are obtained from the soil-column effluent. Some uncertainty arises in the proper selection of the lower boundary condition in such experiments. When dispersion is predominantly hydrodynamic in nature and effluent is removed as it exits the column, experimental and theoretical analyses suggest a semi-infinite lower boundary may most adequately represent the system (Chapters 3 and 4). However, when diffusion is the dominant component of the dispersion coefficient and the column is free-draining or an exit line exists in which dispersion is negligible, the boundary condition to be applied at $x = L$, where L is the column length, is $\partial c/\partial x = 0$ (e.g. Wehner and Wilhelm, 1956). Even in this latter case, it is generally more convenient computationally to analyze effluent data using the solution for a semi-infinite system (Parlange and Starr, 1975).

If we interpret the boundary condition, $\partial c/\partial x = 0$, to result from a vanishing dispersion coefficient beyond $x = L$, then the moments of Table 6.1 can be used to derive a condition for which the assumption of a semi-infinite system can be used without sacrificing accuracy. Putting $D_2 = 0$ and setting $x = L$ we again note from Table 6.1 that the semi-infinite and two-layer assumptions give identical means. By comparison of the normalized variances for each case we see that the semi-infinite solution will closely approximate breakthrough curve predictions obtained from the solution for a finite column if

$$[1 - \exp(-P_1)]/P_1 \ll 1. \tag{6.21}$$

In agreement with Parlange and Starr (1978), we find that the assumption of a semi-infinite layer is justified for $P_1 > 16$. This comparison also predicts that the column Péclet number, P_1, can be obtained from the apparent Péclet number, P_{ap}, where the latter has been derived from breakthrough curve data analyzed using the solution for a semi-infinite column, via

$$\frac{1}{P_1} = \frac{1}{P_{ap}} \left\{1 + \frac{1}{P_{ap}} \left[1 - \exp(-P_{ap})\right]\right\}. \tag{6.22}$$

Using a less direct method, a second-order approximation to (6.22) has been reported by Parlange and Starr (1975).

Semi-Infinite Media Approximation: The Convolution Integral

If we approximate a "spike" of solute having mass per unit area m_o injected at the soil surface ($x = 0$), as a Dirac condition, then its distribution is given by

$$c^{\delta}(x,t) = \frac{m_o}{\theta x} \bar{c}^{\delta}(x,t) \tag{6.23}$$

where $\bar{c}^{\delta}$ is a transfer function representing the Dirac solution normalized to unit injected mass per pore volume. Convolution of (6.23) gives the solution for continuous injection as

$$c(x,t) = \int_o^t m_o(\tau)\bar{c}^{\delta}(x,t-\tau)/(\theta x)\, d\tau. \tag{6.24}$$

In (6.23), m_o has been replaced by $m_o(\tau)d\tau$ where m_o is the mass flux density of material at $x = 0$. For influent concentration $c_o(t)$ at hydraulic flux q we have

$$m_o = qc_o \tag{6.25}$$

and so, for $v \equiv q/\theta$,

$$\frac{m_o}{\theta} = c_o v. \tag{6.26}$$

Equation (6.24) then becomes

$$c(x,t) = \frac{v}{x}\int_o^t c_o(\tau)\bar{c}^{\delta}(x,t-\tau)\, d\tau. \tag{6.27}$$

Generalizing to n soil layers gives

$$c(x_n,t) = \frac{v_n}{L_n}\int_o^t c(x_{n-1},\tau)\bar{c}^{\delta}(L_n,t-\tau)\, d\tau \tag{6.28}$$

where x_i, for $i < n$, is the distance from the surface to the end of the i^{th} layer, x_n is the distance to the measurement point, $L_n = x_n - x_{n-1}$, and $v_n = q/\theta_n$. We will refer to (6.28) as the convolution approximation.

For $c_o(t) = 1$, the solution for c(x,t) in a semi-infinite homogeneous medium is well known (Lapidus and Amundson, 1952)

$$c(x,t) = \frac{1}{2}\left\{\operatorname{erfc}\left[\frac{x - vt}{(4Dt)^{1/2}}\right] + \exp\left[\frac{vx}{D}\right]\operatorname{erfc}\left[\frac{x + vt}{(4Dt)^{1/2}}\right]\right\}. \tag{6.29}$$

For this case $\bar{c}^{\delta}(x,t)$ is calculated by equating (6.27) and (6.29) and differentiating with respect to time,

$$\bar{c}^{\delta}(x,t) = \frac{x^2}{vt(4\pi Dt)^{1/2}}\exp\left[\frac{-(x-vt)^2}{4Dt}\right]. \tag{6.30}$$

We wish to investigate when the convolution approximation will accurately predict breakthrough curves from two soil layers. To do this, note that it is possible to expand the non-exponential terms in the numerator of the right-hand side of (6.10), together with the denominator, as a series. For our purposes it is sufficient to note that the leading term of this series is $\bar{c}_o(s)$. Inverting the remaining exponential term gives (6.28) written for two layers where the integrand is defined by (6.29) and (6.30). Again we assume a Dirac condition and calculate moments for this approximation from the Laplace domain solution. These results have been included in Table 6.1. The convolution

approximation has the same mean as the exact two-layer mean. The approximation will yield accurate predictions if there is little difference between the exact and approximate variances, or

$$\frac{\left|\frac{D_2}{v_2^2} - \frac{D_1}{v_1^2}\right|\frac{D_1}{v_1^2}[1-\exp(-P_1)]}{\frac{D_1 L}{v_1^3} + \frac{D_2(x-L)}{v_2^3}} \ll 1 \qquad (6.31)$$

Although not identical, condition (6.31) and condition (6.20) are very similar and will hold under the same general physical criteria. In the majority of cases then, where it is found that the layer ordering has little effect on the breakthrough curve, we expect that the convolution approximation will be accurate (and vice versa).

To obtain the transfer function for the equilibrium convection-dispersion equation given by (6.30) we equated (6.27) and (6.29) and differentiated with respect to time as noted above. This method can be applied easily to any single-layer model. For example, consider the nonequilibrium convection-dispersion model for a soil with mobile-immobile zones (De Smedt and Wierenga, 1979)

$$R_m\theta_m\frac{\partial c_m}{\partial t} + R_{im}\theta_{im}\frac{\partial c_{im}}{\partial t} = \theta_m D_m\frac{\partial^2 c_m}{\partial x^2} - q\frac{\partial c_m}{\partial x} \qquad (6.32)$$

and

$$R_{im}\theta_{im}\frac{\partial c_{im}}{\partial t} = \alpha(c_m - c_{im}) \qquad (6.33)$$

where the subscripts m and im refer to the mobile and immobile zones respectively and α is the mass transfer coefficient. For a continuous injection of solute applied at x = 0, the solution to (6.32) and (6.33) is

$$c_m(x,t) = \frac{v}{x}\int_0^t c(x,\tau)J\left[\frac{\alpha\tau}{R_m\theta_m},\frac{\alpha(t-\tau)}{R_{im}\theta_{im}}\right]\,d\tau \qquad (6.34)$$

where $c(x,\tau)$ is given by (6.30) written for the mobile region parameters, $D = D_m/R_m$ and $v = v_m = q/(\theta_m R_m)$, and J(a,b) is the Goldstein J-function (Goldstein, 1953):

$$J(a,b) = 1 - \exp(-b)\int_0^a \exp(-\tau)I_0[2(b\tau)^{1/2}]\,d\tau, \qquad (6.35)$$

where I_i denotes an i^{th} order modified Bessel function. For this case the transfer function is

$$c_m^{\delta}(x,t) = \frac{\alpha}{(R_m\theta_m R_{im}\theta_{im})^{1/2}}\int_o^t c(x,\tau)\exp\left[-\frac{\alpha\tau}{R_m\theta_m} - \frac{\alpha(t-\tau)}{R_{im}\theta_{im}}\right]\left[\frac{\tau}{t-\tau}\right]^{1/2} I_1\left\{2\alpha\left[\frac{\tau(t-\tau)}{R_m\theta_m R_{im}\theta_{im}}\right]^{1/2}\right\}d\tau$$

$$+ \exp\left[-\frac{\alpha t}{R_m\theta_m}\right]c(x,t). \qquad (6.36)$$

When computing the integral on the right-hand side of (6.36), it is useful to note that as $\tau \to 0$ and t, the integrand $\to 0$ and $c(x,t)\exp[-\alpha t/(R_m\theta_m)] \times \alpha t/(R_m\theta_m R_{im}\theta_{im})^{1/2}$, respectively.

APPLICATION TO EXPERIMENTAL DATA

Shamir and Harleman (1967)

We now apply the above methods to data from experiments reported by Shamir and Harleman (1967) involving continuous injection of NaCl into a medium consisting of several alternating 3.175 cm thick layers of two different granular silica sands. The condition of no retardation is assumed. Shamir and Harleman (1967) give the dispersion coefficients for the two materials as 0.0115 $cm^2\ h^{-1}$ and 0.0465 $cm^2\ h^{-1}$, for a pore water velocity of 0.154 $cm\ h^{-1}$. We note that for these parameters, conditions (6.19), (6.20) and (6.31) are all satisfied. Because layer ordering does not affect the breakthrough curve, the lengths of the alternating layers can be summed, and the system analyzed as if it consisted of two layers with lengths of, for layer 1, 41.6 cm and, for layer 2, 41.3 cm. The results of the convolution approximation, via (6.28), with $c(x_{n-1},t)$ given by (6.29), and the transfer function by (6.30), previously given by Shamir and Harleman (1967), is shown as the solid line in Figure 6.3. This prediction was checked by comparison with a numerical solution which yielded an identical breakthrough curve.

For a finite-duration input signal, it is of interest to note that although the equivalent single layer has the same mean and variance as the exact two-layer model, its predictions are less accurate than the convolution approximation (Figure 6.3), which has the same mean but different variance. (This statement is meaningless in the case of a continuous input although, as already noted, the equivalent layer parameters remain unaffected.) The reason for this is that the calculated moments of second order and higher can be affected noticeably by the tail of the distribution, in which case the distribution's skewness should be considered explicitly in the calculation of the equivalent parameters. An alternative approach is to calculate the equivalent parameters using *weighted* moments, which weight the main body of the signal at the expense of the less-important tail. The most useful weighting function is $\exp(-\chi t)$, where χ is the weighting factor. Equation

(6.11) becomes

$$w_j = \int_o^\infty t^j \exp(-\chi t) c(x,t)\ dt, \qquad j = 0,\ 1,\ 2,... \qquad (6.37)$$

where the w_j are the exponentially weighted moments. Unweighted moments given by (6.11) are calculated using $\chi = 0$. Nauman and Buffham (1983) suggest the mean as a reasonable weighting factor.

Panigatti (1970)

Panigatti (1970) measured Cl breakthrough curves from homogeneous and two-layered soil columns. Evidence of mobile-immobile soil regions was observed. The breakthrough curves used here are for Norge loam, from Perkins, Oklahoma, and Stratford I soil, from Stratford, Oklahoma. The porosities of these soils were 0.345 and 0.243, respectively, and the experimental hydraulic flux was fixed at 1.78 cm h^{-1}. The columns in the study were 30 cm long (layers of 15 cm were used for the layered experiments) with a diameter of 7.5 cm. Solute was applied as a pulse in each experiment. We found that the mass of Cl calculated by integrating under the given breakthrough curves differed slightly from the input quantities given by Panigatti (1970). We assume that no irreversible reactions of Cl take place and so the durations of the applied solute pulses were adjusted to conserve mass of Cl.

Figures 6.4 and 6.5 show the measured and fitted breakthrough curves for the Stratford I and Norge soils, respectively, obtained using the parameters listed in each figure assuming retardation factors of unity. In this case we make use of the convolution approximation, substituting (6.34) and (6.36) into (6.28). To ascertain the numerical precision of the convolution calculation, results for the homogeneous Stratford I soil, treated computationally as two identical 15 cm layers, were checked against the exact, single-layer solution given by (6.34). No discernible difference between the one- and two-layer curves was observed.

Panigatti (1970) found no significant difference between breakthrough curves for the Norge - Stratford I layering or the reverse order. In Figure 6.6 we show the approximation's accurate predictions for the Norge - Stratford I ordering.

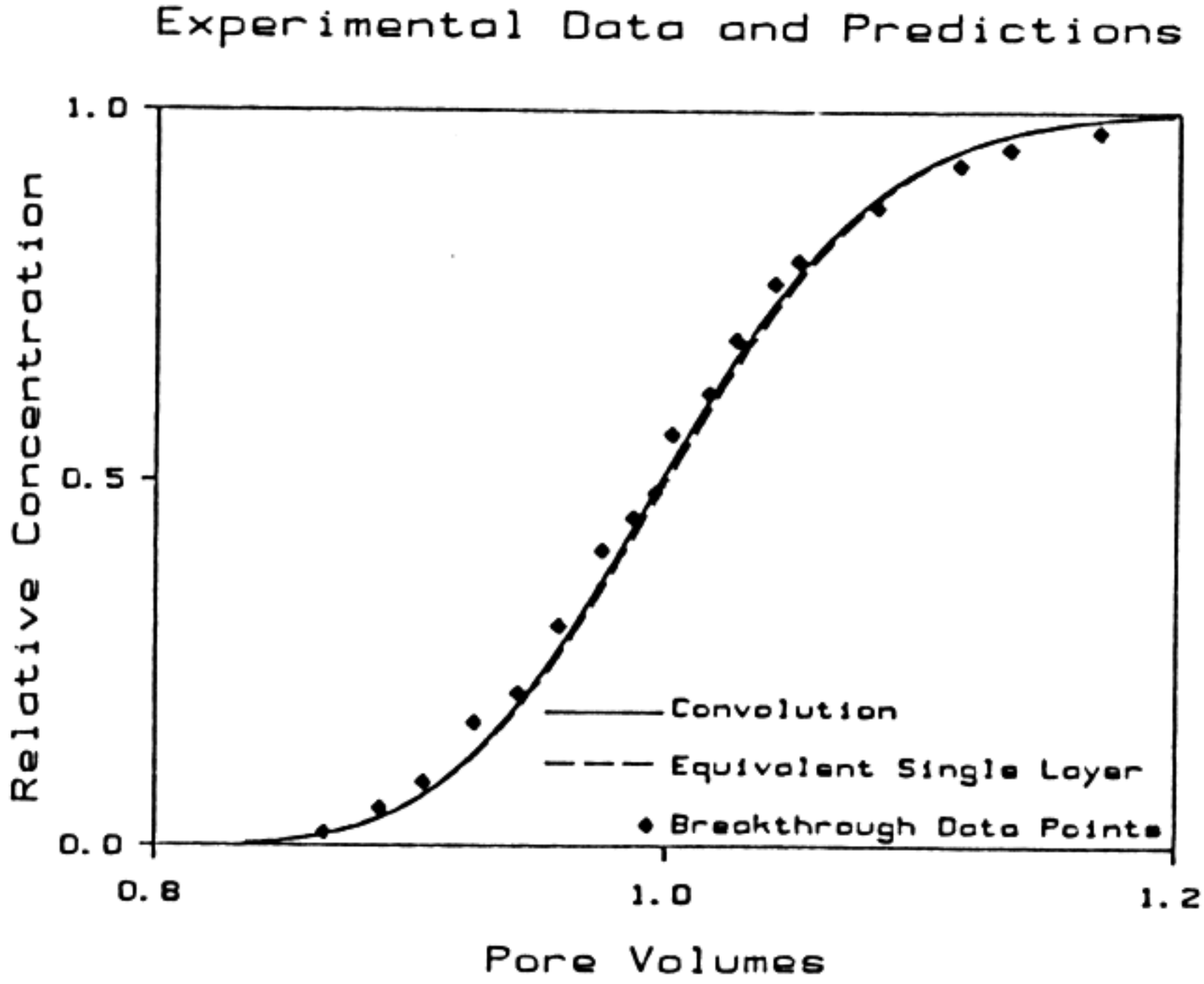

Figure 6.3. Approximations compared with experimental data from Shamir and Harleman (1967).

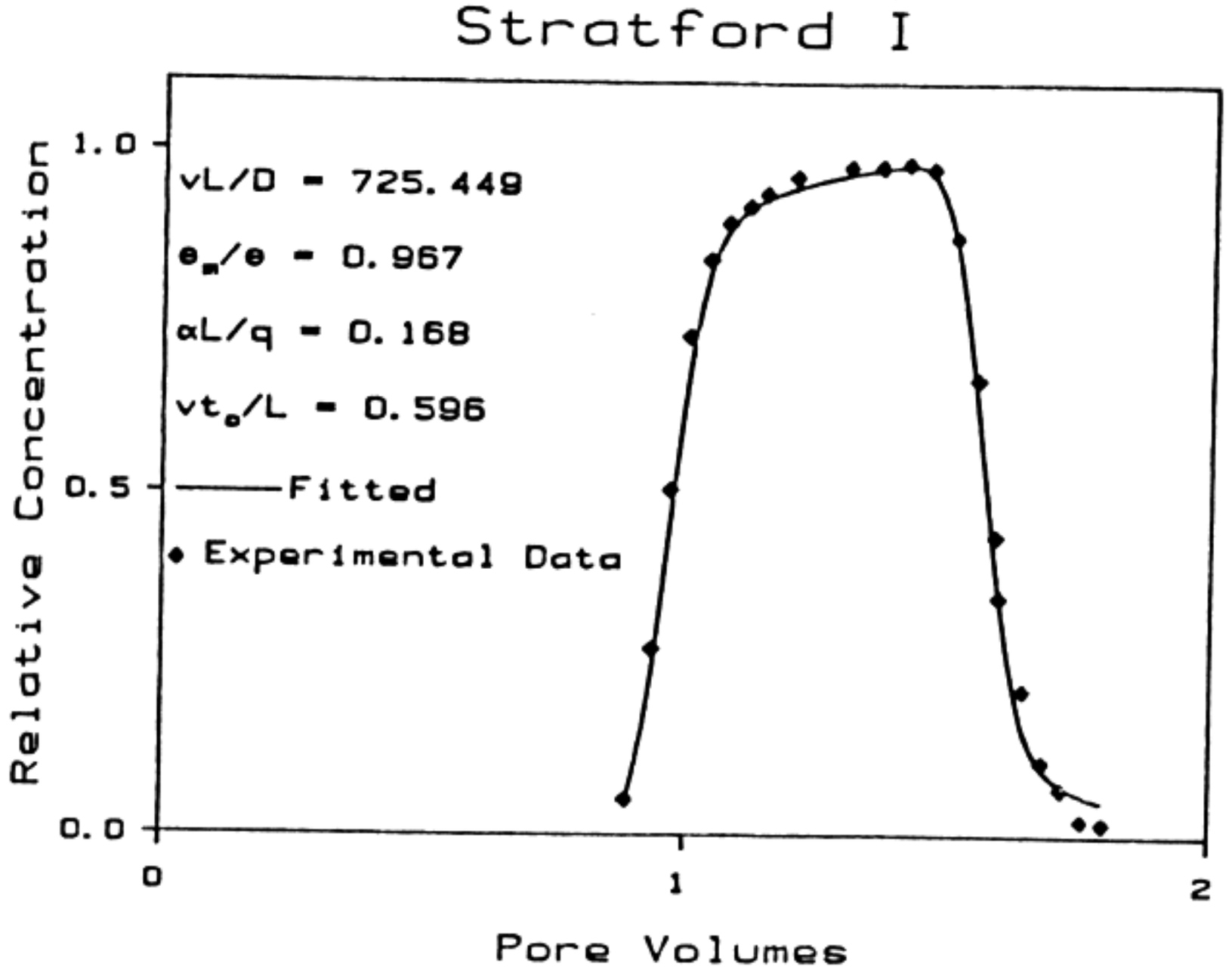

Figure 6.4. Best fit of the mobile-immobile model to experimental data from Panigatti (1970) for the Stratford I soil.

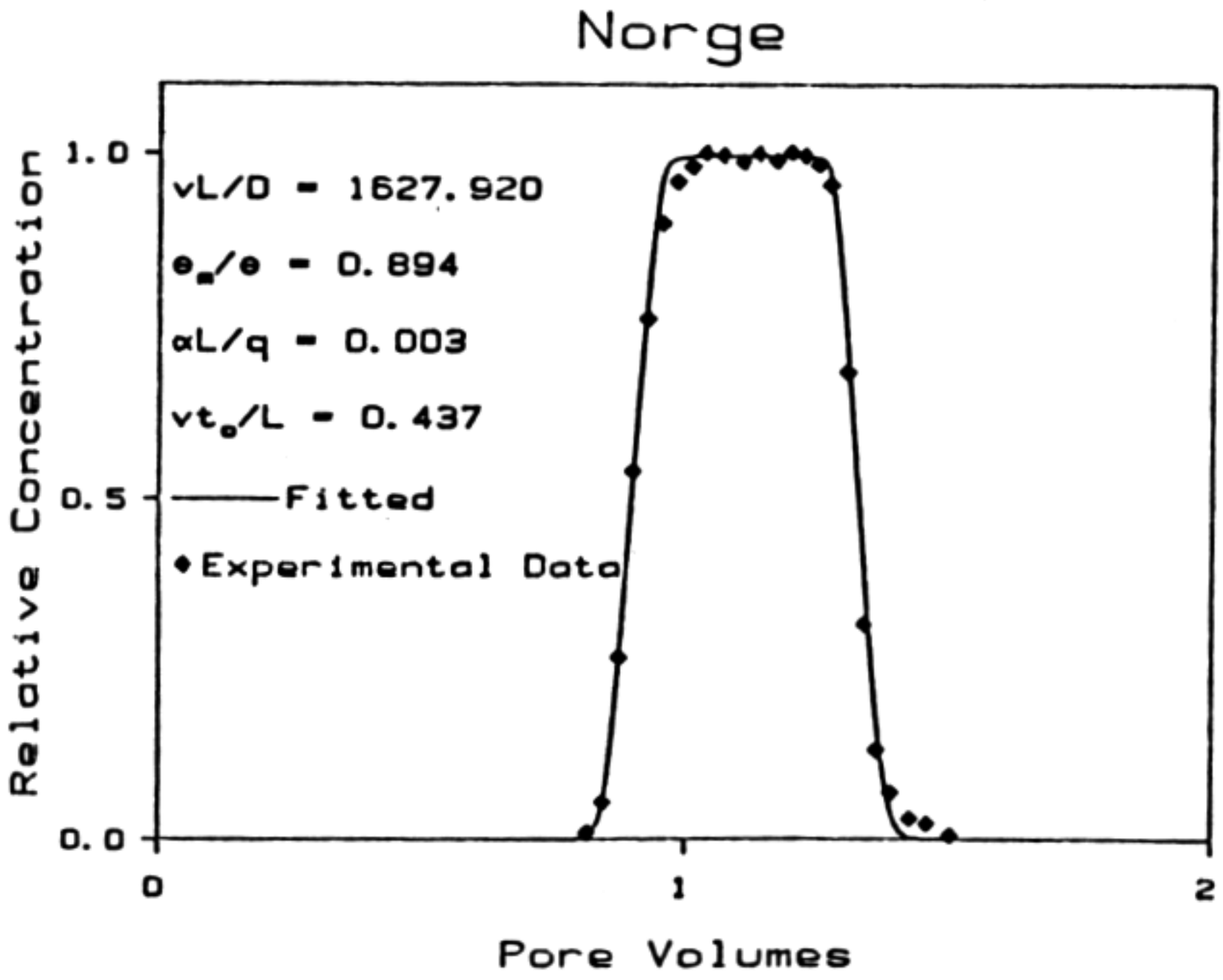

Figure 6.5. Best fit of the mobile-immobile model to experimental data from Panigatti (1970) for the Norge soil.

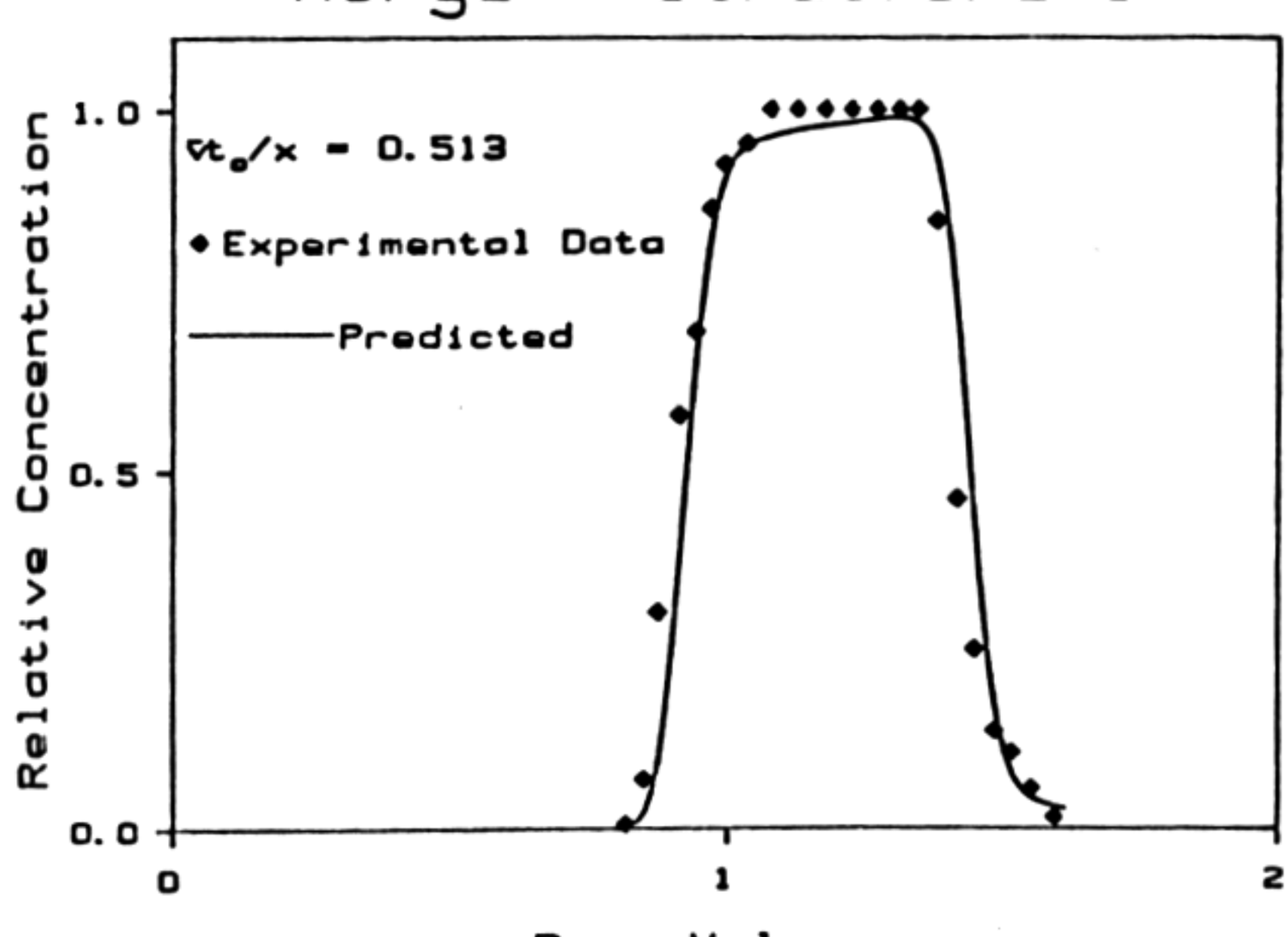

Figure 6.6. Convolution approximation prediction of the breakthrough curve compared with experimental data from Panigatti (1970) for two 15 cm layers consisting of Norge overlaying Stratford I.

CONCLUSIONS

Analytical approaches to transport in layered media may employ averaging techniques to treat the profile as a homogeneous single layer, or treat each layer independently as if there were no interactions between layers and make use of the convolution integral. We have analyzed the feasibility and validity of these approximations with particular reference to predictions of breakthrough curves from two layers. The results of this study can be very useful in practice. For example, Monte Carlo simulations of field solute transport generally require large numbers of realizations of the random process to be generated, and hence substantial computer time, for reasonable estimates of population means and variances (e.g. Persaud *et al.*, 1985). This problem is compounded for layered systems. Thus, if accuracy criteria are satisfied, analytical approximations such as those given here can markedly reduce computational costs without loss of precision in the results.

It is apparent that the simplest and most straightforward way to predict breakthrough curves from a two-layer system is to use the equivalent single-layer approximation. Transport parameters for the equivalent layer are easily found by equating means and variances for the one- and two-layer systems.

A more accurate approximation is given by the convolution integral which assumes that layer interactions have no significant effect on solute transport. Again by comparing the moments of the approximation with the exact moments, a criterion for the validity of this approach was obtained. The approximation was also applied to experimental data using a transport model incorporating the assumption of mobile-immobile zones within the soil.

CHAPTER 7

MONOCONTINUUM ANALYSIS OF UNSATURATED FLOW

Natural soil profiles commonly exhibit pronounced heterogeneities in relation to properties controlling water movement. As a result, measured distributions of these properties, e.g. hydraulic conductivity, tend to log-normal rather than normal (e.g. Nielsen et al., 1973) and the number of data points required to describe the distribution with any precision is relatively large. Unfortunately, it appears that the effort needed to adequately characterize field profiles is too prohibitive to allow accurate predictions of water movement to be made, even if the measurements leave the profile intact. In any case, given that the necessary parameter information is available, the highly nonlinear equations to be solved numerically require substantial computing power and time. Thus we seek methods which will alleviate data collection and computing needs while maintaining accuracy in model predictions.

The nonlinearities involved in the related problem of solute transport can generally be addressed more satisfactorily and, in many cases, a linear version of the particular transport scenario can be devised or assumed. The assumption of a nonreactive chemical or of a linear isotherm would be examples of the latter. Because of the linearity assumption, these cases can be treated by numerous mathematical techniques. Therefore, in the description of chemical transport in saturated aquifers, sophisticated and elegant analyses have been reported (e.g. Smith and Schwartz, 1980; Grisak and Pickens, 1981; Bhattacharya and Gupta, 1983; Gillham et al., 1984; Güven et al., 1984). Similar approaches have been applied to descriptions of water movement in both saturated (e.g. Gelhar, 1974) and unsaturated regimes (e.g. Bhattacharya et al., 1976; Andersson and Shapiro, 1983).

Obvious heterogeneities in field soils are relatively large continuous pores or fractures caused, perhaps, by worms or plant roots which have subsequently decayed. These features are commonly termed macropores and have been shown experimentally to have substantial effects on water infiltration, redistribution and drainage in soil profiles. Bouma and Wösten (1979) found that water and solute moved much more rapidly in soils with macropores, and concluded that extrapolating from "equivalent" pore diameters to prediction of breakthrough curves was not possible. Bouma et al. (1977) showed different behaviors for various types of macropores found in practice under saturated conditions, while the study Bouma et al. (1982) showed that macropores could be cast into functional categories by measuring, rather than calculating, infiltration rates. In another, more recent, paper, Smettem and Collis-George (1985b) were able to predict the steady-state ponded infiltration rate in a field soil from the experimentally-measured macropore distribution.

In a controlled numerical experiment Edwards et al. (1979) showed that the macropore geometry and density in a soil profile have large effects on the amount of infiltration and runoff occurring at the soil surface when there is enough water to supply the macropores, at least for the conditions of their

simulations which were assumed to mimic field conditions. The condition of there being enough water to supply the macropores comes from the assumption that the micropores must reach saturation before water flow in macropores begins. Later laboratory experiments of Germann and Beven (1981) reached similar conclusions.

Beven and Germann (1981) presented an analytical approximation to the above case. Their model distinguished between micropore and macropore regions. Flow in the macropores occurred as the micropores at the upper flux-controlled boundary became saturated and was divided into specific saturated and unsaturated portions. A slightly more realistic model was discussed by Beven and Clark (1986). After in- filtration into a particular macropore was initiated, radial flow into the surrounding micropores was modeled following Green and Ampt (1911). Assuming a Poisson distribution of macropores, the model for a single channel was then extended to a population of channels. It is interesting to note that Smettem and Collis-George (1985a) found that the macropores in their ex- perimental soil also followed a Poisson distribution.

Macropores represent a particular type of heterogeneity found in soils. The mathematical models and experiments discussed here are evidence that there is a perceived need for models considering specific well-defined heterogeneities. Our purpose is to investigate the feasibility of predicting water flow in vertically-stratified two- or three-dimensional soils through a simple averaging procedure to yield an approximately equivalent homogeneous one-dimensional system. The vertical stratification is assumed to be comprised of adjacent zones made up of soils with different retention and hydraulic properties. We focus on soils with saturated conductivities that differ by an order of magnitude or more. It can be seen that macropores are a specific case of the system under consideration.

NUMERICAL EXPERIMENT

To first provide some motivation for the averaging presented later, a numerical simulation will be examined. We consider the profile represented schematically in Figure 7.1. The profile consists of two well-defined regions. Region 1, which accounts for the majority of the profile (85.8% by area), is defined as a low permeability zone with a saturated conductivity, K_s, of 0.1 cm h^{-1}. Region 2 is a zone of relatively high permeability with K_s = 1 cm h^{-1}. We use the retention function proposed by Brooks and Corey (1966),

$$\theta = \frac{\theta - \theta_r}{\theta_s - \theta_r} = \begin{cases} \left[\frac{h_b}{h}\right]^{\lambda}, & h < h_b \\ 1, & h \geq h_b \end{cases} \qquad (7.1)$$

where θ is the normalized water content ($0 \leq \theta \leq 1$), θ [= $\theta(h)$] ($cm^3 cm^{-3}$) is the water content, θ_r ($cm^3 cm^{-3}$) is the residual water content, θ_s ($cm^3 cm^{-3}$) is the saturated water content, h_b (cm water) is the "bubbling" or "air-entry"

pressure, h (cm water) is the matrix tension and λ is an arbitrary exponent which is considered to be an index of the soil pore-size distribution (Lenhard, 1986).

To calculate the relative conductivity we assume an isotropic conductivity tensor and follow Brooks and Corey's prescription and use the so-called Burdine (Burdine, 1953) integral

$$K_r = \frac{K(\theta)}{K_s} = \theta^2 \frac{\int_0^\theta \frac{dw}{h^2(w)}}{\int_0^1 \frac{d\theta}{h^2(\theta)}} \qquad (7.2)$$

where K (cm h^{-1}) is the conductivity, K_r is the relative conductivity and w is the dummy variable of integration. Substituting from (7.1) into (7.2) gives

$$K_r = \theta^{3+2/\lambda} \qquad (7.3a)$$

or, equivalently,

$$K_r = \begin{cases} \left[\frac{h_b}{h}\right]^{3\lambda+2}, & h < h_b \\ 1, & h \geq h_b. \end{cases} \qquad (7.3b)$$

Note that for the scheme to be presented later the specific form of the retention and conductivity functions is unimportant. We could just as easily use any of the retention functions in the literature such as the one presented by van Genuchten (1980). Similarly, Mualem (1976) has suggested an alternative to (7.2), or an empirical "exponential" or "power-law" relative conductivity relation could be used. The advantage of using (7.1) and (7.3) is that they are discontinuous. It will become apparent later that this feature provides a very stringent test of the theory.

Table 7.1. Parameters used to describe the soils of Fig. 7.1.

	θ_r($cm^3 cm^{-3}$)	θ_s($cm^3 cm^{-3}$)	h_b(cm water)	λ	K_s(cm h^{-1})
Region 1	0.1	0.5	-50	0.1	0.1
Region 2	0.05	0.4	-10	0.25	1

We wish to simulate flow through adjacent soils with large differences in hydraulic properties. The parameter values given in Table 7.1 correspond to a sand (region 1) and a clay (region 2) (Clapp and Hornberger, 1978). Using the parameters of Table 7.1 and the system depicted in Figure 7.1, a ponded infiltration event was simulated using the two-dimensional finite-element code HYDRO (Kaluarachchi and Parker, 1986). The profile was in equilibrium prior to the beginning of the simulation, i.e. at time $t = 0$. The coordinate system origin (0,0) is located at the upper left corner of the region in Figure 7.1, with x being the distance in the horizontal direction and z being the distance in the vertical direction (measured positive downwards). For $t > 0$ the boundary conditions shown in Figure 7.1 were imposed.

In this simulation it was observed that the total water flux at the interface of the two regions was at least an order of magnitude less than the corresponding vertical flux in the region from the surface to the wetting front. It is apparent that, as a result of the disparate conductivities between the two regions, the two-dimensional simulation behaves like two separate and essentially independent one-dimensional soil columns. To confirm this, the average retention function for the flow domain of Figure 7.1 was calculated for both the two-dimensional and independent parallel one-dimensional analyses. To determine the average retention function for the two-dimensional analysis, the domain was divided into horizontal slices corresponding to the finite-element discretization. Along each of the slices the average water content was calculated from

$$\theta_{ex} = \frac{\sum_{j=1}^{m} \theta_j A_j}{\sum_{j=1}^{m} A_j} \qquad (7.4)$$

where θ_{ex} is the "exact" averaged water content in the layer and m is the number of elements in that layer. The averaged tension in the layer could be calculated in a manner similar to (7.4) however the average would be skewed towards elements with tensions of large magnitude. Such a procedure would give meaningless results in terms of the mass of water being moved through the profile since large tensions only occur in dry soils. Therefore the tension in each element is weighted by the corresponding mass of water in that element and so the "exact" average tension, h_{ex}, in each layer is given by

$$h_{ex} = \frac{\sum_{j=1}^{m} h_j \theta_j A_j}{\sum_{j=1}^{m} \theta_j A_j}. \qquad (7.5)$$

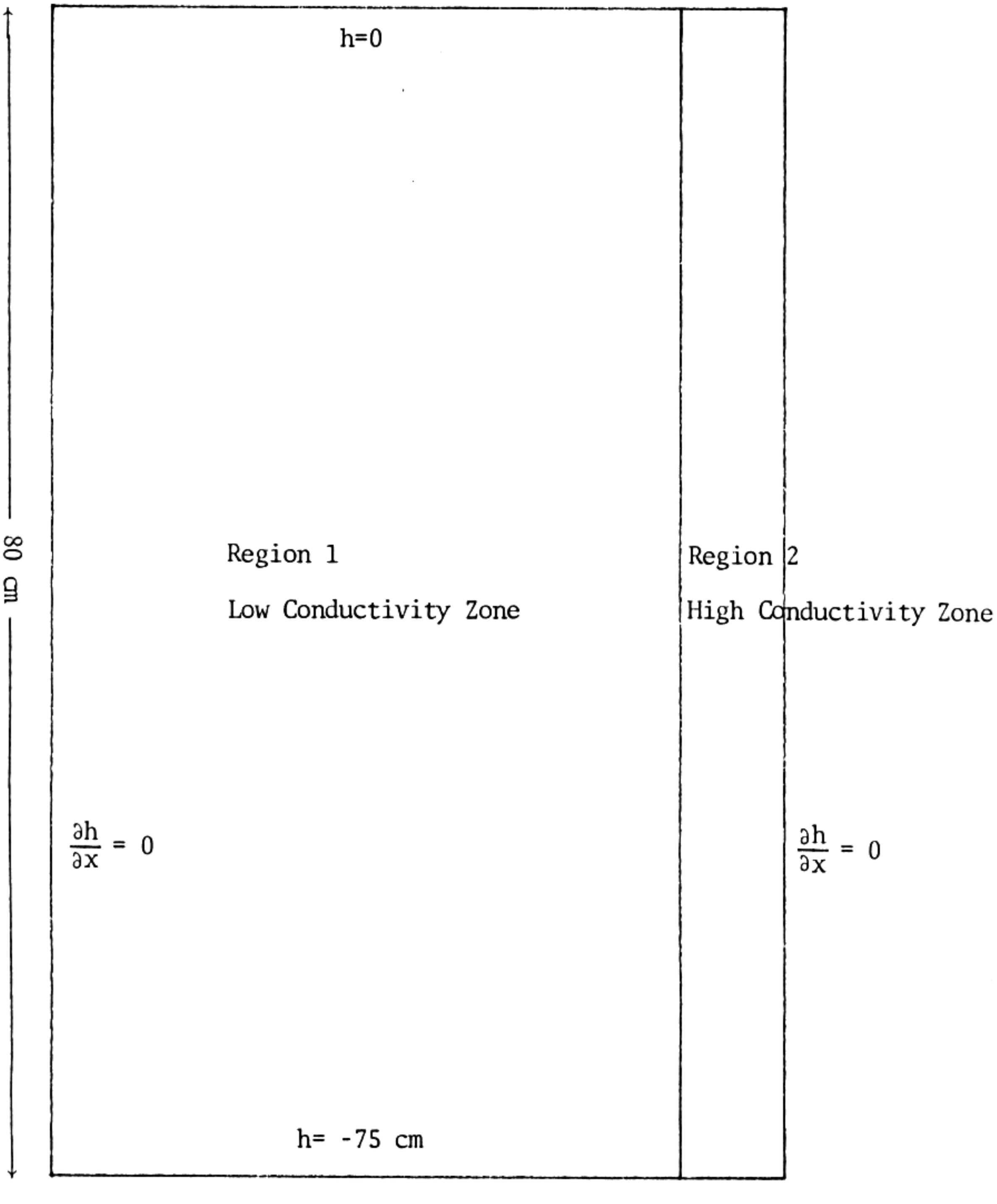

Figure 7.1. Diagram of flow domain used in the numerical experiments.

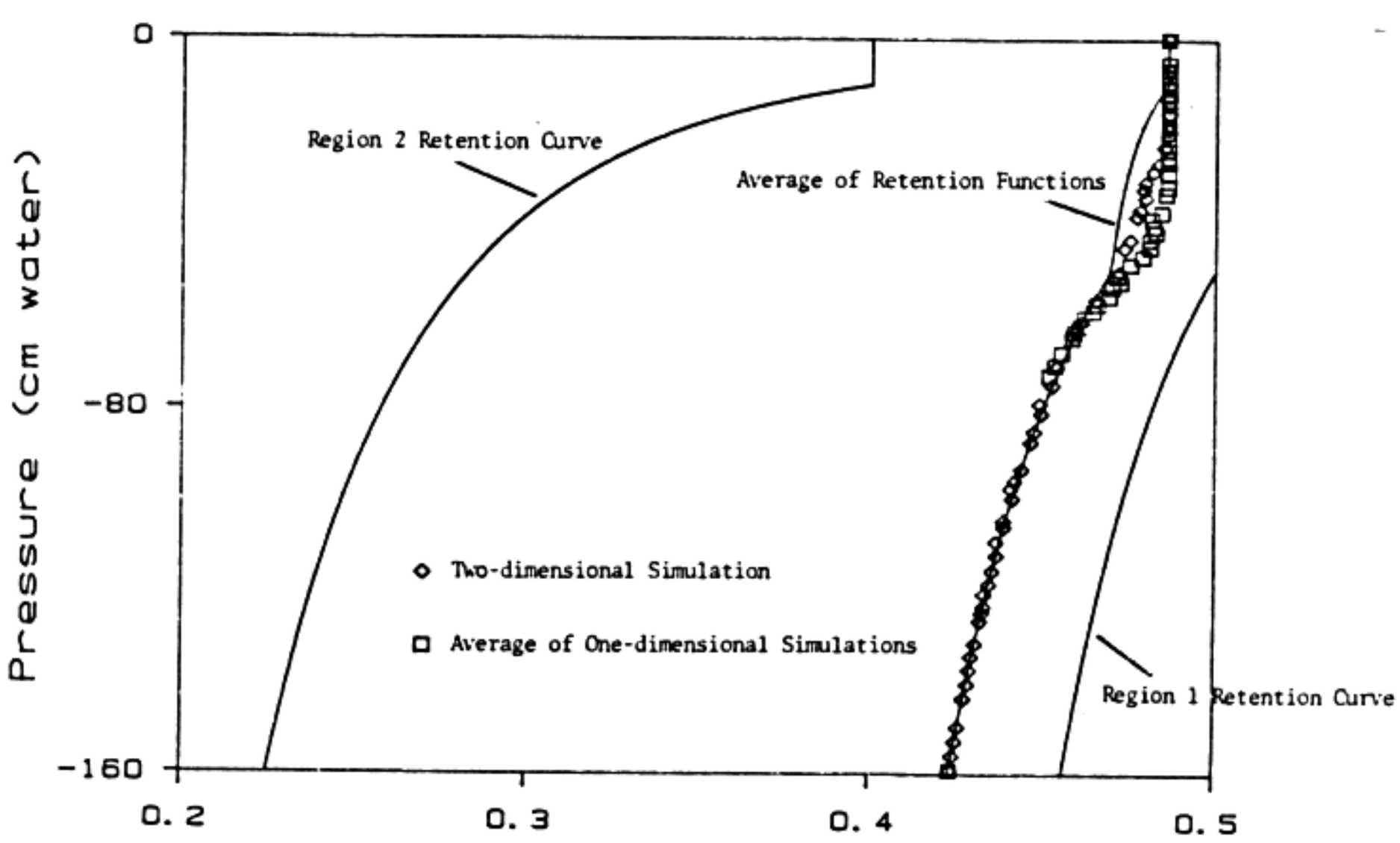

Figure 7.2. Region 1 and Region 2 retention curves and averages.

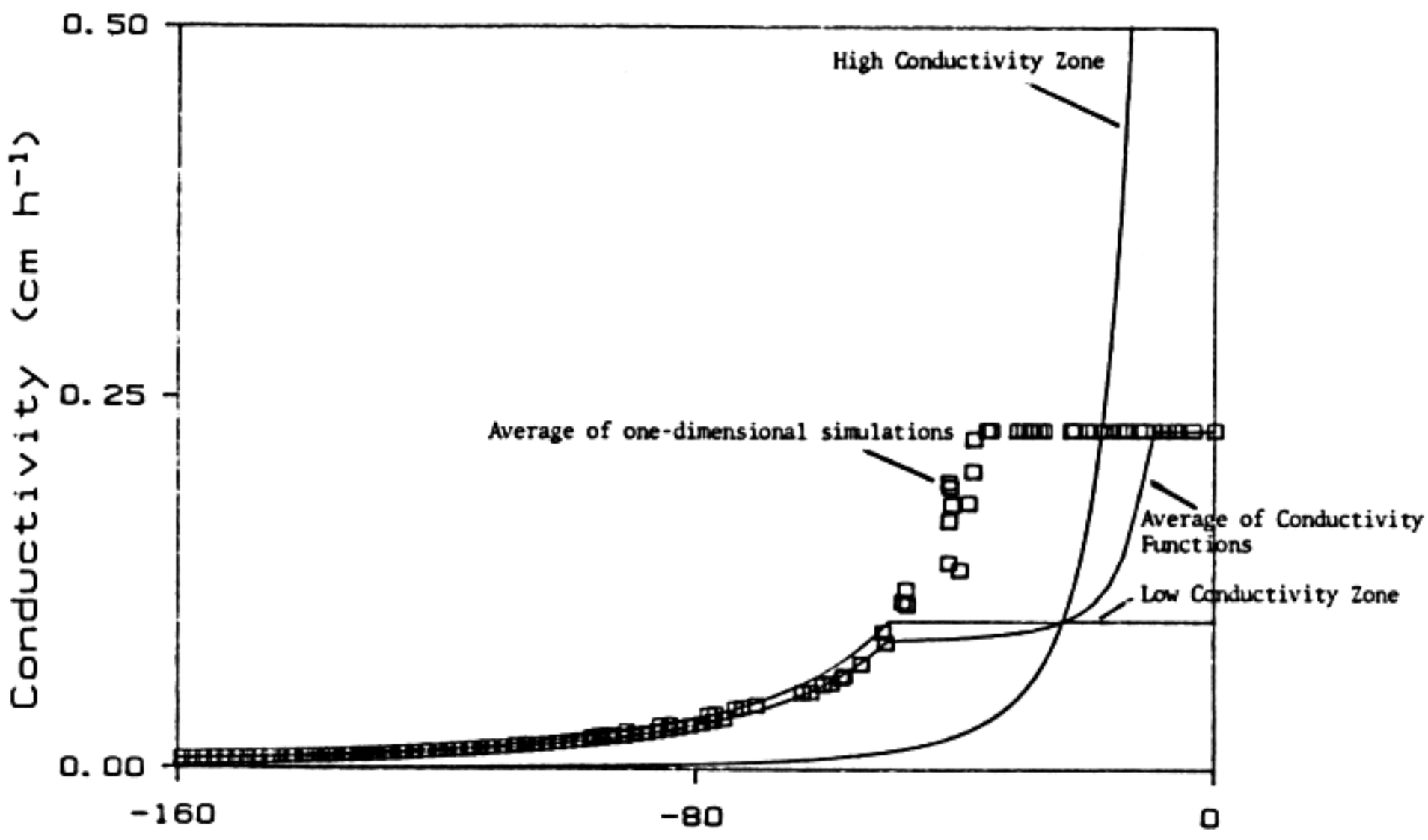

Figure 7.3. Region 1 and Region 2 conductivity functions compared with average of one-dimensional simulations (squares) and average of conductivity functions (————).

The data points (diamonds) in Figure 7.2 were calculated using (7.4) and (7.5) from the two-dimensional simulation results and may be compared with the corresponding function computed as the volume-weighted average of two one-dimensional simulations (squares). Note that in the lower part of the retention curve no squares are plotted as they would obscure the exact results. It is clear that the average of the one-dimensional simulations closely approximate the exact two-dimensional results. Retention curves for the two separate porous media are also given in Figure 7.2.

AVERAGING SCHEME

Our basic assumption is that regions of soil with marked differences in hydraulic conductivities can be treated independently as one-dimensional soil columns. We have indicated above that this is seems a reasonable approximation. Solving a number of one-dimensional problems is far more economical and numerically stable than solving the complete two- or three-dimensional system. The second step is to examine the feasibility of modeling the complete system as a single one-dimensional profile. Our aim is to determine the limits of such an approach using representative simulations of field conditions.

Averaged Retention Function

Assume again that the soil profile is vertically stratified and composed of several well-defined soils, each with a known retention function $\theta(h)$, and that the hydraulic conductivity of adjacent soils differs by an order of magnitude or more. The averaged retention function, $\theta_{av}(h_{av})$, over n such regions at any particular depth is

$$\theta_{av}(h_{av}) = \frac{1}{v_t} \sum_{i=1}^{n} v_i \theta_i(h_i) \qquad (7.6)$$

where the subscript i refers to the particular soil region, v_i is the volume of each soil, v_t is the total volume of soil, θ_i is the retention function for soil i, and h_i is the tension in soil i at the depth of interest. Equation (7.6) will be essentially exact for soils which can be treated as independent columns. In general it will be impossible to predict h_i and so, to calculate θ_{av} we invoke the additional assumption $h_i = h_{av}$ where h_{av} is some mean tension in the system. Equation (7.6) becomes

$$\theta_{av}(h_{av}) = \frac{1}{v_t} \sum_{i=1}^{n} v_i \theta_i(h_{av}) \qquad (7.7)$$

In Figure 7.2 we compare the predictions of (7.7), given by the middle solid line, with the results of the above numerical simulation. In this case we take n = 2 and calculate θ_{av} using (7.1) as

$$\theta_{av} = \begin{cases} \frac{v_1}{v_t}\left[\theta_{r1}+(\theta_{s1}-\theta_{r1})\left(\frac{h_{b1}}{h_{av}}\right)^{\lambda_1}\right] + \frac{v_2}{v_t}\left[\theta_{r2}+(\theta_{s2}-\theta_{r2})\left(\frac{h_{b2}}{h_{av}}\right)^{\lambda_2}\right], & h_{av} < h_{b1} \\ \frac{v_1}{v_t}\theta_{s1} + \frac{v_2}{v_t}\left[\theta_{r2}+(\theta_{s2}-\theta_{r2})\left(\frac{h_{b2}}{h_{av}}\right)^{\lambda_2}\right], & h_{b1} \leq h_{av} < h_{b2} \\ \frac{v_1}{v_t}\theta_{s1} + \frac{v_2}{v_t}\theta_{s2}, & h_{b2} < h_{av} \end{cases} \quad (7.8)$$

where the subscript 1 or 2 refers to Region 1 or 2 respectively. Note that the normalized average water content, θ, is defined as

$$\theta = \frac{\theta_{av} - \theta_{rav}}{\theta_{sav}-\theta_{rav}} \quad (7.9a)$$

where θ_{rav} (cm^3cm^{-3}) and θ_{sav} (cm^3cm^{-3}) are the averaged residual and saturated normalized water contents defined by

$$\theta_{rav} = \frac{1}{v_t}\sum_{i=1}^{n} v_i\theta_{ri} \quad (7.9b)$$

and

$$\theta_{sav} = \frac{1}{v_t}\sum_{i=1}^{n} v_i\theta_{si}. \quad (7.9c)$$

It is clear that the h_{ex} calculated from (7.5) is identical to h_{av} for the limiting case where each element in a particular layer has equal matrix tension. This is the case at the beginning of the simulation since we begin with an equilibrium profile. The approximation given by (7.7) is seen to provide a reasonable description of the "exact" averages, (7.4) and (7.5). The main discrepancy lies between the air-entry pressures and is due partly to the assumption contained in (7.7) but also to the discontinuity in the Brooks-Corey retention function. A continuous retention function would be less prone to such an error. As time increases the exact averages begin to diverge from the approximate average due to the assumption of equal tensions throughout each layer becoming less valid. We observe, however, that the divergence is minimal for several hours; the simulations used to obtain the one-dimensional averages were continued until t = 10 h. Under natural or agricultural conditions, such times for ponded infiltration are unlikely to be exceeded often, and that the approximation (7.7) may have practical use.

Averaged Conductivity Function

We use a volume-weighted average of the conductivity functions (K) in each soil. Similarly to (7.4) we have

$$\mathbf{K} = \frac{1}{v_t} \sum_{i=1}^{n} K_i v_i \qquad (7.10)$$

where K_i is the conductivity function for the i^{th} region. When the entire profile is saturated then (7.10) gives the average saturated conductivity, K_{sav}, as

$$K_{sav} = \frac{1}{v_t} \sum_{i=1}^{n} K_{si} v_i \qquad (7.11)$$

where K_{si} is the saturated conductivity of the i^{th} region. Thus in the limiting case of the profile approaching saturation, (7.10) reduces to the correct averaged saturated conductivity given by (7.11).

In terms of the above example we have n = 2 and substituting (7.3b) into (7.10) gives

$$\mathbf{K} = \begin{cases} v_1 K_{s1} \left[\frac{h_{b1}}{h_{av}}\right]^{\lambda_1} + v_2 K_{s2} \left[\frac{h_{b2}}{h_{av}}\right]^{\lambda_2}, & h_{av} < h_{b1} \\ v_1 K_{s1} + v_2 K_{s2} \left[\frac{h_{b2}}{h_{av}}\right]^{\lambda_2}, & h_{b1} \leq h_{av} < h_{b2} \\ v_1 K_{s1} + v_2 K_{s2}, & h_{b2} < h_{av}. \end{cases} \qquad (7.12)$$

We wish to compare the averaged conductivity predicted by (7.12) with the exact averaged conductivity from the average of the one-numerical simulations. At any arbitrary depth, z, at the i^{th} node of the finite-element grid the flux, q_i, is given by Darcy's law as

$$q_i = K_i \left[\frac{\partial h_i}{\partial z} + 1\right]. \qquad (7.13)$$

Since q_i is known, the "exact" averaged conductivity, K_{ex}, for the total of all the different soils is calculated from

$$K_{ex} = \frac{1}{v_t} \sum_{i=1}^{n} K_i v_i = \frac{1}{v_t} \sum_{i=1}^{n} \frac{q_i}{\frac{\partial h_i}{\partial z}_{+1}} \qquad (7.14)$$

Our purpose in using the Brooks-Corey formulation now becomes clear on examination of Figure 7.3. Similarly to Figure 7.2 the approximation shows most discrepancy between the bubbling pressures. As stated above this error occurs because the tensions in each region differ substantially and so assuming an h_{av} is no longer valid. This error is less apparent for retention functions with no discontinuities. It is clear that the error disappears completely for soils with identical bubbling pressures and it is interesting to note from Figures. 7.2 and 7.3 that the approximation becomes more accurate for increasingly unsaturated conditions.

APPLICATION OF AVERAGING SCHEME

To ascertain the accuracy of the averaging scheme its predictions will be compared with numerical results for three representative cases. In each case the numerical results are obtained from averaging the results of one-dimensional simulations run using the finite element code WORM of van Genuchten (1986) with parameters in Table 7.1

Ponded Infiltration

The first case considered is ponded infiltration into a profile initially at equilibrium. The flow domain is shown in Figure 7.4. We take the pressure at the lower boundary to be fixed at -200 cm water (boundary and initial condition set 1). Figure 7.4 shows the profile is 99 cm in depth and at equilibrium initially. The tension at the surface prior to ponding is -299 cm water. In Figure 7.5 we show the cumulative infiltration into each region from t = 0 through 5 h. The empirical average shows an over-estimation of the cumulative infiltration with increasing time, however its accuracy would seem to be adequate for most purposes.

Infiltration into Macropores

Consider the situation of a soil containing vertical macropores which reach the soil surface. If water is applied to the soil at a constant flux greater than the saturated conductivity of the micropores (i.e. the pores in the soil matrix) then it is assumed (Germann and Beven, 1981) that flow in the macropores will not begin until ponding occurs (at time t_p). At this time the entire surface is ponded.

This case was followed here except that prior to t_p a constant flux of 0.5 cm h^{-1} was applied to the whole surface as shown in Figure 7.4 (boundary and initial condition set 2). Figure 7.6 shows that the predicted average infiltration is essentially exact until t = 4 h. After this time the approximation overestimates the actual infiltration slightly in common with the previous case.

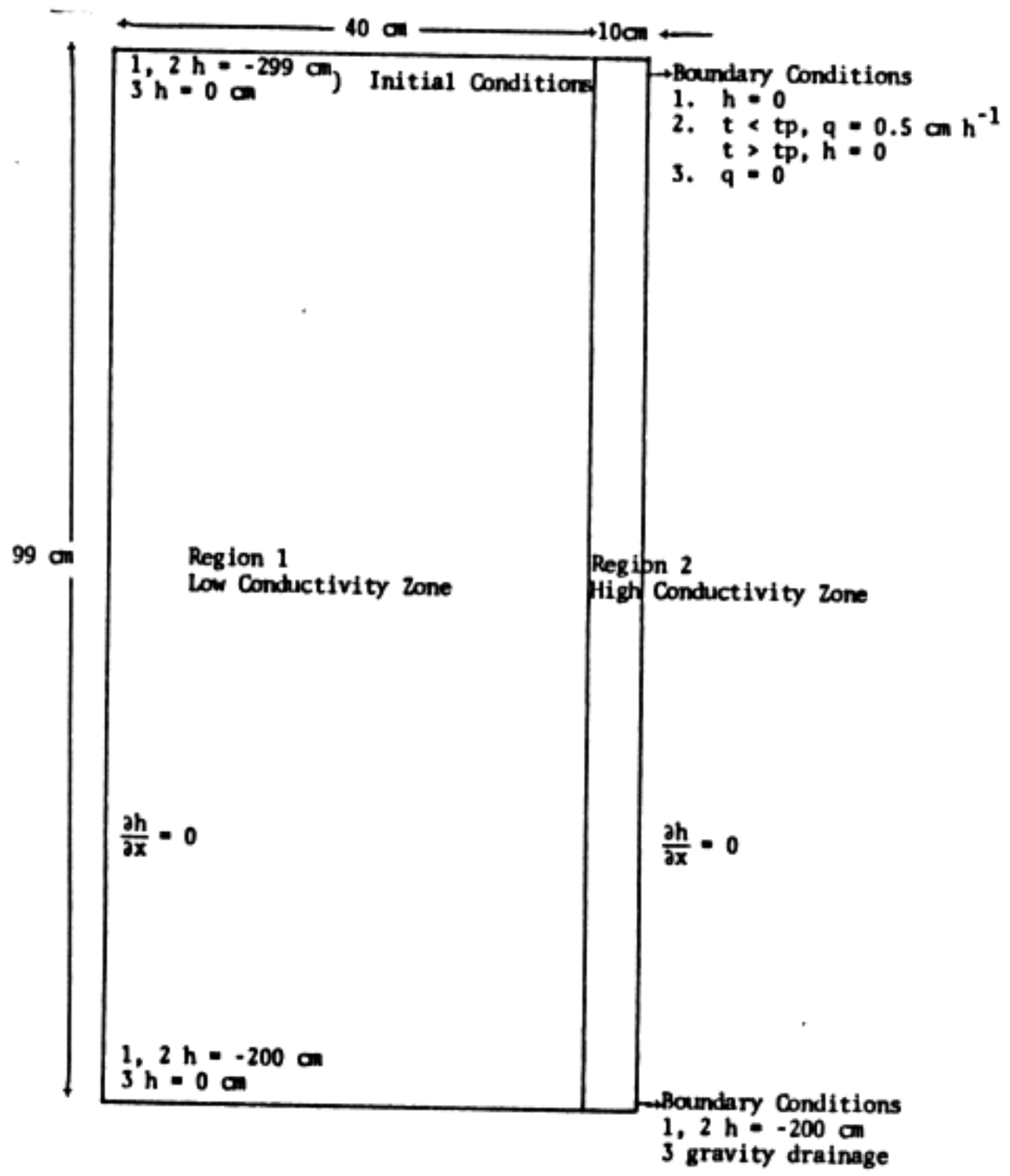

Figure 7.4. Flow domain used in checking the averaging approximation.

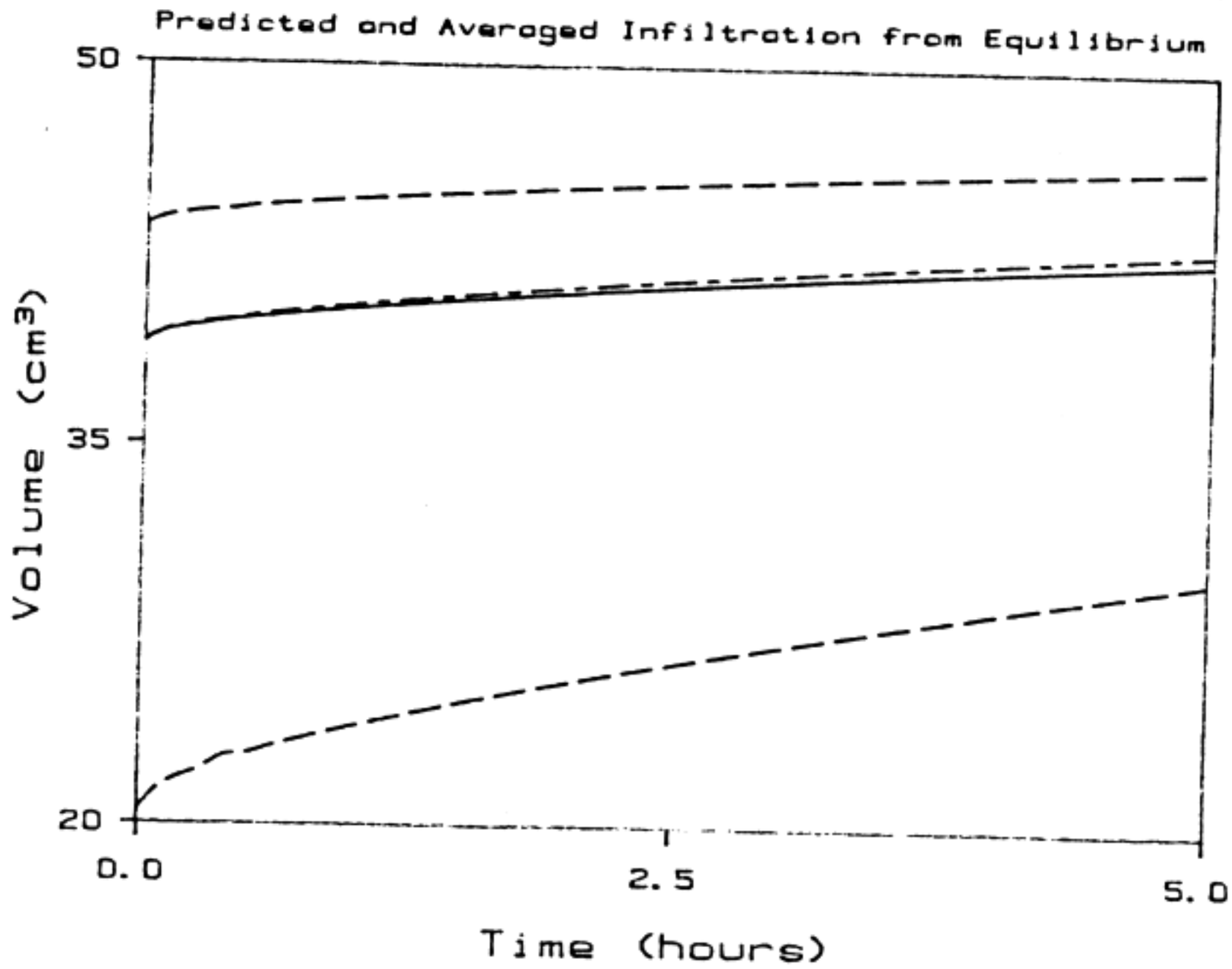

Figure 7.5. Ponded infiltration into the flow domain given by Fig. 7.4. The starting point of each curve is the calculated volume of water in the profile. The cumulative infiltration into each region is given by the dashed lines, with the upper dashed line being for Region 1 and the lower one for Region 2. The volume-weighted average of the two regions is given by the dashed-dotted line with the empirical average given by the solid line.

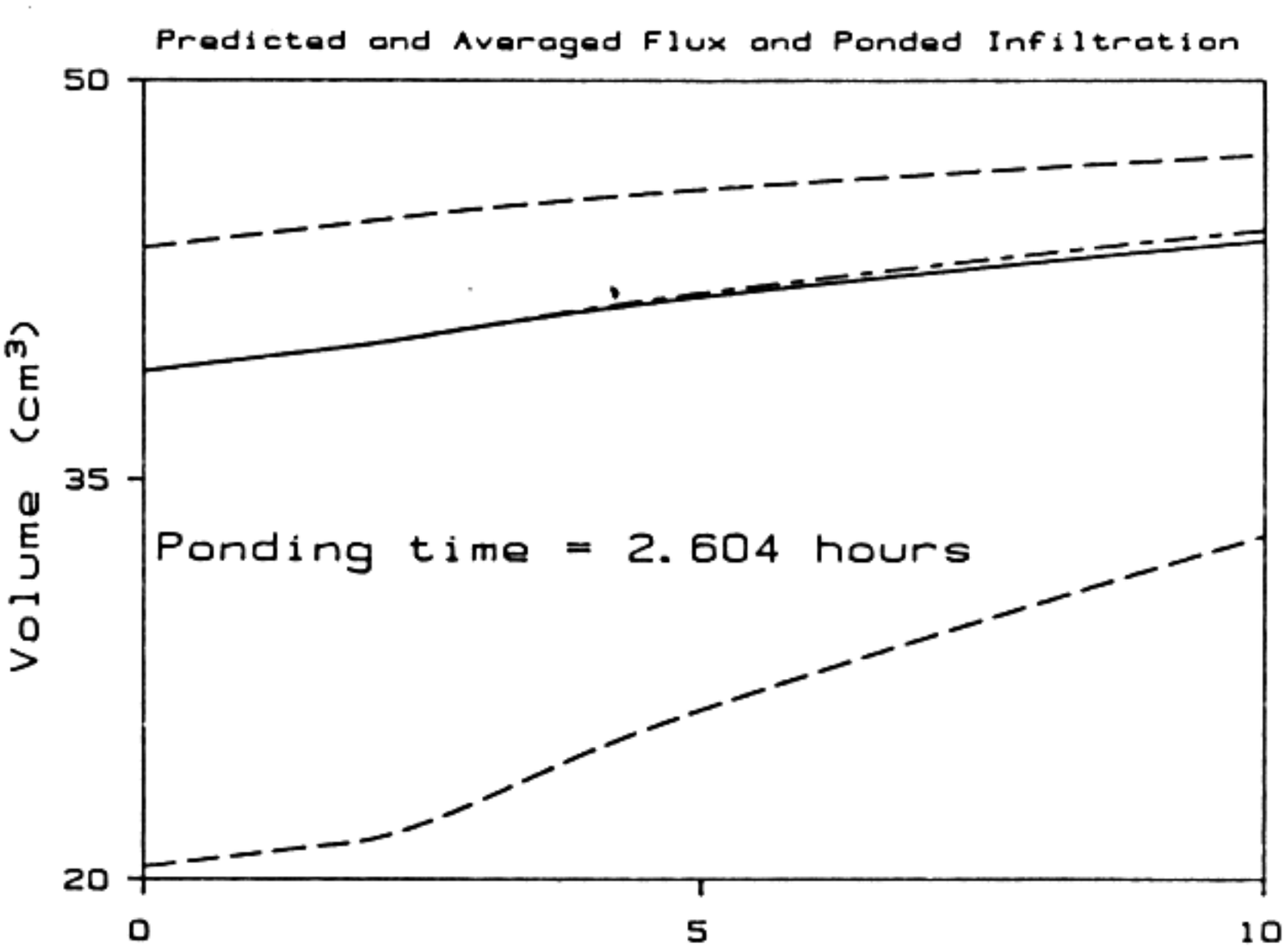

Figure 7.6. Cumulative infiltration into a soil with a macropore. Curves correspond to those in Fig. 7.5. The ponding time is that for the low-conductivity zone but is applied to the whole surface.

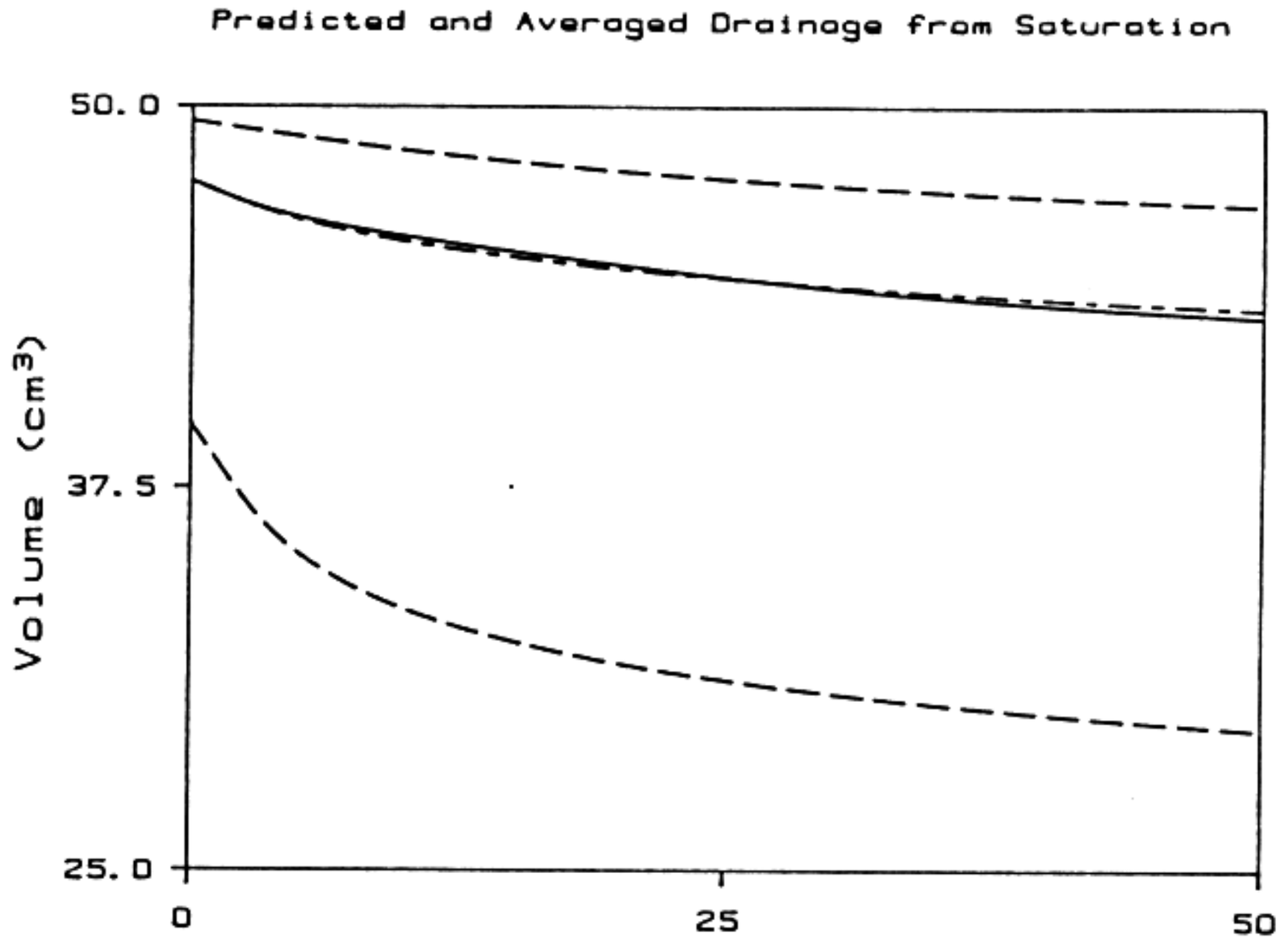

Figure 7.7. Cumulative drainage from a profile initially at saturation. The curves correspond to the previous two figures.

Drainage from Saturation

In this case the initial tension throughout the profile in Figure 7.4 is set to h = 0 cm water (boundary and initial condition set 3). The simulations were terminated at t = 50 h with Figure 7.7 showing that the approximation adequately predicted drainage from the profile for that period.

CONCLUSIONS

The prediction of flow and redistribution of water in heterogeneous soils remains an important practical problem. Our aim here was to investigate the accuracy with which the approximation of one-dimensional averaged flow could predict the average of the "real" two- or three-dimensional case. The approach used was to use volume-weighted averages of the retention and conductivity functions for the particular soil types involved.

Particularly, our interest is directed to the case of vertically-stratified soils in which adjacent soil types have at least an order of magnitude difference in the saturated hydraulic conductivities. This case, which we assume to approximate zones of macroporosity in a soil, was shown to be well approximated by individual soil columns, with the behavior of the entire system being given by the volume-weighted average of the one-dimensional simulations. By itself, this results in a substantial simplification in the flow-domain analysis. Additionally, with this simplification the problem can be easily handled using a microcomputer as opposed to the necessity of using a mainframe for the solution of the original problem.

As stated above the empirical averaging scheme employed took volume-weighted averages of the known retention and conductivity functions. These averaged functions were then used in a one-dimensional code and the results compared with "exact" averages. Three cases were considered; ponded infiltration, infiltration into a soil with a single macropore, and drainage from saturation. Due to the choice of the Brooks-Corey retention function the error of the approximation was shown clearly. Even for this case the approximation was shown to be accurate enough for time scales of interest. However, it is clear that more research is necessary to extend the approach to more practical problems.

REFERENCES

Andersson, J. and A. M. Shapiro, Stochastic analysis of one-dimensional steady state unsaturated flow: a comparison of Monte Carlo and perturbation methods, *Water Resour. Res.*, *19*, 121-33, 1983.

Aris, R., On the dispersion of kinematic waves, *Proc. Royal Soc. of London*, *A245*, 268-277, 1958.

Baker, L. E., Effects of dispersion and dead-end pore volume in miscible flooding, *Soc. Petroleum Eng. J.*, *17*, 219-227, 1977.

Bear, J., and Y. Bachmat, Transport phenomena in porous media - the basic equations, *In J. Bear and M. Y. Corapcioglu* (ed.) Proc. NATO Adv. Study Inst. on Mech. of Fluids in Porous Media, Newark, DE., 18-27 July 1982.

Bear, J., *Dynamics of Fluids in Porous Media*, Elsevier, New York, 1972.

Bear, J., and Y. Bachmat, On the equivalence of areal and volumetric averages in transport phenomena in porous media, *Adv. Water Resour.*, *6*, 59-62, 1983.

Beven, K. J. and R. T. Clarke, On the variation of infiltration into a homogeneous soil matrix containing a population of macropores, *Water Resour. Res.*, *22*, 383-8, 1986.

Beven, K. and P. Germann, Water flow in soil macropores, II. A combined flow model, *J. Soil Sci.*, *32*, 15-29, 1981.

Bhattacharya, R. N. and V. K. Gupta, A theoretical explanation of solute dispersion in saturated porous media at the Darcy scale, *Water Resour. Res.*, *19*, 938-44, 1983.

Bhattacharya, R. N., V. K. Gupta and G. Sposito, On the stochastic foundations of the theory of water flow through unsaturated soil, *Water Resour. Res.*, *12*, 503-512, 1976.

Bolt, G. H., Movement of solutes in soil: principles of adsorption/exchange chromatography, In G. H. Bolt (ed.), *Soil Chemistry: B. Physico-Chemical Models*, (2nd edition), Elsevier, Amsterdam, p. 285-348, 1982.

Bouma, J., C. F. M. Belmans and L. W. Dekker, Water infiltration and redistribution in a silt loam subsoil with vertical worm channels., *Soil Sci. Soc. Am. J.*, *46*, 917-21, 1982.

Bouma, J., and J. H. M. Wosten, Flow patterns during extended saturated flow in two undisturbed swelling clay soils with different macrostructures, *Soil Sci. Soc. Am. J.*, *43*, 16-22, 1979.

Bouma, J. and L. W. Dekker, A case study on infiltration into dry clay soil, 1, Morphological observations, *Geoderma*, *20*, 27-40, 1978.

Bouma, J., A. Jongerius, O. Boersma, A. Jager and D. Schoonderbeek, The function of different types of macropores during saturated flow through four swelling soil horizons, *Soil Sci. Soc. Am. J.*, *41*, 945-50, 1977.

Brenner, H., The diffusion model of longitudinal mixing in beds of finite length: Numerical values, *Chem. Eng. Sci.*, *17*, 229-243, 1962.

Brigham, W. E., Mixing equations in short laboratory columns, *Soc. Pet. Eng. J.*, *14*, 91-99, 1974.

Brooks, R. H. and A. T. Corey, Properties of porous media affecting fluid flow, *Journal of the Irrigation and Drainage Division*, Proceedings of the American Society of Civil Engineers, *92*, 61-88, 1966.

Bruch, J. C., Two-dimensional dispersion experiments in a porous medium, *Water Resour. Res.*, *6*, 791-800, 1970.

Burdine, N. T., Relative permeability calculations from pore-size distribution data. Petroleum Transactions, *Am. Inst. of Mining Engineers*, *198*, 71-7, 1953.

Coats, K. H. and B. D. Smith, Dead-end pore volume and dispersion in porous media, *Soc. Petroleum Eng. J.*, *4*, 73-84, 1964.

Clapp, R. B. and G. M. Hornberger, Empirical equations for some soil hydraulic properties, *Water Resour. Res.*, *14*, 601-4, 1978.

Deans, H. A., A mathematical model for dispersion in the direction of flow in porous media, *Soc. Petroleum Eng. J.*, *3*, 49-52, 1963.

De Smedt, F. and P. J. Wierenga, Solute transfer through columns of glass beads, *Water Resources Res.*, *20*, 225-232, 1984.

De Smedt, F. and Wierenga, P. J., A generalized solution for solute flow in soils with mobile-immobile water, *Water Resour. Res.*, *15*, 1137-1141, 1979.

Dieulin, A., G. Matheron, and G. de Marsilly, Growth of the dispersion coefficeint with mean travelled distance in porous media, *Sci. of the Total Environ.*, *21*, 319-328, 1981.

Dullien, F. A. L., *Porous Meida: Fluid Transport and Pore Structure*, Academic Press, 1979.

Edwards, W. M., R. R. van der Ploeg and W. Ehlers, A numerical study of the effects of noncapillary-sized pores upon infiltration, *Soil Sci. Soc. Am. J*, *43*, 851-856, 1979.

Fried, J. J., *Groundwater Pollution*, Elsevier Scientific Publishing Company, Amsterdam, 1975.

Gelhar, L. W., Stochastic analysis of phreatic aquifers, *Water Resour. Res.*, *10*, 539-45, 1974.

Germann, P. and K. Beven, Water flow in macropores, I. An experimental approach, *J. Soil Sci.*, *32*, 1-13, 1981.

Gillham, R. W., E. A. Sudicky, J. A. cherry and E. O. Friend, An advection-diffusion concept for solute transport in heterogeneous unconsolidated geological deposits, *Water Resour. Res.*, *20*, 369-78, 1984.

Goldstein, F. R. S., On the mathematics of exchange processes in fixed columns, I. Mathematical solutions and asymptotic expansions, *Proc. Roy. Soc. London*, *219*, 151-185, 1953.

Green, W. H. and G. A. Ampt, Studies on soil physics: I, flow of air and water through soils, *J. Agric. Sci.*, *4*, 1-24, 1911.

Grisak, G. E. and J. F. Pickens, An analytical solution for solute transport through fractured media with matrix diffusion, *J. Hydrol.*, *52*, 47-57, 1981.

Gureghian, A. B. and Jansen, G., One-dimensional analytical solutions for the migration of a three-member radionuclide decay chain in a multilayered geologic medium, *Water Resour. Res.*, *21*, 733-742, 1985.

Güven, O., F. J. Molz and J. G. Melville, An analysis of macrodispersion in a stratified aquifer, *Water Resour. Res.*, *20*, 1337-54, 1984.

James, R. V. and J. Rubin, Applicability of local equilibrium assumption to transport through soil of solutes affected by ion exchange, *In Chemical Modeling in Aqueous Systems*, E. A. Jenne (ed.), p. 225-235, Symposium Series 93, American Chemical Soc., Washington, D.C., 1979.

Javandel, I., Doughty, C. and Tsang, C. F., *Groundwater Transport: Handbook of Mathematical Models*, American Geophysical Union, Washington, D.C., 1984.

Kaluarachchi, J. J. and J. C. Parker, Finite element analysis of water flow in variably saturated soils, *J. Hydrol.* (in press), 1986.

Kreft, A., On the residence time distribution in systems with axial dispersed flow, *Bull. Ac. Pol. Tech.*, *29*, 509-520, 1981a.

Kreft, A., On the boundary conditions of flow through porous media and conversion of chemical flow reactors, *Bull. Ac. Pol. Tech*, *29*, 521-529, 1981b.

Kreft, A., and A. Zuber, On the use of the dispersion model of fluid flow, *Int. J. Appl. Rad. Isot.*, *30*, 705-708, 1979.

Kreft, A., and Z. Zuber, On the physical meaning of the dispersion equation and its solutions for different initial and boundary conditions, *Chem. Eng. Sci.*, *33*, 1471-1480, 1978.

Lapidus, L., and N. R. Amundson, Mathematics of adsorption in beds, 6, The effect of longitudinal diffusion in ion exchange and chromatographic columns, *J. Phys. Chem.*, *56*, 984-988, 1952.

Lenhard, R. J., Changes in void distribution and volume during compaction of a forest soil, *Soil Sci. Soc. Am. J.*, *50*, 462-4, 1986.

LePage, W. R., *Complex Variables and the Laplace Transform for Engineers*, McGraw-Hill, New York, 1961.

Lindstrom, F. T., R. Haque, V. H. Freed, and L. Boersma, Theory on the movement of some hebicides in soils: Linear diffusion and convection of chemicals in soils, *J. Environ. Sci. Tech.*, *1*, 561-565, 1967.

Lyman, W. J., W. F. Reehl and D. H. Rosenblatt, *Handbook of Chemical Property Estimation Methods*, McGraw-Hill, 1982.

Marle, C., Simandoux, P., Pacsirszky J. and Gaulier, C., Etude du deplacement de fluides miscibles en milieu poreux stratifie, *Rev. Inst. Fr. Petrole.*, *22*, 272-294, 1967.

Moranville, M. B., Kessler, D. P. and Greenkorn, R. A., Dispersion in layered porous media, *A.I.Ch.E.J.*, *23*, 786-794, 1977.

Mualem, Y., A new model for predicting the hydraulic conductivity of unsaturated porous media, *Water Resour. Res.*, *12*, 523-522, 1976.

Nauman, E. B. and Buffham, B. A., *Mixing in Continuous Flow Systems*, John Wiley and Sons, Inc., New York, 1983.

Nielsen, D. R., J. W. Biggar and K. T. Erh, Spatial variability of field-measured soil-water properties, *Hilgardia*, *42*, 215-58, 1973.

Nkedi-Kizza, P., J. W. Biggar, M. Th. van Genuchten, P. J. Wierenga, H. M. Selim, J. M. Davidson, and D. R. Nielsen, Modeling tritium and chloride 36 transport through an aggregated oxisol, *Water Resour. Res.*, *19*, 691-700, 1983.

Panigatti, J. L., *The Influence of Soil Textural Stratification on Chloride and Fluometuron Movement*, Unpublished M.S. Thesis, Oklahoma State University, Stillwater, Oklahoma, 1970.

Parker, J. C. and Valocchi, A. J., Constraints on the validity of equilibrium and first-order kinetic transport models in structured soils, *Water Resour. Res.*, *22*, 399-407, 1986.

Parker, J. C., Analysis of solute transport in column tracer studies, *Soil Sci. Soc. Am. J.*, *48*, 719-724, 1984.

Parker, J. C., and M. Th. van Genuchten, Determining transport parameters from laboratory and field tracer experiments, *Va. Agric. Exp. Stn. Bull.*, 84-3, 1984.

Parker, J. C., and M. Th. van Genuchten, Flux-averaged and volume-averaged concentrations in continuum approaches to solute transport, *Water Resour. Res.*, *20*, 866-872, 1984a.

Parlange, J.-Y. and Starr, J. L., Linear dispersion in finite columns, *Soil Sci. Soc. Am. Proc.*, *39*, 817-819, 1975.

Parlange, J.-Y. and Starr, J. L., Dispersion in soil columns: effect of boundary conditions and irreversible reactions, *Soil Sci. Soc. Am. J.*, *42*, 15-18, 1978.

Passioura, J. B., Hydrodynamic dispersion in aggregated media, I. Theory, *Soil Science*, *111*, 339-344, 1971.

Pearson, J. R. A., A note on the "Danckwerts" boundary condition for continuous flow reactors, *Chem. Eng. Sci.*, *10*, 281-284, 1959.

Pendse, H., Tien, C., Rajogopalan, R. and Turian, R. M., Dispersion measurement in clogged filter beds: a diagnoistic study on the morphology of particle deposits, *A.I.Ch.E.J.*, *24*, 473-484, 1978.

Persaud, N., Giraldez, J. V. and Chang, A. C., Monte-Carlo simulation of noninteracting solute transport in a spatially heterogeneous soil, *Soil Sci. Soc. Am. J.*, *49*, 562-568, 1985.

Raats, P. A. C., Tracing parcels of water and solutes in unsaturated zones, *In Yaron*, G. Dagan and J. Goldschmid (eds.), Pollutants In Porous Media: The Unsaturated Zone Between Soil Surface and Groundwater, Springer, Berlin, p. 4-16, 1984.

Raats, P. A. C., Transport in structured porous media, *Proceedings Euromech* 143, September 2-4, Delft, Netherlands, p. 221-226, 1981.

Rao, P. S. C. and R. E. Jessup, Sorption and movement of pesticides and other toxic organic substances in soils, *In Chemical Mobility and Reactivity in Soil Systems*, D. W. Nelson (ed.), p. 183-201, Soil Sci. Soc. Am., Madison, Wisconsin, 1983.

Rao, P. S. C., D. E. Rolston, R. E. Jessup, and J. M. Davidson, Solute transport in aggregated porous media: Theoretical and experimental evaluation, *Soil Sci. Soc. Am. J.*, *44*, 1139-1146, 1980.

Rasmuson, A. and I. Neretnieks, Exact solution for diffusion in particles and longitudinal dispersion in packed beds, *Am. Inst. Chem. Eng. J.*, *26*, 686-690, 1980.

Rose, C. W., F. W. Chichester, J. R. Williams, and J. T. Ritchie, Application of an approximate analytic method of computing solute profiles with dispersion in soils, *J. Environ. Qual.*, *11*, 151-155, 1982.

Selim, H. M., Davidson, J. M. and Rao, P. S. C., Transport of reactive solutes through multilayered soils, *Soil Sci. Soc. Am. J.*, *41*, 3-10, 1977.

Sidle, R. C., and L. T. Kardos, Nitrate leaching in a sludge-treated forest soils, *Soil Sci. Soc. Am. J.*, *43*, 278-282, 1979.

Shamir, U. Y. and Harleman, D. R. F., Dispersion in layered porous media, *Proc. Am. Soc. Civil Eng. Hydr. Div.*, *93*, 236-260, 1967.

Shamir, U. Y. and Harleman, D. R. F., 1966, *Numerical and Analytical Solutions of Dispersion Problems in homogeneous and Layered Aquifers, Tech.*, Rep. No. 89, Hydrodynamics Lab., Mass. Inst. Technol., Cambridge, Mass., pp. 206, 1966.

Skopp, J., Analysis of solute movement in structured soils, *Proc. of the ISSS Symposium on Water and Solute Movement in Heavy Clay Soils,* J. Bouma and P. A. C. Raats (eds.), Wageningen: International Institute for Land Reclamation and Improvement - III - (IRLI pub. 37), pp. 220-227, 1984.

Skopp, J., and A. W. Warrick, A two-phase model for the miscible displacement of reactive solutes in soils, *Soil Sci. Soc. Am. Proc., 38*, 545-550, 1974.

Smettem, K. R. J. and N. Collis-George, Prediction of steady-state ponded infiltration distributions in a soil with vertical macropores, *J. Hydrol., 79*, 115-22, 1985a.

Smettem, K. R. J. and N. Collis-George, The influence of cylindrical macropores on steady-state infiltration in a soil under pasture, *J. Hydrol., 79*, 107-14, 1985b.

Smith, L. and F. W. Schwartz, Mass transport, 1. A stochastic analysis of macroscopic dispersion, *Water Resour. Res., 16*, 303-13, 1980.

Sudicky, E. A. and E. O. Frind, Contaminant transport in fractured porous media: Analytical solutions for a system of parallel fractures, *Water Resources Res., 18*, 1634-1642, 1982.

Tang, D. H., E. O. Frind and E. A. Sudicky, Contaminant transport in fractured porous media: Analytical solution for a single fracture, *Water Resources Res., 17*, 555-564, 1981.

Ultman, J. S. and Blatman, H. S., 1977, A compartmental dispersion model for the analysis of mixing in tube networks, *A.I.Ch.E.J., 23*, 169-176, 1977.

Valocchi, A. J., Validity of the local equilibrium assumption for modeling sorbing solute transport through homogeneous soils, *Water Resources Res., 21*, 808-820, 1985.

van Genuchten, M. Th., A numerical model for water and solute movement in and below the root zone, (In prep.), 1986.

van Genuchten, M. Th., A general approach for modeling solute transport in structured soils, Proc. 17th Int. Congress, Int. Assoc. of Hydrogeologists, "Hydrogeology of Rocks of Low Permeability," Tucson, Arizona, January 1985, *Memoires IHS*, vol. 17, part 2, p. 513-526, 1985.

van Genuchten, M. Th., D. H. Tang and R. Guennelon, Some exact solutions for solute transport through soils containing large cylindrical macropores, *Water Resources Res., 20*, 335-346, 1984.

van Genuchten, M. Th. and J. C. Parker, Boundary conditions for displacement experiments through short laboratory soil columns, *Soil Sci. Soc. Am. J., 48*, 703-708, 1984.

van Genuchten, M. Th., and Alves, W. J., *Analytical Solutions of the One-Dimensional Convection-Dispersion Equation*, U.S. Department of Agriculture, Technical Bulletin No. 1661, 151 p., 1982.

van Genuchten, M. Th., Non-equilibrium transport parameters from miscible displacement experiments, USDA-SEA *Res. Rep.* 119, U.S. Salinity Lab., Riverside, Calif., 1981.

van Genuchten, M. Th., A closed-form equation for predicting the hydraulic conductivity of unsaturated soils, *Soil Sci. Soc. Am. J., 44*, 892-8, 1980.

van Genuchten, M. Th., and P. J. Wierenga, Mass transfer studies in sorbing porous media, 1, Analytical solutions, *Soil Sci. Soc. Am. J., 40*, 473-480, 1976.

Weast, R. C. (ed.), *CRC Handbook of Chemistry and Physics*, CRC Press, Boca Raton, Florida, 1985.

Wehner, J. F. and Wilhelm, R. H., Boundary conditions of flow reactor, *Chem. Eng. Sci., 6*, 89-93, 1956.

PUBLICATIONS FROM THIS PROJECT

1. Parker, J. C. and B. Caplin, Evaluation of solute transport parameters from laboratory tracer experiments in soils with large pores, *Agron. Abst., Soil Sci. Soc. Am.*, p. 142, 1983.

2. Parker, J. C. and M. Th. van Genuchten, Flux-averaged and volume-averaged concentrations in continuum approaches to solute transport, *Water Resources Res.*, 20,866-872, 1984.

3. Parker, J. C., Analysis of solute transport in column tracer studies, *Soil Sci. Soc. Am. J.*, *48*,719-724, 1984.

4. Parker, J. C. and M. Th. van Genuchten, Reply to "Comment on flux-averaged and volume-averaged concentrations in continuum approaches to solute transport," *Water Resources Res.*, *22*,1301-1302, 1985.

5. Parker, J. C. and A. J. Valocchi, Modeling of diffusional nonequilibrium in structured porous media, *Trans. Am. Geophys. Union, 66*, 274, 1985.

6. Barry, D. A. and J. C. Parker, Analysis of solute transport through layered soils, *Trans. Am. Geophys. Union, 66*, 881, 1985.

7. Parker, J. C. and D. A. Barry, Theoretical and experimental analysis of transport in fractured porous media, *Trans. Am. Geophys. Union, 66*, 881, 1985.

8. Parker, J. C. and A. J. Valocchi, Constraints on the validity of equilibrium and first-order kinetic transport models in structured soils, *Water Resources Res.*, *22*,399-407, 1986.

9. Barry, D. A. and J. C. Parker, Approximations for solute transport through porous media with flow transverse to layering, *Transport in Porous Media*, (in press).